



Helmholtz-Zentrum für Ozeanforschung Kiel

**FS MARIA S. MERIAN
Fahrtbericht / Cruise Report
MSM-34 / 1 & 2**

SUGAR Site

Varna – Varna,
06.12.13 – 16.01.14



Berichte aus dem GEOMAR
Helmholtz-Zentrum für Ozeanforschung Kiel

Nr. 15 (N. Ser.)

März 2014



Helmholtz-Zentrum für Ozeanforschung Kiel

FS MARIA S. MERIAN
Fahrtbericht / Cruise Report
MSM-34 / 1 & 2
SUGAR Site

Varna – Varna,
06.12.13 – 16.01.14



Berichte aus dem GEOMAR
Helmholtz-Zentrum für Ozeanforschung Kiel

Nr. 15 (N. Ser.)

März 2014

ISSN Nr.: 2193-8113



Das GEOMAR Helmholtz-Zentrum für Ozeanforschung Kiel
ist Mitglied der Helmholtz-Gemeinschaft
Deutscher Forschungszentren e.V.

The GEOMAR Helmholtz Centre for Ocean Research Kiel
is a member of the Helmholtz Association of
German Research Centres

Herausgeber / Editor:

Jörg Bialas, Ingo Klaucke, Matthias Haeckel

GEOMAR Report

ISSN Nr. 2193-8113, DOI 10.3289/GEOMAR_REP_NS_15_2014

Helmholtz-Zentrum für Ozeanforschung Kiel / Helmholtz Centre for Ocean Research Kiel

GEOMAR
Dienstgebäude Westufer / West Shore Building
Düsternbrooker Weg 20
D-24105 Kiel
Germany

Helmholtz-Zentrum für Ozeanforschung Kiel / Helmholtz Centre for Ocean Research Kiel

GEOMAR
Dienstgebäude Ostufer / East Shore Building
Wischhofstr. 1-3
D-24148 Kiel
Germany

Tel.: +49 431 600-0
Fax: +49 431 600-2805
www.geomar.de

Content

1. Summary	5
2 Participants	6
2.1 Scientists of cruise MSM34/1	6
2.2 Scientists of cruise MSM34/2	6
3 Research Program	7
4 Narrative of the cruise	8
4.1 Cruise narrative MSM34-1	8
4.2 Cruise narratives of MSM34/Leg 2	10
5 Preliminary results	12
5.1 Sound Velocity Profiles (SVPs)	14
5.2 Bathymetry and sediment sounding	15
5.2.1 Bathymetry	15
5.2.2 Parasound	16
5.2.3 Flare imaging	16
5.3 Seismic	18
5.3.1 Regional 2D Seismic	18
5.3.1.1 Semblance velocity analysis	20
5.3.1.2 Stacking and post stack migration	21
5.3.2 High resolution 2D seismic	22
5.3.3 3D P-Cable Seismic	26
5.3.3.1 P-Cable area 1	26
5.3.3.2 P-Cable area 2	26
5.3.4 OBS data and results	27
5.3.4.1 Work area 1	27
5.3.4.2 Work area 2	29
5.4 Geochemistry	31
5.4.1 Introduction	31
5.4.2 Materials and Methods	31
5.4.2.1 Sediment and porewater sampling	31
5.4.2.2 Porewater analyses	31
5.4.2.3 Headspace gas analyses	32
5.4.3 Results	32
5.4.3.1 Late Glacial to Holocene Black Sea Sediment Lithology	33
5.4.3.2 General Black Sea Sediment Geochemistry	35
5.4.3.3 IFREMER piezometer site at shallow water depth	35
5.4.3.4 SW channel-levee system / multiple BSRs	37
5.4.3.5 NE channel-levee system / upward bending BSR	38
5.5 Heatflow measurements	39
5.5.1 Working area 1	39
5.5.2 Working area 2	40
5.6 Piezometer installation	41
6 Ship's Metrological Station	42
7 Station List	43
7.1 Stationsliste MSM34-1	43
7.2 Stationsliste MSM34-2	45
8 Data and Sample Storage and Availability	56
9 Acknowledgements	56
10 References	56

11 Appendix	61
11.1 <i>Regional setting</i>	61
11.1.1 Introduction	61
11.1.2 Regional Geology of the Black Sea	61
11.1.2.1 Morphology	61
11.1.2.2 Black Sea basin evolution	61
11.1.3 Regional Geology of the NW Black Sea	65
11.1.3.1 Tectonic	65
11.1.3.2 Sediment structure	67
11.1.3.3 The Messinian event in the Black Sea	68
11.1.3.4 Danube levee system	69
11.1.4 Additional References	71
11.2 <i>Equipment of the scientific party</i>	73
11.2.1 GI-gun	73
11.2.1.1 External trigger	73
11.2.2 Seismic navigation MSM-34/2	74
11.3 <i>Streamer systems</i>	76
11.3.1 SeisLab 2D streamer	76
11.3.1.1 Definition of Navigation Data	78
11.3.1.2 Definition of Multichannel Seismic Data	79
11.3.1.3 Analyzing the Seismic Data and QC	80
11.3.2 2D GEOMAR high resolution streamer	81
11.3.3 P-Cable	81
11.3.4 OBS-Instrumentation	88
11.3.4.1 The GEOMAR three-leg Ocean Bottom Seismometers:	88
11.3.4.2 The GEOMAR Ocean Bottom Seismometer 2002 (OBS-2002):	88
11.3.4.3 Recording and processing of OBS-Data	89
11.4 <i>Coring devices</i>	90
11.5 <i>OBS station list</i>	91
11.5.1 Core descriptions	92
11.5.1.1 Site IFREMER Piezometer (in shallow water)	92
11.5.1.2 Site SW channel-levee with multiple BSR (on seismic line 8b)	93
11.5.1.3 Site SW channel-levee with multiple BSR (channel)	94
11.5.1.4 Site SW channel-levee with multiple BSR (levee)	95
11.5.1.5 Site NE channel-levee with upward bending BSR (slump area)	96
11.5.1.6 Site NE channel-levee with upward bending BSR (slump area)	97
11.5.1.7 Site NE channel-levee with upward bending BSR (gas seep at slump head wall)	98
11.5.1.8 Site NE channel-levee with upward bending BSR (slump area)	99
11.5.1.9 Site NE channel-levee with upward bending BSR (channel)	100
11.6 <i>Heatflow probe</i>	100
11.6.1 Heatflow probe station protocol	101
11.7 <i>Piezometer</i>	107
11.7.1 Specifications of the piezometer:	108
11.7.2 Deployment procedure for bridge and deck	108

1. Summary

Jörg Bialas

During the two legs of cruise MSM34 of R/V MARIA S. MERIAN regional 2D seismic surveying, high resolution 2D and 3D seismic imaging, geo-chemical sampling, heatflow measurements and long-term piezometer installations were undertaken.

A grid of 28 2D seismic profiles was collected across the palaeo Danube delta. A number of inactive and partly buried channel systems could be mapped. Most of them were underlain by one or more bottom simulation reflectors (BSR). Based on the seismic brute stack images and the limits of the MeBo drilling device a prospective channel system with indications for possible gas hydrate formation at shallow depth (BSR, inverted strong amplitudes) could be identified in about 1500 m water depth. High resolution 2D seismic and 3D P-Cable seismic were used together with OBS deployments in order to allow structural mapping and physical description of the channel infill. Heatflow measurements and geochemical analyses of gravity and multi corer samples accompany these investigations. Neither the multibeam water column images nor Parasound records show any evidence of flares (gas bubbles in the water column) in this working area suggesting a well sealed hydrate reservoir.

Active gas expulsion from the seafloor was observed at about 200 m water depth circling around a slump area. The base plane of the failed sediment volume builds the current seafloor at about 600 m to 700 m water depth. On regional 2D seismic profiles a BSR has been mapped underneath the slope failure with unexpectedly strong upward bending. High resolution 2D and 3D P-Cable seismic investigations with complementary OBS deployment will allow imaging the BSR outline. Moreover velocity analyses, heatflow measurements and geo-chemical samples will be available for a detailed description of hydrate distribution and sediment parameters.

In a third working area high resolution 2D seismic reflection profiles were acquired across a fully buried channel system. Together with the regional seismic lines slope failure of the channel fill material can be studied across the slope extension of the system.

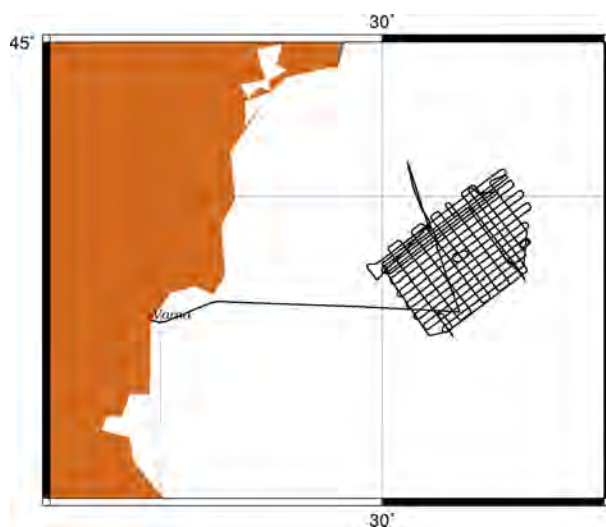


Figure 1.1 Trackplot of cruise MSM-34 leg-1

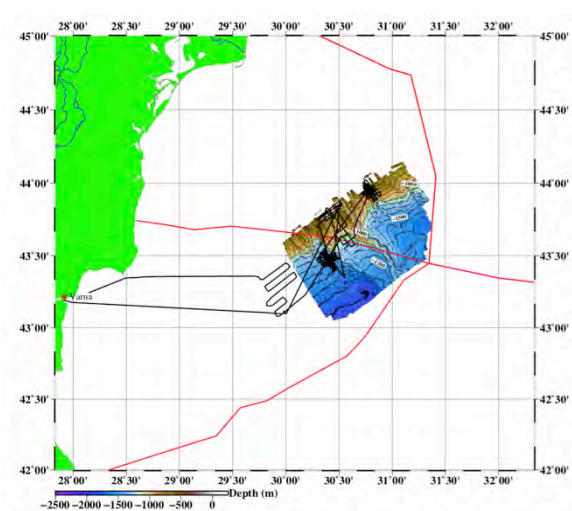


Figure 1.2 Trackplot of cruise MSM-34 leg-2

2 Participants

2.1 Scientists of cruise MSM34/1

#	Name	Expertise	Institute
1	Klaucke, Ingo	Chief scientist	GEOMAR
2	Hoffmann, Jasper	Bathymetry	GEOMAR
3	Schroeder, Henning	Parasound	GEOMAR
4	Zander, Timo	Seismic Interpretation	GEOMAR
5	Ferrrant, Anthony	Geotechnics	IFREMER
6	Roudaut, Mickael	Geotechnics	IFREMER
7	Bayol, Efe	Seismic	IMST-Seislab
8	Barin, Burcu	Seismic	IMST-Seislab
9	Duymaz, Sermet	Seismic	IMST-Seislab
10	Dondurur, Derman	Seismic	IMST-Seislab
11	Cifci, Günay	Seismic	IMST-Seislab
12	Atgin, Orhan	Seismic	IMST-Seislab
13	Nasif, Aslihan	Seismic	IMST-Seislab
14	Küçük, Hilmi Mert	Seismic	IMST-Seislab
15	Özel, Özkan	Seismic	IMST-Seislab
16	Vasilev, Atanas	Seismic / Observer	IO-BAS

2.2 Scientists of cruise MSM34/2

#	Name	Expertise	Institute
1	Bialas, Jörg	Chief scientist / seismic	GEOMAR
2	Dannowski, Anke	OBS	GEOMAR
3	Koch, Stefanie	Seismic processing	GEOMAR
4	Sakar, Sudipta	Seismic interpretation	GEOMAR
5	Zander, Timo	Seismic interpretation	GEOMAR
6	Wetzel, Gero	Electronic engineering	GEOMAR
7	Matthiesen, Torge	Mechanic engineering	GEOMAR
8	Sauermilch, Isabel	OBS	GEOMAR
9	Gross, Felix	Parasound/Multibeam	GEOMAR
10	Schroeder, Henning	Seismic / OBS	GEOMAR
11	Schroller, Dirk	Geochemistry	GEOMAR
12	Haeckel, Matthias	Geochemistry	GEOMAR
13	Dibbern, Meike	Geochemistry	GEOMAR
14	Bigalke, Nikolaus	Geochemistry	GEOMAR
15	Pape, Thomas	Geochemistry	MARUM
16	Atgin, Orhan	Seismic	IMST-Seislab
17	Küçük, Hilmi Mert	Seismic	IMST-Seislab
18	Özel, Özkan	Seismic	IMST-Seislab

GEOMAR	Helmholtz-Zentrum für Ozeanforschung Kiel
IFREMER	Institut Français pour la Recherche et l'Exploitation de la Mer, Brest
IMST-Seislab	Institute of Marine Science and Technology, Dokuz-Eylül University, Izmir
IO-BAS	Institute of Oceanography, Bulgarian Academy of Science, Varna
MARUM	Centre for Marine Environmental Sciences, Bremen

3 Research Program

Jörg Bialas

Gas hydrates have been the focus of scientific and economic interest for the past 15-20 years, mainly because the amount of carbon stored in gas hydrates is much greater than in other carbon reservoirs. Several countries including Japan, Korea and India have launched vast research programmes dedicated to the exploration for gas hydrate resources and ultimately the exploitation of the gas hydrates for methane. The German SUGAR project that is financed by the Ministry of Education and Research (BmBF) and the Ministry of Economics (BmWi) aims at developing technology to exploit gas hydrate resources by injecting and storing CO₂ instead of methane in the hydrates. This approach includes techniques to locate and quantify hydrate reservoirs, drill into the reservoir, extract methane from the hydrates by replacing it with CO₂, and monitor the thus formed CO₂-hydrate reservoir. Numerical modelling has shown that any exploitation of the gas hydrates can only be successful, if sufficient hydrate resources are present within permeable reservoirs such as sandy or gravelly deposits. The ultimate goal of the SUGAR project being a field test of the technology developed within the project, knowledge of a suitable test site becomes crucial. Within European waters only the Norwegian margin and the Danube deep-sea fan show clear geophysical evidence for large gas hydrate accumulations, but only the Danube deep-sea fan most likely contains gas hydrates within sandy deposits.

Prior to cruise MSM34 limited information about the Danube delta was available, only. Preparation was mainly based on three sources. Publications by [Lericolais *et al.*, 2009; Popescu *et al.*, 2007; Popescu *et al.*, 2006], a Diploma thesis by [Baristeas, 2006] and reports on the EU projects ASSEMBLAGE and BLASON.

The work of Baristeas (2006) was based on a selection of seismic profiles from a 3D survey undertaken by TOTAL in 1994 and 2001. This data set was not available for the cruise MSM34. Baristeas (2006) mapped two areas of BSR distribution north and south of the Viteaz canyon and interpreted irregular and increased amplitudes underneath channel axes as indications for free gas. Similar patches were interpreted underneath the levees. Baristeas (2006) speculates that microbial gas migrates along the coarse grained high permeable sediment-fill of the channel axis upwards towards the hydrate stability zone. Vertical migration is limited or inhibited by fine grained sediments. Formation of hydrates provides a seal indicated by the BSR. Further distribution of gas will be guided horizontal into the permeable levee system. Baristeas (2006) observed patches of a double BSR in the northern area. Discussions of models for the formation of a multiple BSR were not concluded. Nevertheless in his summary Baristeas assumes that upward migration of thermogenic gas may have contributed increased amounts of higher carbon gases, which may have caused secondary BSRs due to modified stability boundaries.

Popescu *et al.* (2006, 2007) used data provided from the BLASON cruise undertaken by IFREMER and GeoEcoMar in 1998 and 2002. Selected data sets were provided by IFREMER. Popescu *et al.* (2006) interpreted multiple BSRs in the Danube fan area closely connected to channel-levee systems. They conclude that the uppermost BSR marks the current equilibrium depth of the base of the gas hydrate stability zone (BGHSZ) for gas compositions of more than 99% methane. This BSR1 has been mapped within three areas of the Danube

fan. Chaotic reflection patterns underneath the BSR1 were found underneath the channel axis indicating the accumulation of free gas. The levees are partially underlain by stacks of up to four additional BSRs. Indications of free gas are provided by amplitude reversals of the reflection events where they cross the BSRs. Successive steps of climate warming are thought to be the cause of the additional BSRs. Free gas resulting from destabilization through the climate changes is expected to migrate within the strata. Mineral reaction may have taken place locally and provide a seal for fluid migration, which is imaged as paleo-BSR (Popescu et al., 2006).

Seismic data from EU projects ASSEMBLAGE and BLASON were made available by IFREMER, but did not provide a reasonable data coverage of the working area. Industry data used by Baristeas were not available. Therefore cruise MSM34 set out to establish the bathymetric and seismic database to prepare selection of further high resolution seismic study areas. Leg 1 of cruise MSM34 acquired the necessary grid of 2D seismic profiles and deployed two long-term piezometers operated by IFREMER. Based on the acquired 2D seismic data two target areas were selected for high resolution 3D seismic imaging during leg 2. Both 3D volumes could be acquired. Due to unexpectedly favourable weather conditions additional high resolution 2D seismic profiles could be acquired.

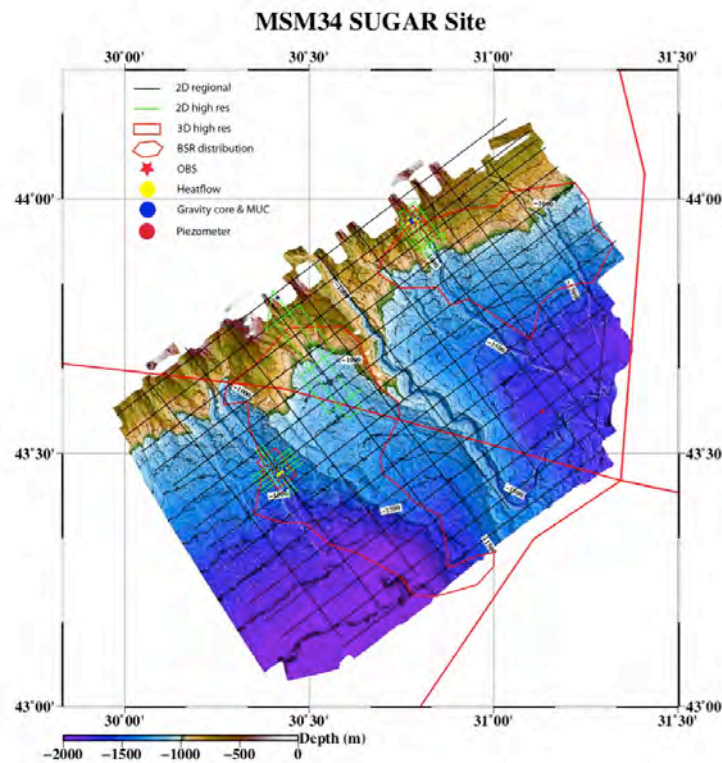


Figure 3.1: Overview map with outline of the working areas and deployments of cruise MSM34-1 & 2

4 Narrative of the cruise

4.1 Cruise narrative MSM34-1

Ingo Klaucke

The first leg of RV MARIA S. MERIAN cruise MSM34 started on December 5, 2013 when a first group of six scientists from Germany and France arrived in Varna, Bulgaria. Cruise MSM34 is dedicated to investigations of marine gas hydrate deposits offshore Bulgaria and Romania in general and the Danube deep-sea fan in particular. During the first leg we intend to acquire 2D-seismic, bathymetry and Parasound data together with in-situ pore pressure measurements while the second leg will acquire 3D seismic and OBS data together

with heat-flow measurements and sediment cores for geochemical analyzes. All the necessary equipment for both legs was already sent for the very beginning of the MSM34 campaign.

On December 6, 2013 RV MARIA S. MERIAN arrived in the port of Varna and berthed at the container pier for unloading of the equipment from the previous cruise. While waiting for the authorisation to disembark the containers, the equipment of cruise MSM34 arriving by two trucks from Kiel and one truck from Brest, France was already loaded onboard. In the afternoon, RV MARIA S. MERIAN changed berth to the passenger terminal that is just a few hundreds of meters away. The following day, a delayed truck with further equipment from Izmir, Turkey finally arrived and the seismic streamer winch and all the necessary electronics were put onto the vast after-deck of RV MARIA S. MERIAN. In the meantime our colleagues from Brest began installing the piezometer underneath the A-frame and the work stations for the seismic interpretation were mounted in the lab. On December 8 the seven scientists from Germany, France and Bulgaria that already had reached Varna boarded RV MARIA S. MERIAN while waiting for nine colleagues from Turkey. They had missed a connecting flight in Istanbul and only arrived in the afternoon at 16:00 after a very long journey. However, soon after their arrival they started setting up the seismic equipment in the deck's lab.

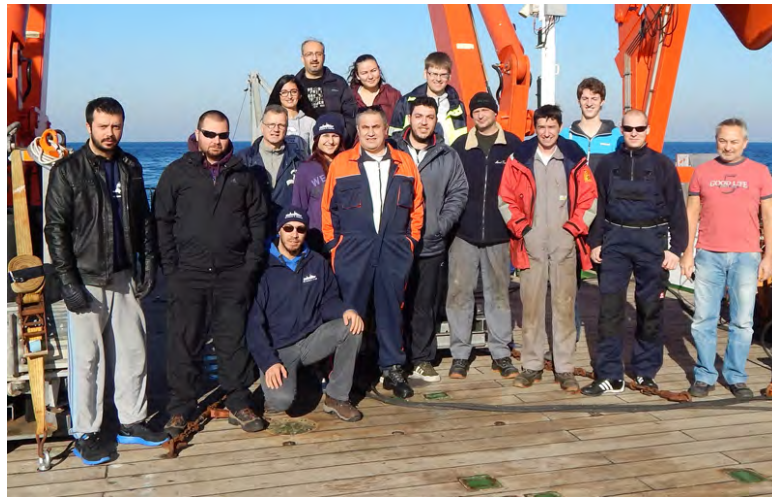
December 9 started with a safety instruction and a familiarization tour of the vessel at 08:00 o'clock. Departure was scheduled for that morning, but had to be delayed because of strange noises and lack of power of one of the pod propulsions. After many different checks and consultation with the manufacturer, the problem was finally overcome by a renewed complete reboot of the system and RV MARIA S. MERIAN finally sailed out of the port of Varna at 18:00 for an 11 hours transit to our first station. At 05:00 on December 10, 2013 we reached the station and deployed a sound velocity probe in order to obtain a sound velocity profile for the EM122 multibeam system. The subsequent multibeam and Parasound profile towards the locations of the first piezometer deployment had to be stopped at mid-way due to deteriorating weather conditions. Average winds of force 7-8 with gusts of force 9 did not allow collecting useful data and all operations were stopped at 08:10.

By the early morning of December 11 the weather conditions had improved and following a safety and abandon ship drill at 10:30, a first attempt to deploy the piezometer at was carried out at mid-day. This test run intended to determine the possible length of the piezometer was successful and the actual piezometer pipe equipped with sensors was installed on the deployment frame. By 19:30 the first piezometer of the cruise was deployed and RV MARIA S. MERIAN headed towards the starting point of our first seismic profile. At 22:00 the 1050-m long streamer of our Turkish colleagues was deployed and at 01:00 on December 12 we started recording our first seismic profile. Unfortunately, the EM122 multibeam system stopped working properly in the early morning hours of December 12 and it took until the evening before the problem could be fixed. Seismic recording continued smoothly until 12:00 on December 16, when a strange signal on the hydrophone of the airgun urged us to bring the airgun back on deck for verification. After replacement of the airgun umbilical, seismic recording resumed at 16:30 and continued until December 18 at 14:30 when the airgun showed signs of leakage. In order to save time, the airgun was replaced with a spare GI-gun and seismic data acquisition resumed at 17:30.

On December 20 the seismic gear was recovered at 12:45 the seismic gear was recovered for a change of batteries of the bird system. The afternoon and early evening was then used to deploy the second piezometer station that was installed in a location where gas hydrates are expected to be close to the seafloor. By 23:30 the piezometer station was successfully completed and we started a short bathymetry survey to allow the CGG Symphony to move away from our survey area.

At 12:30 on December 21 we redeployed the seismic equipment under perfect weather

conditions for seismic acquisition. A loose connection in the acquisition electronics slightly delayed the beginning of the next profile so that we eventually came quite close to the CGG Symphony the next morning. Luckily, although interferences became very strong, they could still be filtered out. By December 24, 12:00 we had completed our preliminary lines and could add several additional lines that appeared to be necessary after initial inspection of the seismic data. With seismic data acquisition still going on, we all celebrated Christmas Eve with a nice special evening program prepared by the crew with a little help of the scientific party. Seismic acquisition was finished on December 26 at 08:00 after 2200 line kilometers of high-resolution and high-quality seismic profiling. By 9:30 the seismic gear was back on deck and we finished our scientific program with a couple of bathymetry and Parasound profiles dedicated at filling some remaining gaps in the bathymetry grid. At 22:00 we had to leave the study area and arrived in time to meet the pilot at 08:00 on December 27 at the entrance to the port of Varna. By 09:00 RV MARIA S. MERIAN had berthed at the pier and by 12:00 the equipment of our colleagues from IFREMER, Brest and SeisLab, Izmir had been loaded onto two trucks waiting at the pier. That was the end of the first leg of cruise MSM34, which was extremely successful, as all goals have been fully achieved.



4.2 Cruise narratives of MSM34/Leg 2

Jörg Bialas

(All times are local times)

On Friday 27.12.13 R/V MARIA S. MERIAN returned from cruise MSM34/ Leg 1 to the port of Varna. PIs of Leg 2, Dr. Bialas and Dr. Haeckel, joined with the PI of Leg1 Dr. Klaucke on board the vessel to discuss the results of the cruise. Seismic 2D profiling on Leg 1 was dedicated to provide a regional overview for the search of buried channel levee systems within the hydrate stability zone of the ancient Danube fan. On a first glance only one promising channel levee system, which seems to be accessible for a future drilling campaign with the mobile drilling device MeBo, could be identified. The outline of the BSR distribution across the 2D seismic grid shows substantial differences to those published previously. Along seismic 2D line 15 the BSR could be mapped upwards the slope until it coincides almost with the seafloor. This area was chosen of second most interest. A third target area was the possible slump distribution within the vicinity of the shallow piezometer deployment site at the shelf break.

In the evening of 27.12.13 the remaining 11 scientific crew members arrived at the port of Varna. Together with 5 crew members of Leg 1 a total of 18 scientists joined for geophysical and geochemical investigations during cruise MSM34/ Leg 2 on board. To avoid delays

caused by season holidays all equipment was already shipped with two trucks for the port call of leg 1.

A safety familiarization was undertaken in the afternoon of the 29.12.13 with all scientists. After two days of preparation major set up of equipment was completed on deck and in the laboratories when R/V MERIAN left the port of Varna on 29.12.13 at 19:00 hrs. Weather conditions were calm with less than 4 Bft. wind and wave heights less than 1.5 m. Weather conditions were stable through the following days.

During transit to the working area two short PARASOUND profiles were recorded across a possible vent site that was observed by our colleagues from NIOZ in early 2013. At this time no flare was observed in the water column. In the morning of 30.12.13 a safety instruction training was undertaken with all crew on board. At 10:30 hrs scientific investigations of MSM34 Leg 2 began with multicore, gravity core and heatflow sampling next to the shallow piezometer site of Leg 1. At 15:30 the acoustic releases of the OBS were tested at 1400 m water depth. A calibration of the heatflow probe and a sound velocity profile were taken as well. Next 15 OBS were deployed within the foreseen area of the 3D seismic cube.

On the 31.12.13 at 01:20 deployment of 15 OBS was completed. After some bathymetric profiles a gravity core was taken at the southern limits of the 3D area before deployment of the P-Cable system. Due to water penetration in the wet end termination of the P-Cable umbilical a 2D seismic survey was run to serve airgun shots for the OBS array. At 18:30 a 45 / 45 cinch GI airgun and 5 streamer sections were deployed. Q/C tests for shot gathers did show interfering signals from M/V CGG SYMPHONY, a seismic 3D industry vessel operating in the Han Asparuh block. Due to far offsets and orthogonal survey outline the signals disappeared in filtered and stacked section display.

At 13:30 on 01.01.14 the 2D seismic survey was completed. Deployment of the P-Cable was completed at 18:30 with 14 nodes. Nodes 5 to 8 were equipped with doubled streamer sections. Airgun shots were fired at 5 sec. interval. Q/C tests did not show any remaining interferences caused by the M/V CGG SYMPHONY operations.

P-Cable operation was continued until 13:00 hrs on 04.01.14. In the afternoon two multicorer stations were sampled. At 18:30 hrs the heatflow probe was deployed. 11 stations were sampled until 01:30 of the 05.01.14. The night hours were used to recover the 15 OBS.

On the 05.01.14 at 10:00 hrs sampling of two gravity cores at the western and eastern end of the heatflow profile followed. Next the seismic survey was continued after deployment of the P-Cable at 16:30 hrs.

On the 06.01.14 at 10:00 hrs the injector of the airgun failed and the gun was replaced. Some time later the data connection to the P-Cable streamers was lost. It turned out that the data umbilical between vessel and P-Cable needed to be changed. The repair time was used to deploy a Mini-Corer at 17:30 hrs. At 22:00 hrs the P-Cable survey was continued.

At 03:00 hrs on 07.01.14 streamer section 6 delivered incomplete data. Node four of the P-Cable was taken out of the configuration scheme of the recording software and the survey was continued without recovery of the P-Cable.

The remaining 3D survey could be completed without system failure. Acquisition was stopped on 09.01.14 at 10:00 hrs. After a short transit R/V MARIA S. MERIAN arrived in the second work area. At 13:00 hrs research work continued with acquisition of gravity corer, Multi-Corer samples and a third heatflow profile. Starting at 20:00 hrs 12 OBS were deployed until 23:00 hrs.

At 01:30 on 09.01.14 hrs acquisition of the second 3D seismic data volume started. The survey area covered parts of a slump area and the neighbouring canyon system.

The survey was completed without interruption on 13.01.14 at 13:00 hrs. Gravity coring,

Multi-Corer and heatflow profiling was undertaken in the afternoon and night hours.

At 14.01.14 at 02:00 hrs 2D seismic profiling began to extend the survey area beyond the limits of the 3D cube. At 23:00 hrs recovery of 12 OBS took place until 03:30.

On 15.01.14 heatflow profiling began in order to connect measures from the slump area into the depression of the canyon system. Due to anomalous temperatures measured at the base of the canyon additional temperature and heatflow measurements were taken to better estimate the limits of the anomaly. For ground truthing a gravity core was taken on short notice prior to transit for the third working area. At 14:00 hrs a final 2D seismic survey began across a buried slump volume.

On 16.01.14 seismic data acquisition was terminated at 08:15 hrs. Following a short transit a last multibeam and Parasound survey investigated the so-called NIOZ bubble site with water column imaging. Scientific work of cruise MSM34 was terminated at 24:00 hrs when R/V MARIA S MERIAN set course towards the port of Varna.



5 Preliminary results

During leg 1 a grid of regional 2D seismic profiles has been acquired (Fig. 5.1) and has been the basis for choosing three detailed working areas for leg 2. Figures 5.2 to 5.4 summarize the high resolution seismic profiles and station work, first results of which are described below.

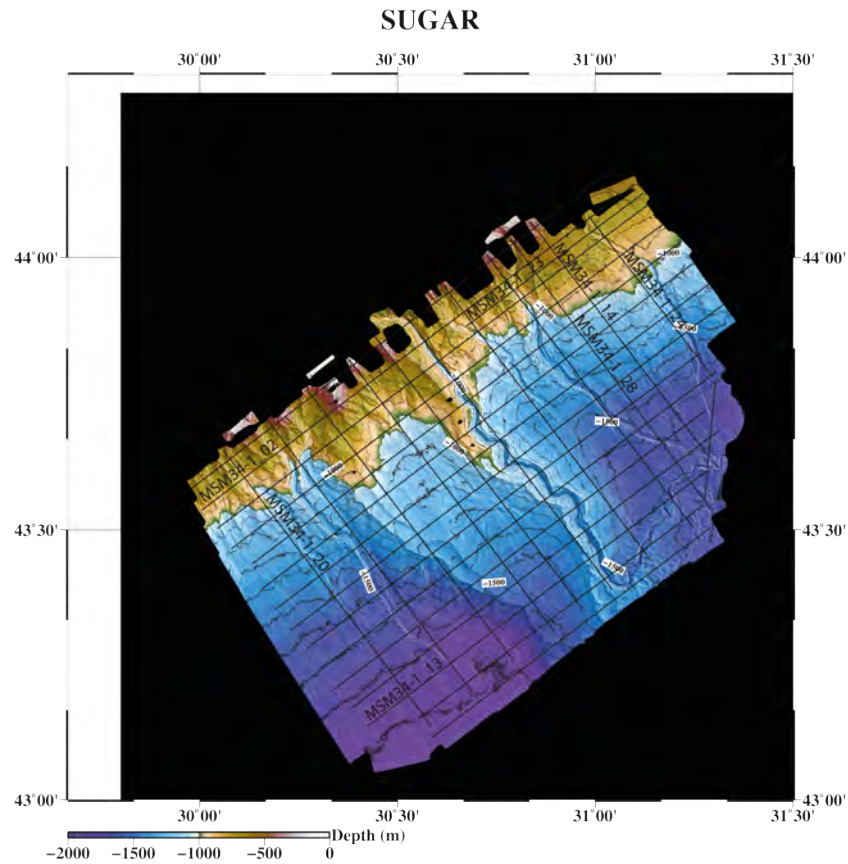


Figure 5.1: Bathymetric map of the MSM34 working area with the grid of 2D seismic profiles acquired during leg-1 of cruise MSM34 using the one kilometre long streamer of SeisLab

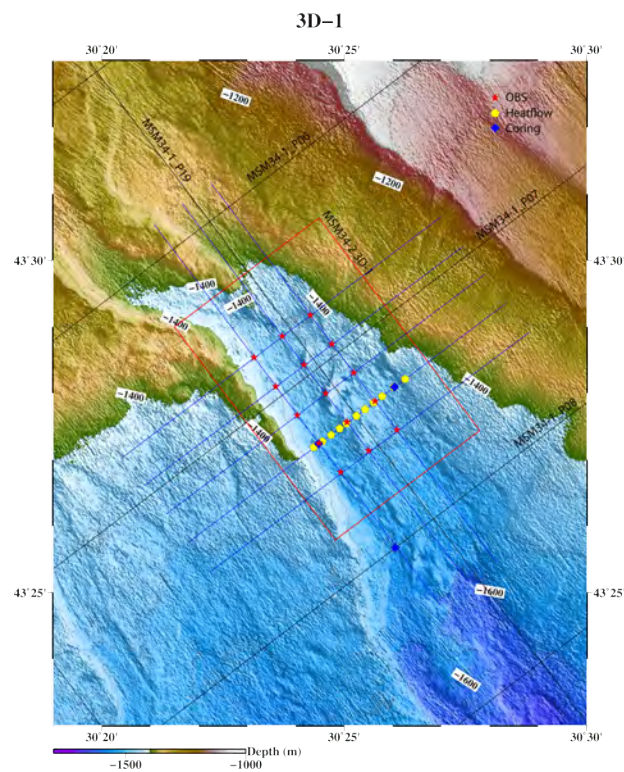


Figure 5.2: Overview map of working area 1 indicating seismic profiles and sampling stations

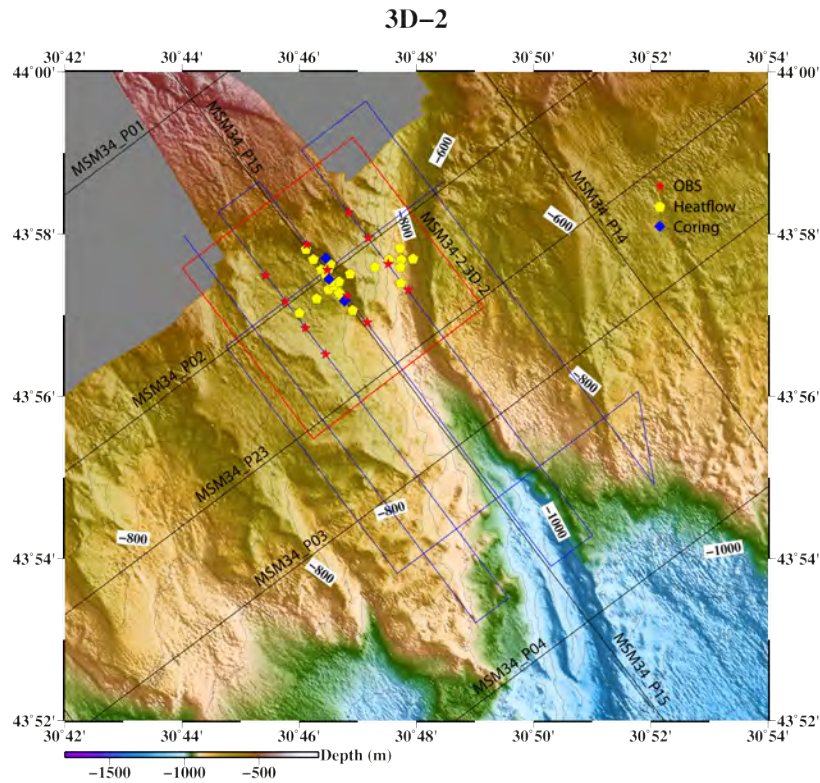


Figure 5.3: Overview map of working area 2 indicating seismic profiles and sampling stations

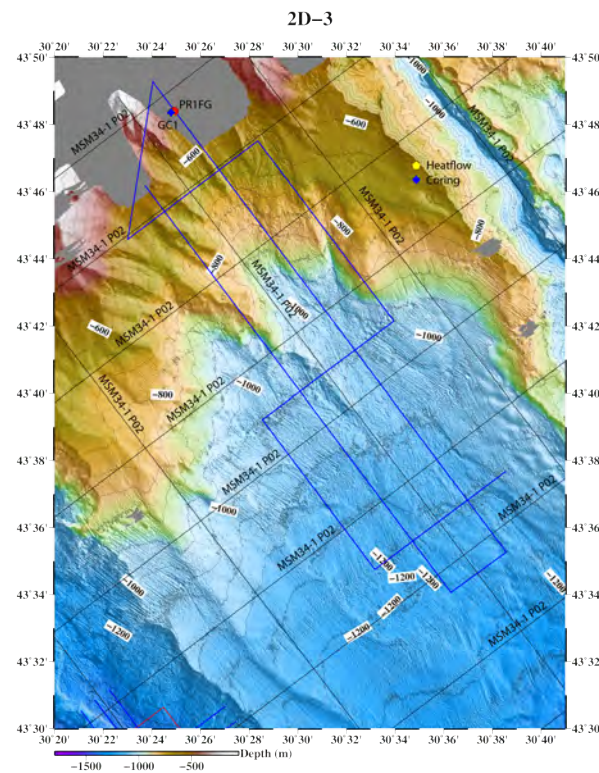


Figure 5.4: Overview map of working area 3 indicating seismic profiles and sampling stations

5.1 Sound Velocity Profiles (SVPs)

Felix Gross, Jasper Hoffmann

Three SVPs were acquired during MSM34 (Fig. 5.1.1). The data was acquired with an AML Oceanographic Plus X probe and were needed for multibeam calibration. The probe

measures the sound velocity every meter in depth up to 5000 dBar. The SVP stations are located in the studied area at highest possible water depth (up to 1840m) for a continuous profile. Data was extracted from the Probe using Seacast software and immediately loaded into the multibeam control software SIS for correct ray tracing through the water column.

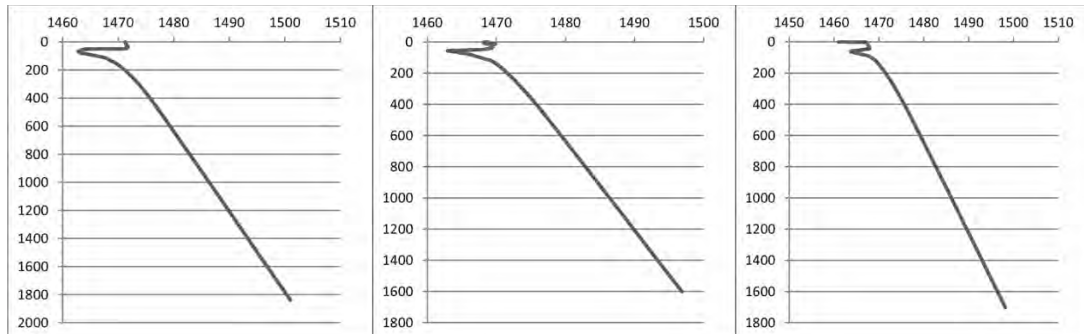


Figure 5.1.1: From left to right: SVP1 (MSM34-1) SVP2 (MSM34-1) SVP3 (MSM34-2)

5.2 Bathymetry and sediment sounding

5.2.1 Bathymetry

Jasper Hoffmann, Timo Zander, Henning Schröder, Felix Gross

Bathymetric data were recorded with the EM122 during the complete cruises MSM34 1 and 2. During the acquisition of the 2D seismic lines it was possible to achieve a sufficient overlapping of the outer beams between adjacent profiles. Thus, it was possible to generate a very detailed 25 m by 25 m bathymetry grid of the main study area (Fig 5.2.1.1). During the second leg of the cruise, additional bathymetry data could be retrieved only on the first and last days of the cruise during the observation of the NIOZ bubble site at the southwestern part of the study area.

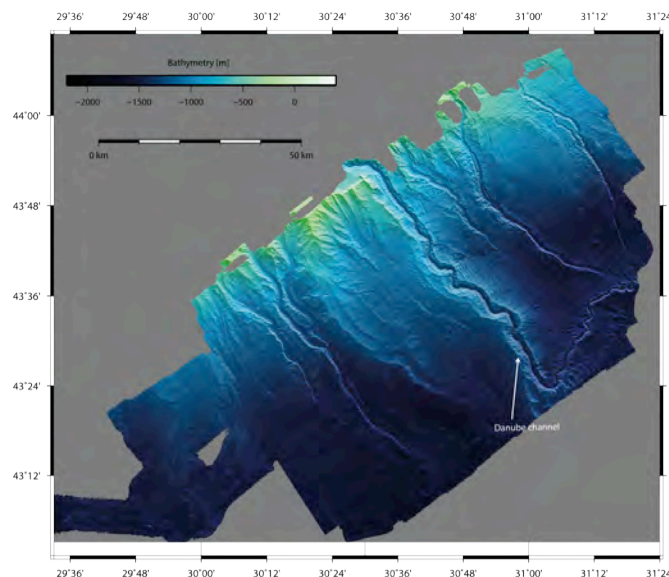


Figure 5.2.1.1: Bathymetric map of the Danube delta acquired during cruises MSM34-1 & 2

The multibeam bathymetry collected in the work area shows several paleo-channels of the Danube river, but only one channel was active at a time (Popescu et al., 2006), controlled by sea-level. The most recent channel-levee system that was active during the last sea-level lowstand is the Danube channel in the centre of the study area. The Danube channel cuts deeply into the sediments as shown in the surface profile (Fig. 5.2.1.2)

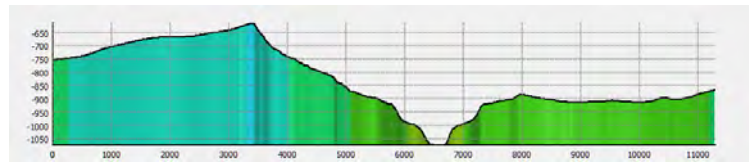


Figure 5.2.1.2: bathymetry cross-section through the Danube channel

The area towards the east of the Danube channel shows a rough surface structure with several blocks (Fig.5.2.1.3), while the area towards the west shows a flat surface in comparison.

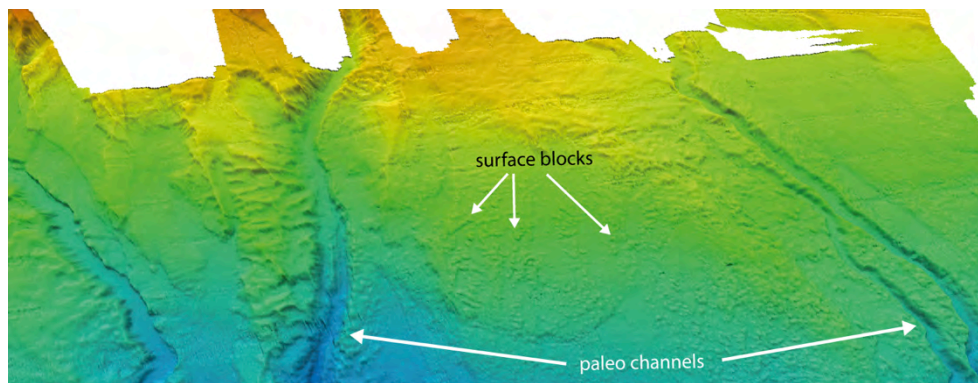


Fig. 5.2.1.3: bathymetric chart of the eastern part of the work area

5.2.2 Parasound

Felix Gross, Jasper Hoffmann, Timo Zander, Henning Schröder

The PARASOUND System was operated in a 24/7 mode during the entire cruise and a significant amount of echo-sounder data were collected. As the PARASOUND PS70 is able to resolve sedimentary structures at the cm scale, this system is very helpful for detailed sedimentary studies and the combination with sediment core data.

The general heterogenic geology of the working area is also visible in the PARASOUND data.

Fig. 5.2.2.1 left presents a representative PARASOUND profile from the western part of the working area. It features a high penetration of up to 175 ms two-way traveltime (TWT) and exhibits finely laminated sediment packages in the west and a chaotic/transparent facies overlying well-stratified deposits further East. These chaotic/transparent units are typical for mass transport deposits in PARASOUND data and in particular for debris flow deposits.

Fig. 5.2.2.1 right presents a representative PARASOUND Profile from the eastern part of the working area. In comparison to the western area, this area can be characterized by less penetration and therefore indicates a significant change in lithology. Less penetration indicates a high absorption of energy in the upper strata, which generally points towards a higher proportion of coarse-grained deposits.

5.2.3 Flare imaging

Felix Gross

During MSM 34/2 the Primary High Frequency (PHF) of the PARASOUND P70 was used for flare imaging. The high frequency of 18.8 kHz enables this echo sounder system for water column imaging and images horizontal, as well as vertical structures. This capability makes

the PARASOUND P70 feasible for high resolution 2D gas flare imaging within the water column. For less interference and signal distortion in the water column, the PARASOUND was operated in single pulse mode during flare imaging. In addition to the PARASOUND P70, the Kongsberg EM 122 was used for water-column imaging (WCI). The water column was recorded during the second P-Cable survey site. During acquisition, the system showed vertical features in the water column. The data was not processed on board due to missing software.

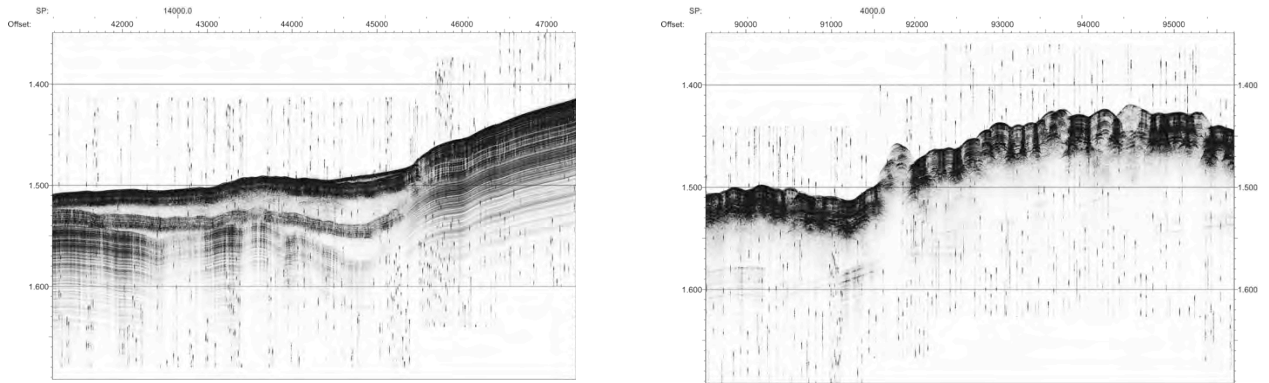


Figure 5.2.2.1: left: PARASOUND Profile in the western part of the working area with high penetration. right: PARASOUND Profile in the eastern part of the working area with low penetration.

Beside the gas flares, observed in shallow water depths of ca. 200 m, a special target for flare imaging was the second P-Cable survey area. In this area an unusual upward bended BSR is a possible indicator for gas emissions at the seafloor.

Several gas flares could be imaged within the water column at the second 3D survey area. Their origin at the seafloor lies in water depths between ca. 580 m – 750 m and is clearly associated with prominent morphological expressions at the seafloor (Fig. 5.2.3.1). The abundance of these flares can be traced in the entire second P-Cable survey. The gas emissions seemed to be constant during the survey, as some of the flares were imaged several times by the cruise track. The flares are not influenced by any currents in the water column, as they rise vertically without any bending towards the water surface.

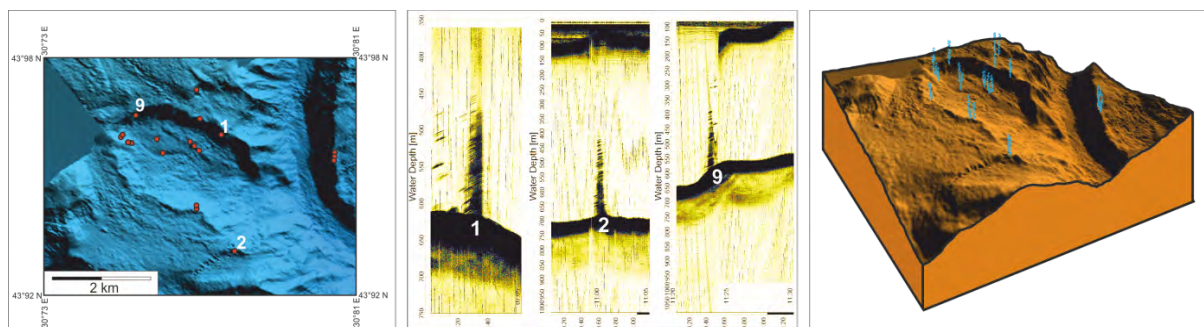


Figure 5.2.3.1: Left: Overview map on the second 3D survey area. Several flares were imaged in water depths ranging between 580 m and 750 m. Center: Examples of flares, observed in the working area. Their location is marked in the overview map to the left. Right: 3D view on the flare sites. Gas emissions are indicated by gas bubbles.

5.3 Seismic

5.3.1 Regional 2D Seismic

Orhan Atkin, Burcu Barin, Efe Bayol, Gunay Cifci, Derman Dondurur, Sermet Duymaz, Ingo Klaucke, Mert Küçük, Aslihan Nasif, Özkan Özel, Timo Zander

A total of 28 regional 2D seismic profiles have been acquired during leg 1. Despite the presence of an industry seismic ship (CGG Symphony) in the vicinity of the working area, the interferences from this vessel could be filtered out (Fig. 5.3.1.1) and a set of high quality seismic profiles has been obtained.

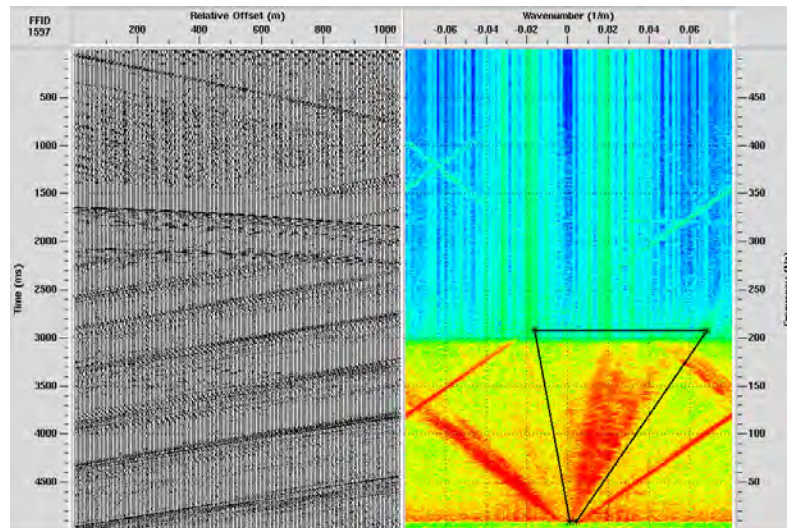


Figure 5.3.1.1: Seismic interference from far to near end and its FK spectrum related to of symphony (CGG) ship.

Brute stacks of the 2D seismic acquisition of leg 1 (fig. 5.3.1.2-4) were prepared in a Kingdom project for inspection prior to the beginning of leg 2. The main goal of cruise MSM34 was to identify gas hydrate bearing locations, which were favourable for a possible SUGAR test site. Boundary conditions for a test site are given by the request for a reasonable permeability to enable a productive gas flow. To enable application of the MeBo drilling device the hydrates need to be available as shallow as about 100 m below seafloor. It is the assumption of the MSM34 proposal that reasonable permeability is most likely to be expected within the centre and the levees of buried canyon systems. With this in mind the 2D seismic data of leg 1 were discussed between the party chiefs of cruise MSM34 leg 1 and leg 2 prior to start of leg 2 in the port of Varna.

Among the large number of buried channel levee systems only one was found, which seems to fulfil the requirements of the SUGAR project. The system further named work area 1 was identified along profile MSM34-1_19 between the crossing with profile MSM34_07 (Fig. 5.3.1.2) and MSM34-1_08. It is underlain by a continuous BSR indicating availability of free gas. Within the old channel centre at about 1500 m water depth a significant reflector of inverted polarity was identified within a depth of about 100 m below seafloor. It is assumed that above this horizon hydrate formation has taken place in porous sediment suitable for a test production site.

A second target of investigation was identified in water depth of about 700 m along profile MSM34-1_15 (Fig. 5.3.1.3) at the cross points with profiles MSM34-1_23 and MSMS34-1_28. At the cross point of profiles 15 and 23 the bathymetric depression of a channel system deviates from its NW-SE trend to north-south heading. Underneath an adjacent oval shaped area of slope failure the seismic section shows a significant upward bending of the BSR. The projected intersection of the BSR with the seafloor would be in roughly 700 m water depth. It

is assumed that variations in the subsurface temperature regime are responsible for the anomaly in the hydrate stability.

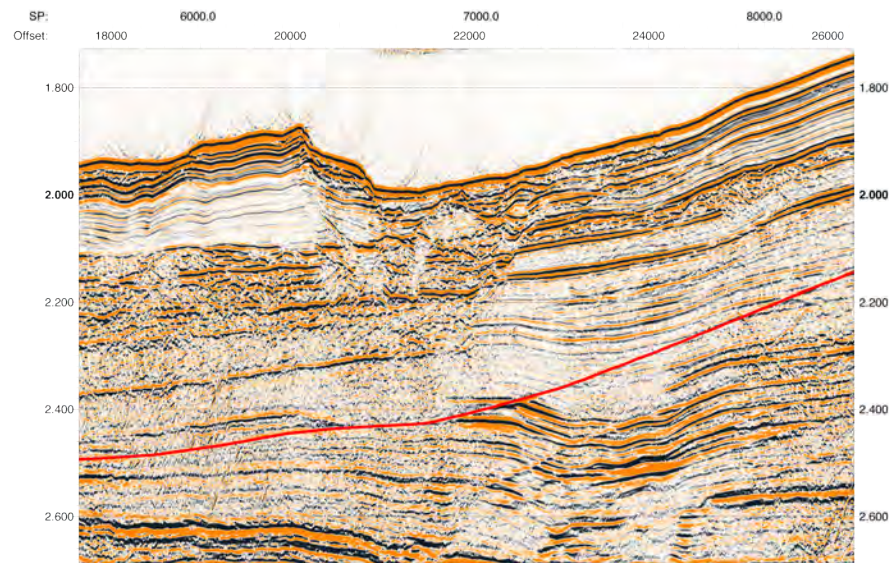


Figure 5.3.1.2: Zoom of seismic profile MSM34-1_07. The selected window shows the buried channel system chosen for the first 3D acquisition (offset 20000 to 24000). The main BSR is marked in red. Additional BSRs are visible between offset 22000 to 24000 at about 2.4 s TWT and 2.5 s TWT.

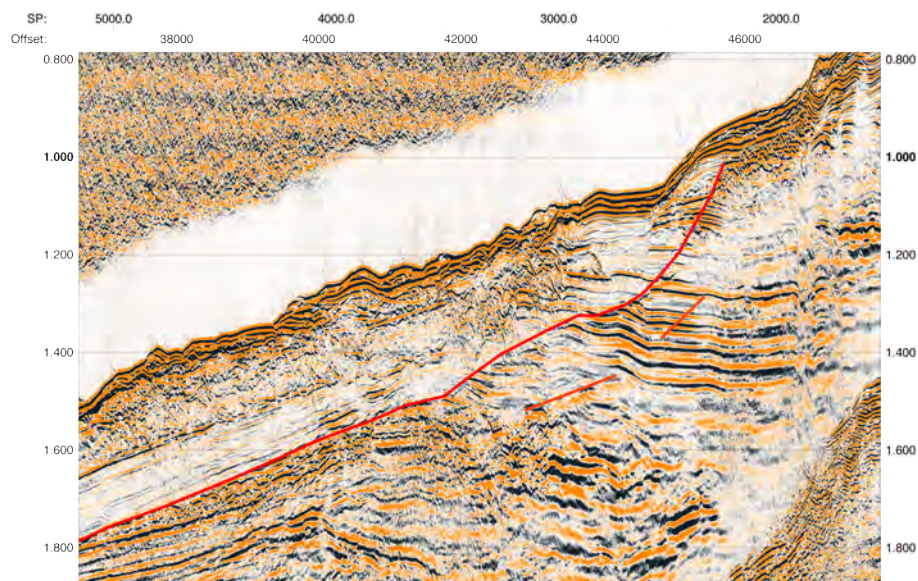


Figure 5.3.1.3: Zoom of the seismic profile MSM34-1_15. The main BSR is marked continuously (red). An additional BSR could be identified at offsets 44000 and 45000 (red). The remarkably increased upward bending of the BSR indicate a change in the hydrate stability conditions. Therefore this area was chosen as second 3D seismic target.

Two buried channel levee systems were chosen as a potential third target for the investigations of leg-2. At the cross points of profiles MSM34-1_18 and MSM34-1_02 well layered sediment horizons are interrupted by a sequence of chaotic reflection patterns. The base of these structures extend over 6 km on line MSM34-1_02 (Fig. 5.3.1.4). Downslope the reflection pattern could be followed towards the cross point of profiles MSM34-1_18 and

MSM34-1_07, where the width of the chaotic pattern reduces to about 4 km.

Based on the 2D seismic grid of MSM34-1 an outline of the BSR extension in the working area was mapped (red polygon in Fig. 5.3.1.5). In the northeast the BSR limits of this investigation are almost coincident with the observations of [Baristead, 2006] (yellow polygon in Fig. 5.3.1.5). Due to a wider data coverage [Popescu *et al.*, 2006] (orange polygon in Fig. 5.3.1.5) continuously mapped the BSR further outside the MSM34 working area. Although the data coverage of this investigation and the work of [Baristead, 2006] cover a similar region, the BSR was mapped to larger water depth in the MSM34-1 data. [Popescu *et al.*, 2006] deviate slightly from the MSM34-1 BSR distribution in water depth greater than 1500 m. While the BSR outline of MSM34-1 and [Baristead, 2006] cover a similar area at water depth shallower than 1500 m, the outline by [Popescu *et al.*, 2006] extends only half as wide (Fig. 5.3.1.5). Most likely the variations in BSR distribution of the three data sets are caused by different data coverage and data quality.

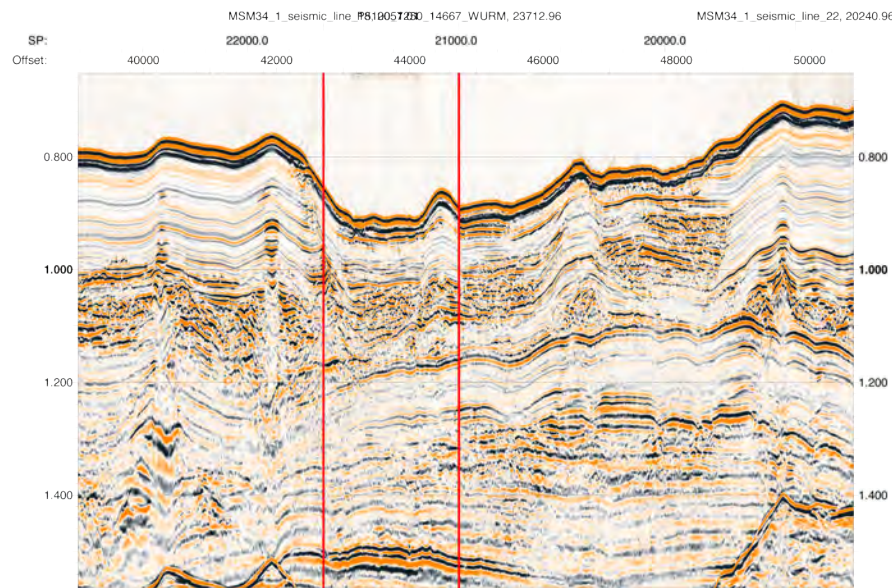


Figure 5.3.1.4: Zoom of the seismic profile MSM34-1_02. Chaotic reflection pattern between offsets 42000 to 46000 and 47000 to 49000 outline the bottom limits of ancient channel systems.

5.3.1.1 Semblance velocity analysis

Sudipta Sarkar, Orhan Atkin, Mert Küçük, Özkan Özel

We used ProMAX™ to carry out semblance velocity analyses and deduce root mean square (RMS) velocities for normal move-out (NMO) correction (fig. 5.3.1.1). For this we made common mid-point (CMP) supergathers using 9 adjacent CMPs and then computed semblance. We picked velocities for which the hyperbolic reflections were best flattened in the CMP-offset display. Once the RMS velocities were computed we used the velocity table to flatten (NMO correction) the reflections.

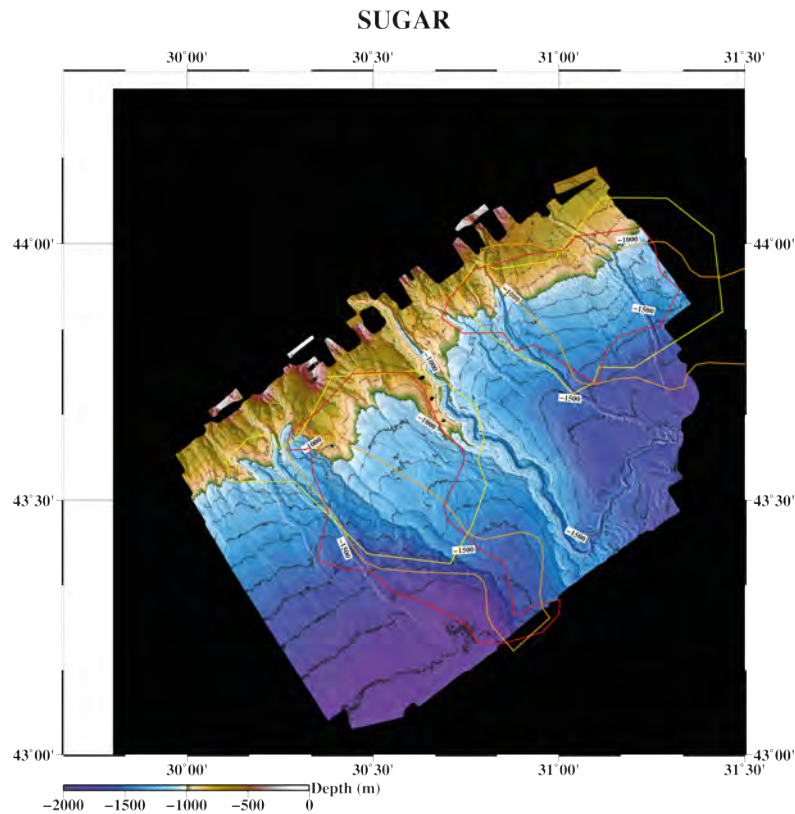


Figure 5.3.1.5: Bathymetric map of the MSM34 working area. Polygons outline the BSR extend mapped from MSM34 2D seismic data (red), published by [Popescu et al., 2006] (orange) and mapped by [Baristeas, 2006] (yellow).

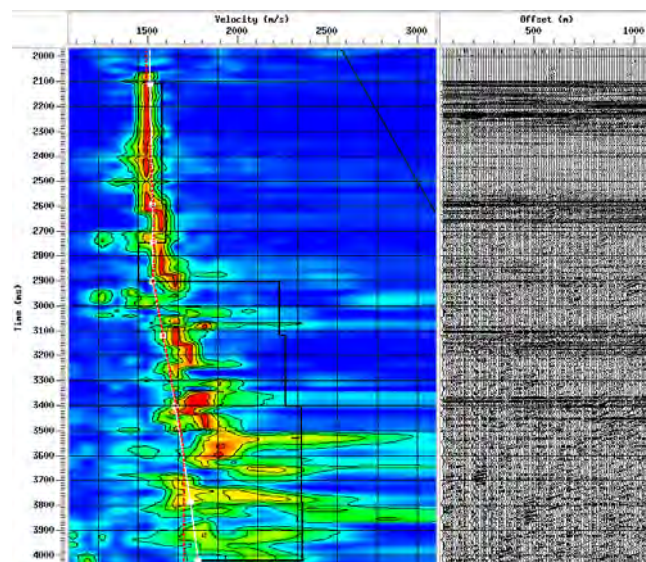


Figure 5.3.1.1. Semblance velocity panel (left) showing the picks (white points) for which the hyperbolic reflections were best flattened (image on the right). Interval velocity profile (black curve on left image) following Dix's equation was computed from the stacking velocity that was picked on the semblance panel.

5.3.1.2 Stacking and post stack migration

We stacked the NMO corrected CMP gathers and produced a final stacked image. An interval velocity model (Figure 5.3.1.2) was generated from RMS velocities and was finally

used to carry out post-stack Stolt migration. An example of a migrated profile is shown in Figure 5.3.1.3. This profile was finally loaded into kingdom for a general comparison with the brute stacked data. The velocity model from this analysis can be further used as an initial input model to prestack time migration processing.

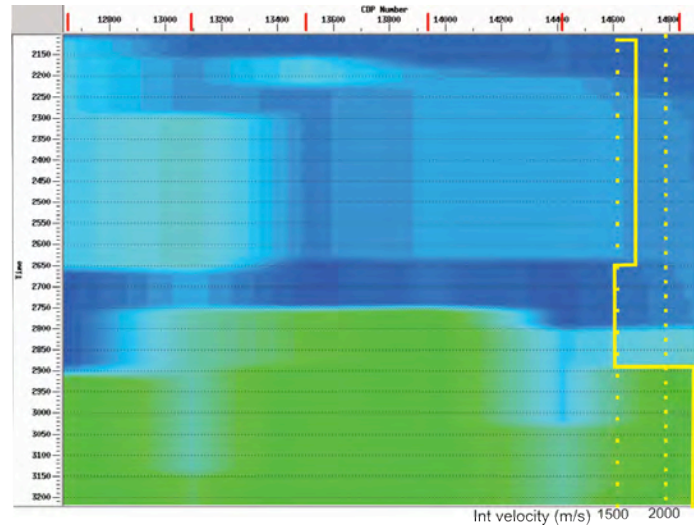


Figure 5.3.1.2. Interval velocity profile generated from stacking velocities for the seismic section shown in Figure 5.3.1.3.

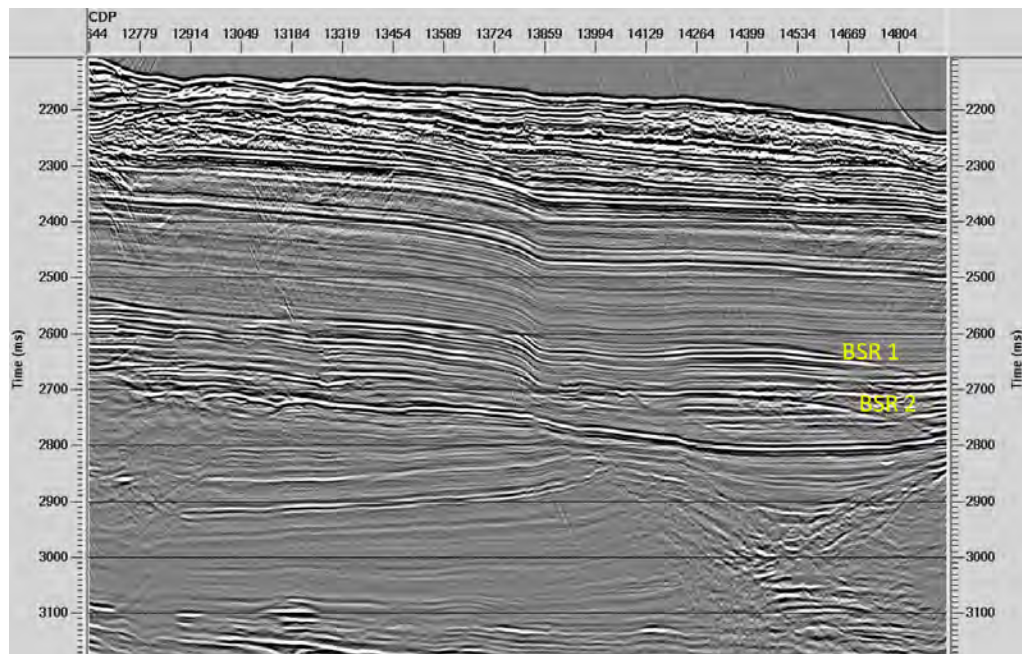


Figure 5.3.1.3. Post stack Stolt migration result of a seismic profile showing multiple BSRs. The velocity model for this profile is shown in Figure 5.3.1.2.

5.3.2 High resolution 2D seismic

Timo Zander, Jörg Bialas, Stephanie Koch

The first set of high resolution 2D seismic lines was acquired across an ancient channel-levee system of the Danube paleo-fan (Fig. 5.1). Seismic line P1107 is shown in fig 5.3.2.1.

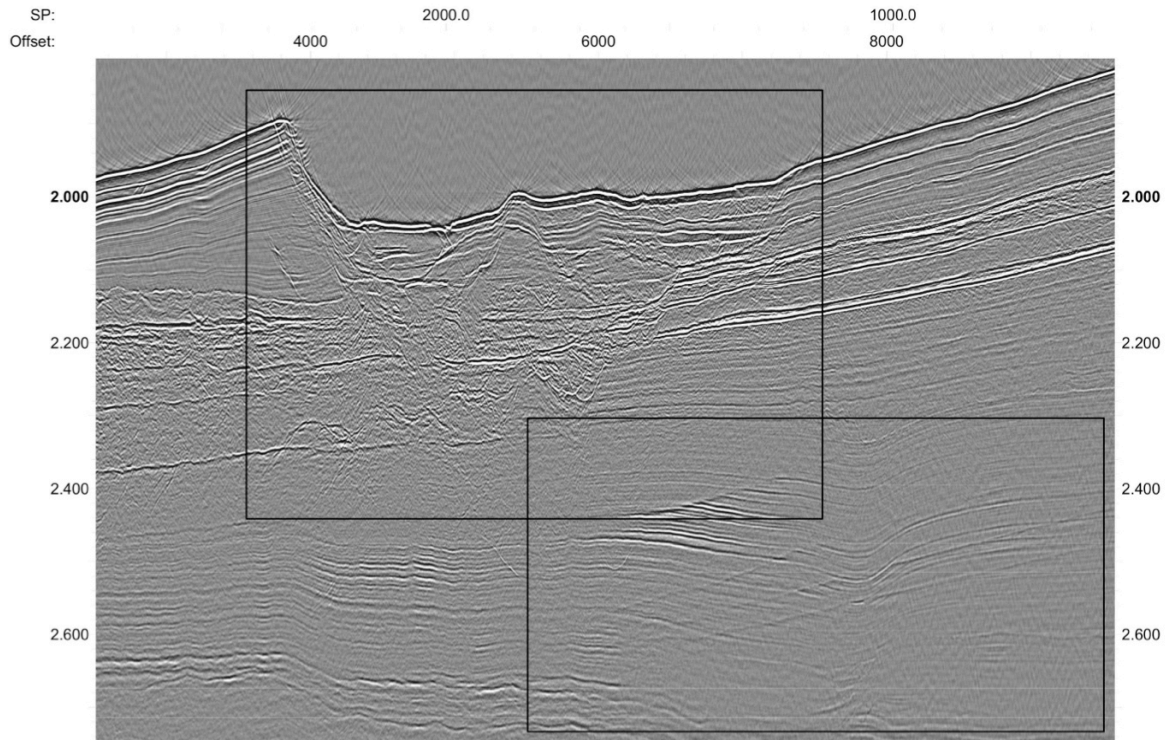


Figure 5.3.2.1: High resolution 2D seismic profile P1107 across a buried channel levee system in working area 1

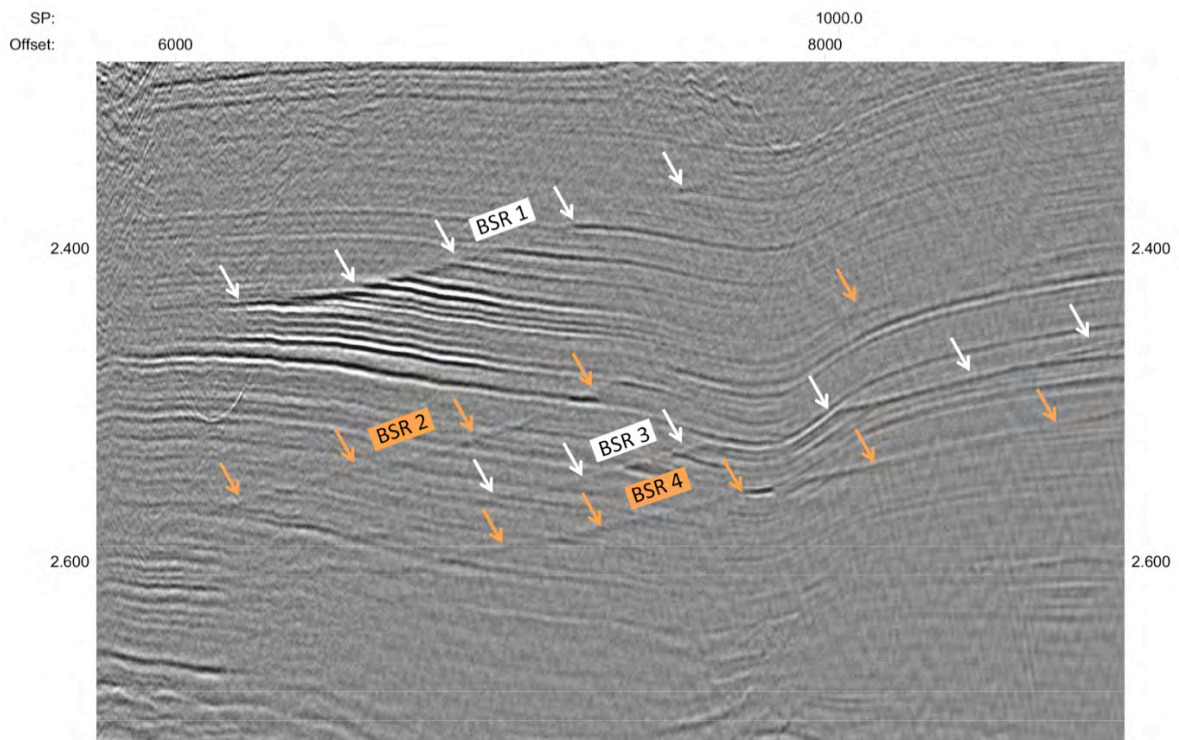


Figure 5.3.2.2: Zoom of profile P1107 indicating the multiple BSR event in working area 1

In a depth of about 200 ms TWT below the seafloor on the eastern levee of the channel, a distinct BSR can be identified (BSR 1, fig. 5.3.2.2). It shows a reversed polarity, mimics the seafloor and thus crosscuts strata. Towards the axis of the channel, the BSR signature decreases and fades out, but also shows increased amplitudes in the underlying well-stratified

sediments indicating a high gas-reservoir potential. The free gas might be trapped below the BGHSZ. Furthermore, up to three additional BSRs could be detected in the seismic data, each with a slightly varying dip (fig. 5.3.2.2). The observation of multiple BSRs agrees with the observations of Popescu et al. (2006).

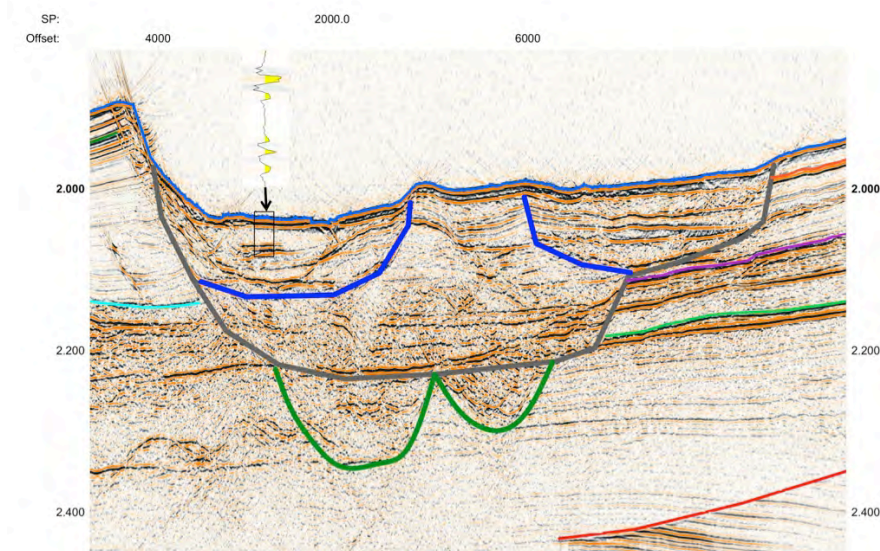


Figure 5.3.2.3: Zoom of profile P1107 indicating the variability in channel levee systems in working area 1

The seismic line P1107 also reveals the complexity of the channel-levee system (fig. 5.3.2.3). Channel signatures can be identified up to 350 ms subseafloor depth. Only one channel was active at a time, with the most recent active channel in this area on top (west, highlighted dark blue in fig. 5.3.2.3) neighboring and overlying older channel pathways (gray, dark green in fig. 5.3.2.3). The channel sediments are expected to consist of varying coarse grained sand beds depending of the history of channel activity. Several HARs (high amplitude reflections) can be identified in the channel axes, often of reversed polarity as highlighted in (fig. 5.3.2.3).

The levees to both sides of the channel system are well stratified, but show variations in amplitudes. Some strong reflectors (orange, pink, light green, turquoise in fig. 5.3.2.3) are interpreted as facies changes.

BSR 1 is marked red in fig. 5.3.2.3 and is characterized by crosscutting the strata, marking the upper boundary of a package of high amplitude reflections in the well-stratified reflectors below. Therefore, the coarse grained channel sediments in this area are interpreted as a reservoir facies of high gas-hydrate potential.

The BSR could be mapped in two areas by picking the BSR horizon on the dense grid of 2D seismic lines which were acquired during MSM34-1. After the picking, two separated BSR areas were identified, and a gridding algorithm interpolated the picks to a 3D horizon (fig. 5.3.2.4).

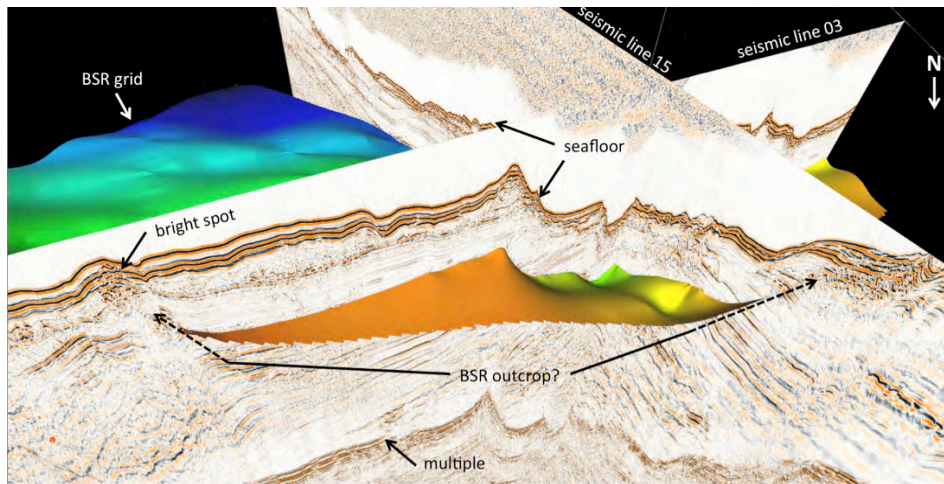


Figure 5.3.2.4: 3D perspective view of BSR1 interpreted from regional seismic 2D profiles

The eastern area shows a potential outcropping of the BSR from deep towards shallow water depths of about 700 m, which marks the upper boundary of the GHSZ in the Black Sea. Increased amplitudes below the BSR in seismic data as well as disturbed reflections and bright spots close to the seafloor indicate high gas content that migrates along the BSR towards shallower depths. The secondary low frequency SLF PARASOUND data show acoustic blanking in about 30 m depth below the seafloor that might be attributed to shallow gas at the projected BSR outcrop (fig. 5.3.2.5)

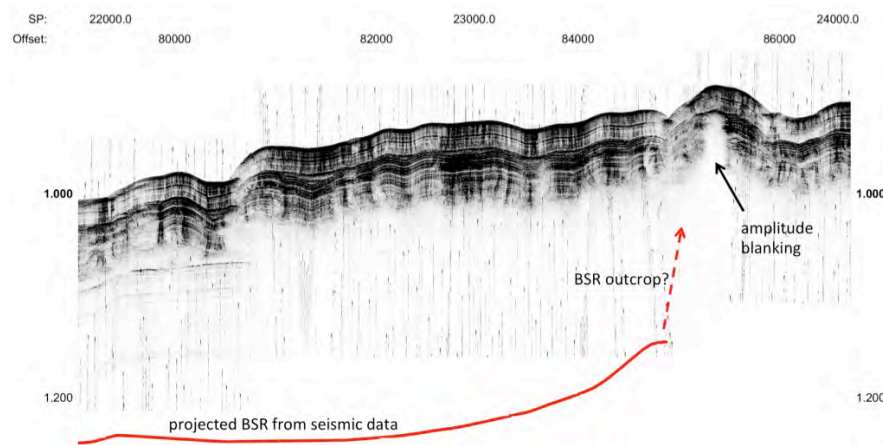


Figure 5.3.2.5: Parasound image coincident with seismic profile MSM34-1 / 15 indicating a possible gas accumulation above the upward bending and termination of the BSR

A comparison of the seismic line 15 acquired during MSM34-1 with the 1 km SEISLAB streamer section and the seismic line p4103 acquired during MSM34-2 with the 2D P-Cable is shown in fig. 5.3.2.5. Both lines are almost identical in direction with a small parallel offset of about 90 meters. Deeper reflections are much better resolved on long streamer data allowing more channels to be stacked.

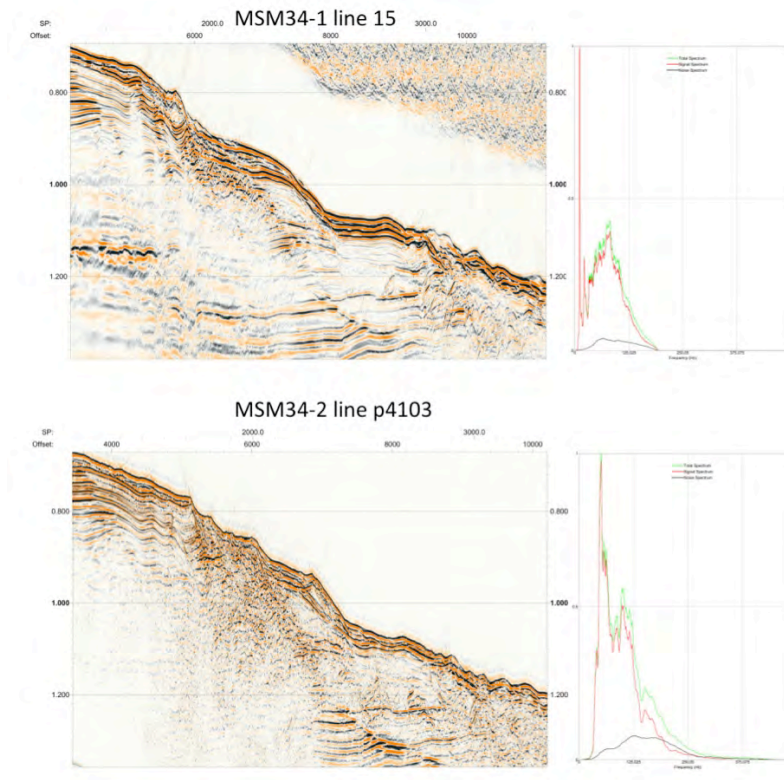


Figure 5.3.2.6: Comparison of coincident 2D seismic profiles MSM34-1 / 15 and MSM34-2 P4103

5.3.3 3D P-Cable Seismic

Jörg Bialas, Stephanie Koch, Torge Matthiessen, Gero Wetzel, Orhan Atkin, Felix Gross, Mert Küçük, Sudipta Srakar, Özkan Özel

5.3.3.1 P-Cable area 1

As outlined in figure 5.1 an area of about 8 km * 6 km was chosen for a first high resolution 3D P-Cable survey.

Restricted to 14 nodes in a first deployment the array could be widened to 15 nodes in the subsequent deployments. The setup of the streamer array is listed in appendix 11.3.3 for configurations P2xxx. Source signals were generated by a 45 cinch / 45 cinch GI airgun at 3 sec shot interval. During three days of profiling 15 OBS were recording the airgun shots as well.

QC test during the time of recording confirmed data quality and navigation information storage for later post processing of the data volume.

5.3.3.2 P-Cable area 2

The second work area for the high resolution 3D seismic studies was chosen above an unusual upward bending of the BSR (chapter 5.3.1). The 4 km * 4 km wide area of the 3D multichannel seismic survey covers a failed part of the slope. Water depth in this area increases from about 600 m to 900 m, including the top of the hydrate stability at about 650 m water depth.

Again the P-Cable array could be deployed with 15 nodes (app. 11.3.3 P3xxx). Source signals were generated by a 45 cinch / 45 cinch GI airgun at 3 sec shot interval. The entire volume was acquired without any interruption. 12 OBS were deployed for a complete record of the 3D airgun shots.

QC test during the time of recording confirmed data quality and navigation information storage for later post processing of the data volume.

5.3.4 OBS data and results

Anke Dannowski, Isabel Sauermilch, Henning Schröder

Ocean Bottom Seismometer (OBS) were deployed in the two main research areas of the cruise MSM34-2. The main target of the deployment was to provide velocity information for 2D and 3D seismic processing and to get a second imaging possibility apart from the streamer and P-Cable seismics. Moreover wide angle OBS observation provide the possibility to apply AVO analyses in order to investigate physical parameters. In case of PS conversion the horizontal components of the OBS can be used for development of a shear wave velocity model.

5.3.4.1 Work area 1

A total of 15 OBS were deployed in three lines with 5 instruments per line (Fig. 5.2). The water depth varied between 1420 m and 1515 m. The instruments were deployed in the evening of December 30th 2013. Afterwards the streamer was deployed and eight profiles (P1101 - P1108) of 2D seismic, crossing the OBS were shot during the following 20 hrs. The shot interval was 5 s with an GI-airgun volume of 45 in³/ 45 in³.

After one day the streamer was replaced by the P-Cable system, while the OBS remained on the seafloor. The shot interval was reduced to 3 s the airgun volume remained at 45 in³/ 45 in³. During the night from January 4th to 5th 2014 while the P-cable system was on deck for maintenance all OBS were recovered. Thus, the instruments did not record all the shots from the 3D P-cable cube. However shots were recorded from all azimuths around each station. In general the 15 instruments worked continuously well while three geophone components on two different stations failed during recording only. All stations can be used to generate a high resolution velocity model as further input for the 3D and 2D processing and interpretation. A receiver gather example from OBS-1014 along line P1107 is shown in Fig. 5.3.4.1. It represents the overall data quality.

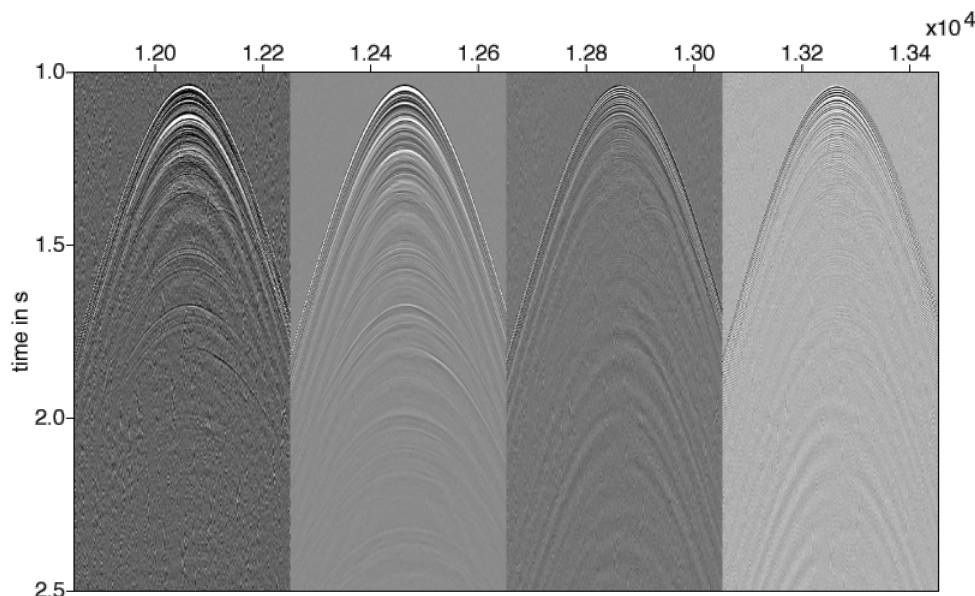


Fig. 5.3.4.1: Receiver gather of OBS-1014 along profile P1107

From left to right: hydrophone, vertical, H1, H2 component

OBS and 2D seismic data can directly be compared which is illustrated in Fig. 5.3.4.2.

using OBS-1004 along line P1107. By this method it is easier to follow the horizons from instrument to instrument to pick travel times for the further modelling procedure. A first rough 2D model using apparent velocities (assuming non dipping topography) shows very low seismic P-wave velocities for the uppermost portion of the sedimentary layers. The few first 10th of meters have velocities of about 1600 m/s.

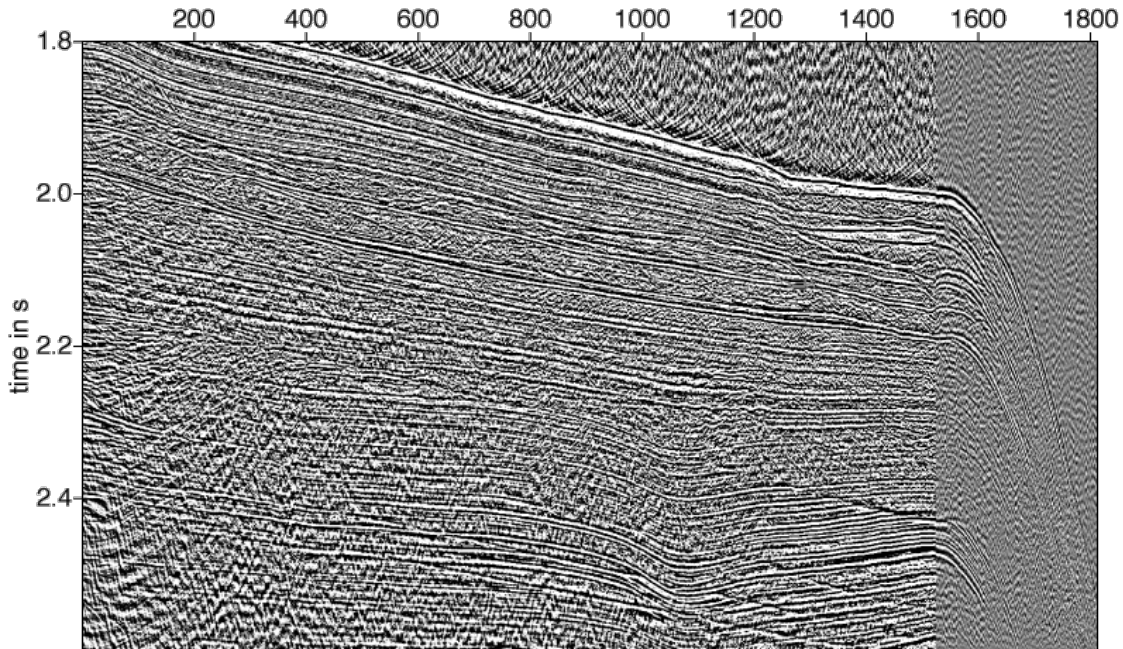


Fig. 5.3.4.2: Simultaneous plot of 2D MCS data of profile P1107 (shots 0 – 1500) and corresponding records of OBS-1004 (shots 1501 – 1800)

Although the seafloor is very muddy and loose, the geophones, separated from the system carrier, provided a good coupling to the seafloor resulting in good quality data. However, a high frequency ringing could be observed with frequencies higher than 150 Hz (fig. 5.3.4.3).

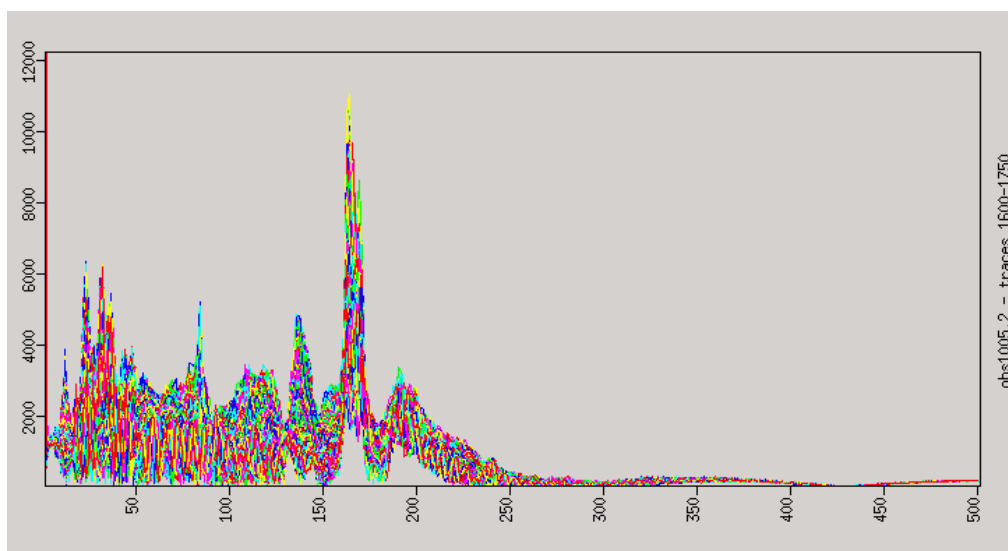


Fig. 5.3.4.3 Frequency spectra of OBS-1005 with a noticeable frequency peak at 160 Hz

Figures 5.3.4.4.a-c display OBS-1005 without filtering and with two different filter settings, respectively. The ringing might be caused due to the soft seafloor in the observation

area since it did not appear so strong during deployments with seafloor having higher P-wave velocities.

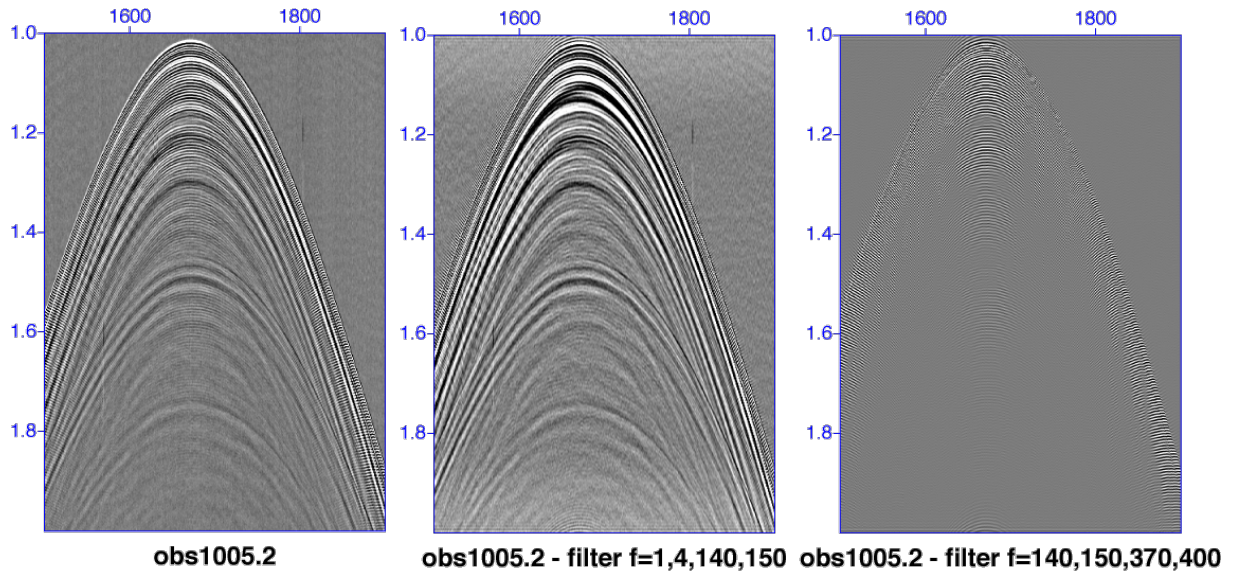


Fig. 5.3.4.4 from left to right vertical component of OBS-3005 a) raw data , b) bandpass filtered excluding the 160 Hz peak, c) remaining high frequency energy

5.3.4.2 Work area 2

In the second working area 12 instruments were again deployed in three lines in the centre of the 3D seismic cube (fig. 5.3). In the evening of January 09 2014 they were deployed and remained on the seafloor until January 14 2014. This area was shallower than area 1. The deployment depth for the OBS ranged between 600 and 860 m. The 12 OBS recorded all the shots from the second 3D cube of the P-cable acquisition. Additionally, they recorded the airgun shots of the following 2D seismic lines that were acquired in the night from January 13 to 14 2014. Some of the instruments went low on battery and may not record all 2D seismic lines, but still kept their synchronisation. The data quality of the OBS in the second area is again very high and this time each instrument delivered data for every single component without any failure. A shot gather example of OBS-3008 is shown in (fig. 5.3.4.5).

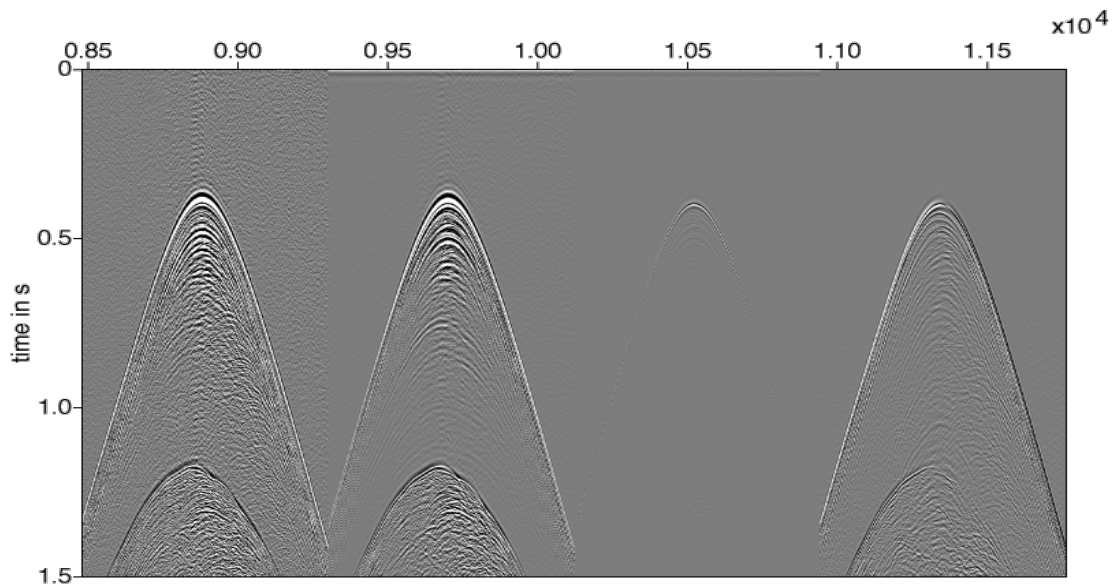


Fig. 5.3.4.5: Receiver gather of OBS-3008

From left to right: hydrophone, vertical, H1, H2 component

Figure 5.3.4.6 displays the OBS receiver gather compensated for direct arrival of station OBS-3001 during relocation processing of the OBS. All stations showed a similar difference between deployment position and recording position, thus, the OBS drifted while sinking to the seafloor in the direction of sea currents.

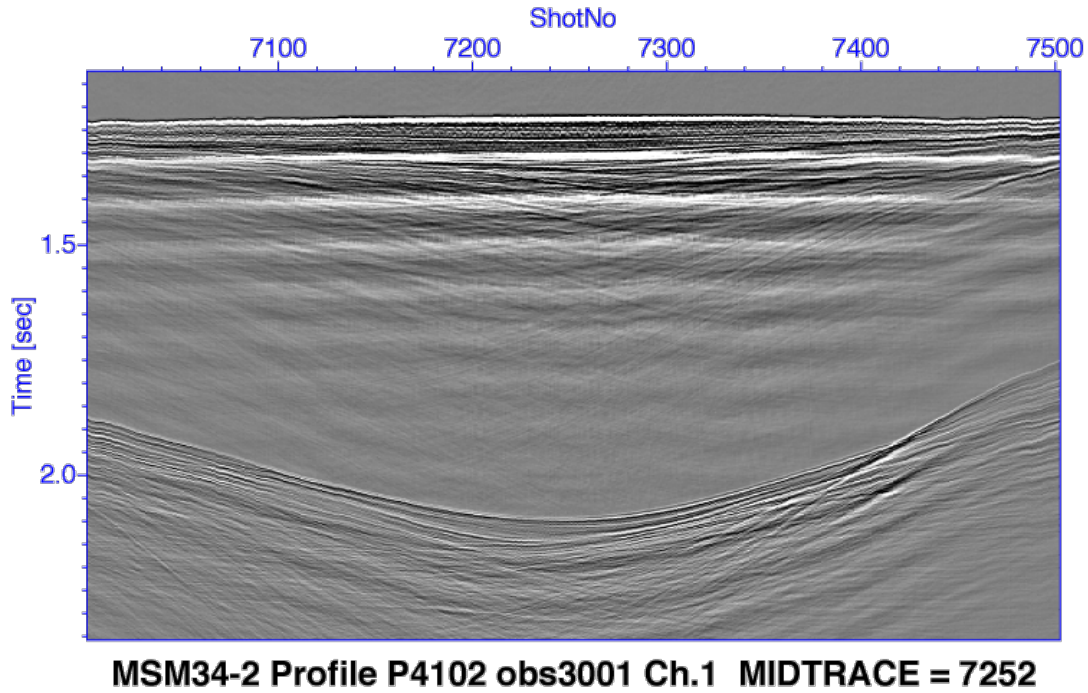


Fig. 5.3.4.6: Receiver gather of OBS-3001 displayed with direct arrival compensation for verification during relocation processing

A comparison of OBS-3005 with the MCS data from line P4103 can be seen in Figure 5.3.4.7. Major phases seen in the MCS data can be resolved in both datasets down to the first multiple. This comparison helps to correlate the phases between the OBS, a crucial step for further data interpretation and the generation of a background velocity field for the MCS data and the processing of the 3D P-cable cube.

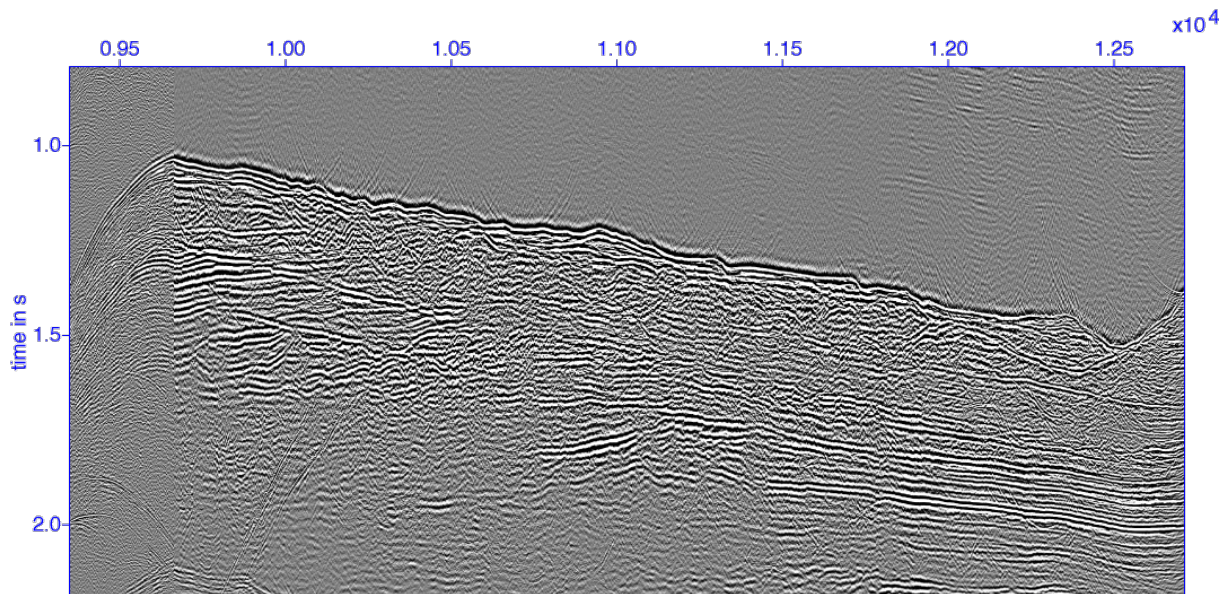


Fig. 5.3.4.7: Simultaneous plot of 2D MCS data of profile P4103 (shots 9800 – 12500) and corresponding records of OBS-3005 (shots 9400 – 9800)

5.4 Geochemistry

M. Haeckel¹, T. Pape², M. Dibbern¹, N. Bigalke¹, D. Schroller¹ (1GEOMAR, 2MARUM)

5.4.1 Introduction

The geochemical analyses of the porewaters and sediments of the Paleo Danube deltas in the Black Sea aim at quantifying methane fluxes and turnover rates of associated biogeochemical processes as well as determining the sources of gases and fluids migrating in the subsurface and forming gas hydrate accumulations in the area. Therefore, a comprehensive geochemical dataset has been collected on this cruise.

Onboard, the collected samples were analysed for their content of NH_4^+ , PO_4^{3-} , SiO_4^{4-} , H_2S , total alkalinity, and dissolved methane. In addition, sub-samples were taken for further shore-based analyses: methane $\delta^{13}\text{C}$ and δD isotope ratios, DIC content and its $\delta^{13}\text{C}$ isotope ratio, dissolved metal cations, SO_4^{2-} , Br^- , Cl^- , and I^- concentrations, isotopic ratios of Sr, Cl, Li, H, and O in the porewater as well as porosity, carbonate, POC, PON, and sulfur content of the solid phase (Table 5.4.1). The sampling locations were chosen, where gas and gas hydrate accumulations in the deeper subsurface are anticipated from the 2-D seismic information collected on the first leg (Fig. 5.1 & 5.2).

5.4.2 Materials and Methods

5.4.2.1 Sediment and porewater sampling

Surface and subsurface sediment samples were retrieved using a mini-corer (MIC) and a gravity corer (GC). The sediments were extruded out of the MIC plastic liners with a piston and cut into 0.5 to 2 cm thick slices, whereas GC cores were cut in half and 3-5 cm thick slices were taken in approximately 20-40 cm intervals. Subsequently, the porewater was extracted in the ship's cold room (4 °C) using a low pressure-squeezer (argon at 3-5 bar, sometimes up to 7 bar). While squeezing, the porewater was filtered through 0.2 μm cellulose acetate Whatman filters and collected in recipient vessels.

About 5 ml of wet sediment of each sediment slice was collected for porosity, carbonate and CNS element analyses at home. Aliquots of the extracted porewater were sub-sampled for various onboard and further shore-based analyses (Table 5.4.1). Subsamples for ICP-AES analysis were acidified with 30 μl of conc. suprapure HNO_3 per 3 ml of porewater sample (i.e. $\text{pH} < 1$) and subsamples (~1.9 ml) for $\delta^{13}\text{C}$ and DIC were treated with 10 μl of HgCl_2 to inhibit further microbial degradation. All samples for home-based analyses were stored refrigerated. In total, 364 samples from 17 cores were collected for porewater analysis (Table 5.4.1).

For analysis of light hydrocarbons dissolved in porewater in MIC and GC cores, 3 ml of wet sediment was subsampled with cut-off syringes and transferred into 20-ml glass vials prefilled with 5 ml of a 1M NaOH solution for onboard headspace methane and higher hydrocarbon analyses. The vials were closed with butyl rubber stoppers and capped, thoroughly shaken and stored at 4 °C for at least 12 h before analysing. From the 17 cores retrieved during the cruise a total of 520 sediment samples was collected and analysed during the cruise (Table 5.4.1).

5.4.2.2 Porewater analyses

Analyses for the nutrients NH_4^+ , PO_4^{3-} , SiO_4^{4-} as well as H_2S were completed onboard using a Hitachi UV/VIS spectrophotometer. The respective chemical analytics followed standard procedures (Grasshoff et al., 1999), i.e. ammonium was measured as indophenol blue, phosphate and silicate as molybdenum blue, and sulfide as methylene blue. Since high sulfide contents ($> 1 \text{ mM}$) interfere with the reactions of NH_4^+ , PO_4^{3-} , and SiO_4^{4-} , the respective sub-samples were bubbled with argon to strip any H_2S prior to the analysis.

The total alkalinity of the porewater was determined by titration with 0.02 N HCl using a mixture of methyl red and methylene blue as indicator. The titration vessel was bubbled with argon to strip any CO₂ and H₂S produced during the titration. The IAPSO seawater standard was used for calibration.

The analytical precision and accuracy of each method are given in Table 6.3.2.

5.4.2.3 Headspace gas analyses

Gases (methane and higher hydrocarbons) dissolved in the porewater were analyzed onboard using an Agilent Technologies 6890N gas chromatograph equipped with a capillary column and a flame ionization detector. Calibrations and performance checks of the analytical system were conducted regularly using commercial pure methane standards and hydrocarbon mixtures. The coefficient of variation determined for the analytical procedure was lower than 2%.

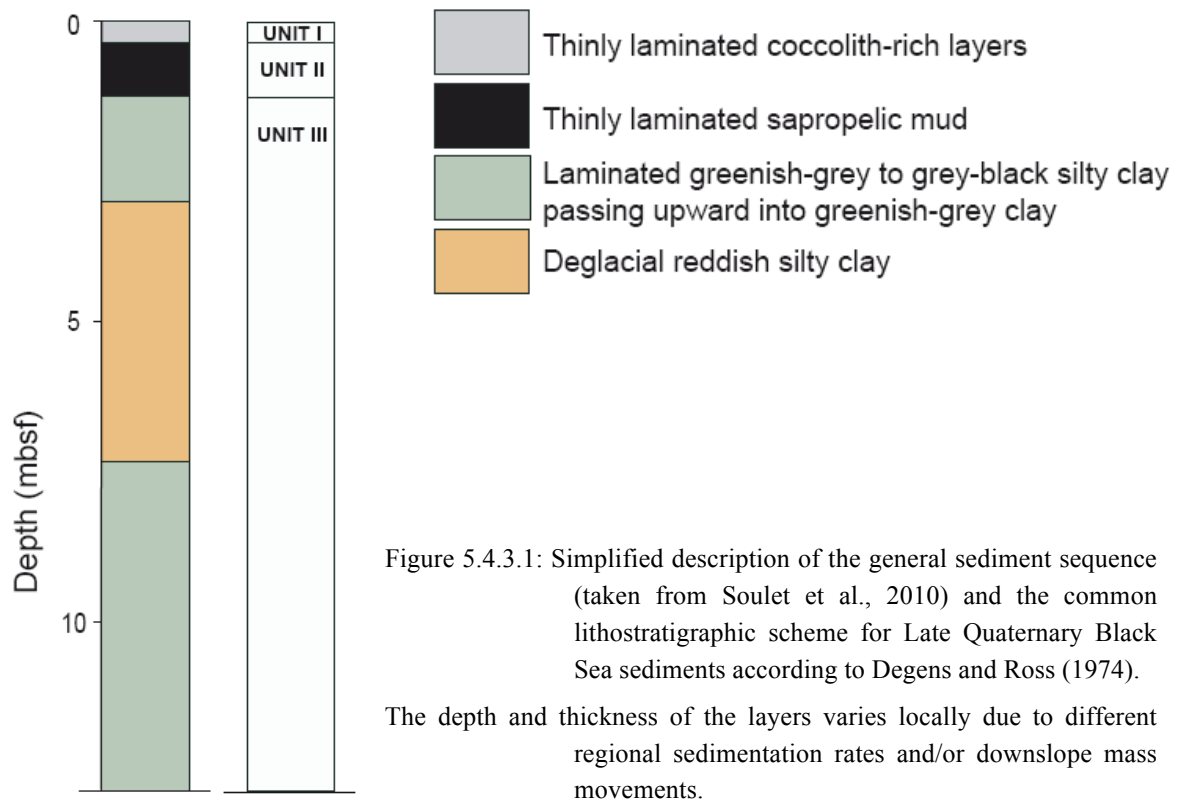
Table 5.4.2: Analytical methods of onboard geochemical analyses.

Parameter	Method	Detection limit	Analytical precision/accuracy
H ₂ S	Photometer	3 µmol/l	3 %
NH ₄ ⁺	Photometer	5 µmol/l	5 %
PO ₄ ³⁻	Photometer	1 µmol/l	5 %
SiO ₄ ⁴⁻	Photometer	5 µmol/l	2 %
Alkalinity	Titration	0.1 meq/l	2 %
CH ₄	Gas chromatograph	0.1 ppmV	2 %

5.4.3 Results

The geological stratigraphy and geochemical processes in Black Sea sediments as well as their associated porewater profiles are well-known from previous cruises, e.g. TTR-15, M72/3, M84/2, SPUX. Observed variations in stratigraphy, geochemical gradients and solid phase compositions reflect the local setting, which may be influenced by turbidites and mass wasting at the slopes and upward migrating methane gas along faults and fractures. Hence, the sediment sequences and porewater profiles observed in cores retrieved during MSM34/2 are discussed against the general Black Sea lithology and geochemistry of the upper few meters below seafloor, which are recapitulated here.

A complete photo documentation of individual cores retrieved with GC and MIC is given in Appendix 11.xx.



5.4.3.1 Late Glacial to Holocene Black Sea Sediment Lithology

Typical Black Sea sediments comprise of finely laminated coccolith ooze (Unit 1; Fig. 5.4.3.1) at the top, followed by a finely laminated sapropel (Unit 2; Fig. 5.4.3.1) with distinct light laminations rich in needle-shaped authigenic aragonite towards the base. Both, Unit 1 and 2, represent the current marine stage of the Black Sea. Further downcore grayish mud of lacustrine origin follows (Fig. 5.4.3.1), representing the limnic stage of the Black Sea during the last glacial. During this time, the global sea level fell below the sill depth of the Bosphorus (~35 m; Bahr et al., 2008), leading to a disconnection of the Black Sea from the Sea of Marmara and the Mediterranean Sea. The reconnection of the Black Sea with the Sea of

Marmara occurred at around 9.4 ka (Major et al., 2006). The inflow of saline marine water caused the formation of the present stratification of the Black Sea water column and the manifestation of anoxic conditions below ~150 m water depth. These anoxic conditions lead to the accumulation of the organic-rich sediments of Units 1 and 2. The base of the sapropel (Unit 2) has been dated to 7.5 ka by Jones and Gagnon (1994), an age that has later been refined to 8.0 ka (Lamy et al., 2006). The first prolonged invasion of coccolithophorides occurred at 2.7 ka (Jones and Gagnon, 1994) marking the base of Unit 1. An often recurring feature of Unit 3 is a distinct blackish-dotted/-banded interval (in 250-350 cm) rich in amorphous Fe-sulfides (Neretin et al., 2004), termed “hydrotroilite” (Limonov et al., 1994). These black horizons are related to the anaerobic oxidation of methane (AOM, see geochemistry further below) that produces hydrogen sulfide as one reaction product and which is subsequently precipitated below the AOM reaction zone. The black color is lost within a few hours if the core is opened, since these Fe-sulfides oxidize rapidly. Seep-influenced cores often show disturbed bedding and a “moussy” consistency due to degassing during core retrieval (see e.g., 66-2 GC7), making exact assignment of unit boundaries difficult.

Table 5.4.1: List of sampled cores and collected sub-samples.

Station Device	Area	Latitude (N)	Longitude (E)	Water depth / m	PW	Poros / CNS	IC	ICP-AES / ^{87/86} Sr	CH ₄ / $\delta^{13}\text{C}_{\text{CH}_4}$	DIC / $\delta^{13}\text{C}_{\text{DIC}}$	Iso	Length of core / cm	No. of PW samples	No. of gas samples
3-2 MIC1	IFREMER Piezometer	43°48.353'	30°24.792'	420	X	X	X	X		X	X	50	29	20
3-3 GC1	IFREMER Piezometer	43°48.354'	30°24.786'	420	X	X	X	X	X	X	X	500	22	24
22-1 GC2	SW channel-levee multiple BSR, seismic 8b	43°25.679'	30°26.055'	1550	X	X	X	X	X	X	X	485	17	28
26-1 MIC2	SW channel-levee multiple BSR, channel	43°27.237'	30°24.470'	1498	X	X	X	X		X	X	51	24	30
27-1 MIC3	SW channel-levee multiple BSR, levee	43°28.099'	30°26.040'	1465	X	X	X	X		X	X	40	21	28
39-1 GC3	SW channel-levee multiple BSR, channel	43°27.245'	30°24.472'	1500	X	X	X	X	X	X	X	485	17	32
40-1 GC4	SW channel-levee multiple BSR, levee	43°28.093'	30°26.036'	1470	X	X	X	X	X	X	X	484	20	35
42-1 MIC4	SW channel-levee multiple BSR, seismic 8b	43°25.675'	30°26.055'	1550	X	X	X	X		X	X	42	21	38
43-1 GC5	NE channel-levee, upbending BSR, slump	43°57.443'	30°46.506'	674	X	X	X	X	X	X	X	484	19	33
43-2 MIC5	NE channel-levee, upbending BSR, slump	43°57.443'	30°46.508'	680	X	X	X	X		X	X	38	20	39
51-1 GC6	NE channel-levee, upbending BSR, slump	43°57.177'	30°46.272'	724	X	X	X	X	X	X	X	448	22	31
65-1 MIC6	NE channel-levee, upbending BSR, slump	43°57,177'	30°46,722'	726	X	X	X	X		X	X	41	22	38
66-1 MIC7	NE channel-levee, upbending BSR, slump	43°57,177'	30°46,530'	638	X	X	X	X		X	X	44	22	40
66-2 GC7	NE channel-levee, upbending BSR, slump	43°57,177'	30°46,529'	635	X	X	X	X	X	X	X*	500	21	30
74-1 MIC8	NE channel-levee, upbending BSR, slump	43°57,439'	30°46,513'	679	X	X	X	X		X	X	42	21	39
74-2 GC8	NE channel-levee, upbending BSR, slump	43°57,440'	30°46,512'	678	X	X	X	X	X	X	X	500	21	35
89-1 GC9	NE channel-levee, upbending BSR, channel	43°57.685'	30°47.750'	827	X	X	X	X	X	X	X	500	25	45

GC = gravity corer; MIC = mini-corer; PW = porewater analyses of TA, H₂S, NH₄, PO₄, SiO₄; IC = ion chromatography (SO₄, Br, Cl, I); ICP-AES = inductively-coupled atomic emission spectroscopy (for various dissolved cations); Iso = Isotope ratios of porewater O, H, Cl, Li; *no Li

2.1.1.1 General Black Sea Sediment Geochemistry

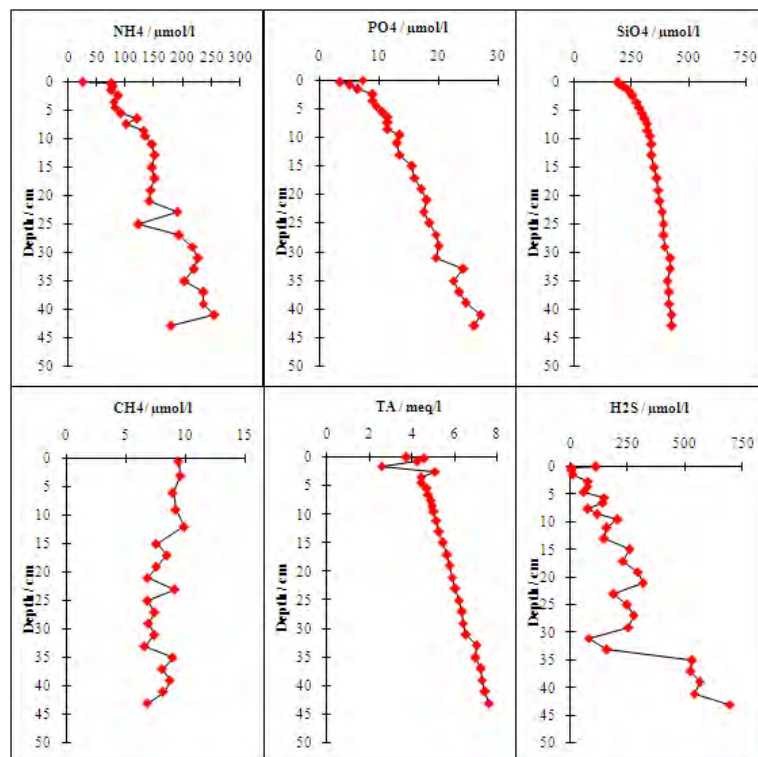
Background sediments in the Black Sea are those not influenced by gas (methane) and/or oil seepage or mud expulsion. Since these sediments are overlain by completely anoxic bottom water – in the Black Sea oxygen and nitrate are typically consumed within the upper ~150 m of the water column – sulfate reduction and methanogenesis are the dominant early diagenetic processes. In fact, the upward diffusing methane typically consumes the dissolved sulfate that is diffusing into the sediment within the upper 250-350 cm of the sediment. This anaerobic oxidation of methane (AOM) leads to an increase in total alkalinity and hydrogen sulfide. The produced hydrogen sulfide then reacts with dissolved iron in the porewater forming FeS that is readily recognized as black spots and layers in the sediment and often builds up a continuous zone of several decimeters to a meter in thickness (see ‘hydrotroilite’ discussion in the above lithology section). Similarly, dissolved phosphate is consumed by mineral formation with e.g., dissolved iron, roughly 100 cm below the depth of H₂S depletion. Dissolved ammonium and phosphate are released during the microbially mediated degradation of organic material in the sediment, which occurs primarily via sulfate reduction and methanogenesis. In contrast to phosphate, ammonium is not involved in any mineral formation or other reactions and hence continuously accumulates in the porewater leading to concentrations of 1-2 mM in the upper 5-6 m of the sediment. Likewise, concentrations of methane, one of the final products of organic carbon degradation, are also increasing below the depth of sulfate penetration. This can be witnessed on deck by a downcore increasing intensity of degassing of the sediment, since methane solubility drops drastically due to pressure reduction during core retrieval.

Another peculiarity of Black Sea porewaters is the linearly decreasing chloride concentration in the surface sediments. Chloride and other sea salt ions are still diffusing from the overlying, marine and thus, saline, water body into the salt-depleted lacustrine sediments from before 10,000 years ago. Minimum Cl concentrations of 25-30 mM are reached in 20-25 m sediment depth (Manheim and Schug, 1978; Soulet et al., 2010). This circumstance will be used to determine, how much surface sediment was lost during recovery and overpenetration of the GCs (see coring device appendix 11.xx). For overpenetrated cores, we, consequently, report sediment depths as ‘coring depth’, whereas if the sediment surface was recovered, i.e. with the MIC, we report actual sediment depths.

2.1.1.2 IFREMER piezometer site at shallow water depth

A mini-MUC and a GC core (3-2 MIC1 and 3-3 GC1) were retrieved at a shallow water site (~420 m), where the piezometer of IFREMER was deployed on the first leg (see chapter 5.6). The GC overpenetrated a lot and we currently estimate that the top ~150 cm were lost during recovery. The site is characterized by higher POC degradation at larger depth, i.e. below core penetration, as indicated by the NH₄ concentrations that increase linearly to almost 2.5 mM at 500 cm sediment depth (Fig. 5.4.3.2).

3-2 MIC1



3-3 GC1

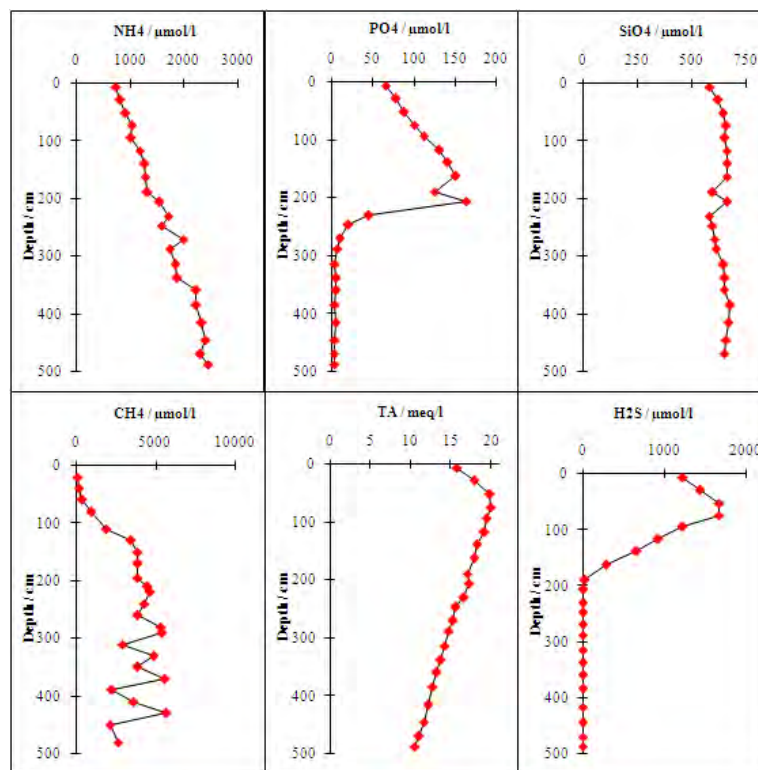
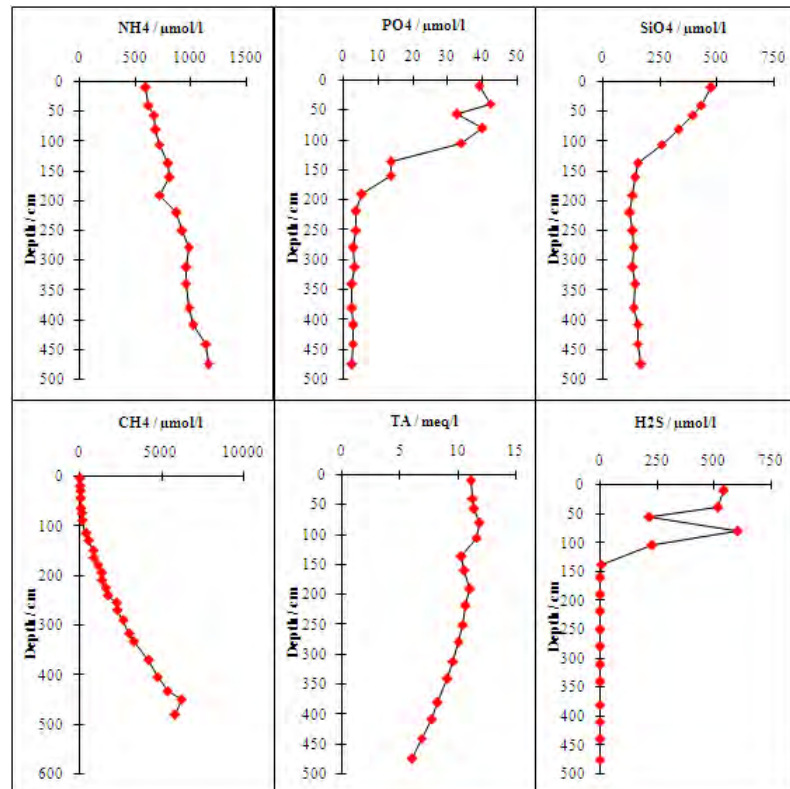


Figure 5.4.3.2: Measured concentrations of porewater constituents of 3-2 MIC1 (top) and 3-3 GC1 (bottom) at the 420-m piezometer location. Note the different concentration scales for MIC and GC. The sediment gap between MIC and GC is an estimated 150 cm.

The POC degradation rate is slightly higher than observed in other areas of the Black Sea (see previous cruise reports from TTR15, M72/3, and M84/2). The typical diffusively fueled AOM is observed with a reaction peak at ~75 cm coring depth, as indicated by a maximum total alkalinity (TA) value of ~20 meq/l and linearly decreasing values towards the sediment surface (see also MIC1) and towards the bottom of the core. H₂S peaks at a similar coring depth. A strong CH₄ concentration gradient occurred between ca. 40 and 150 cm coring depth.

39-1 GC3



40-1 GC4

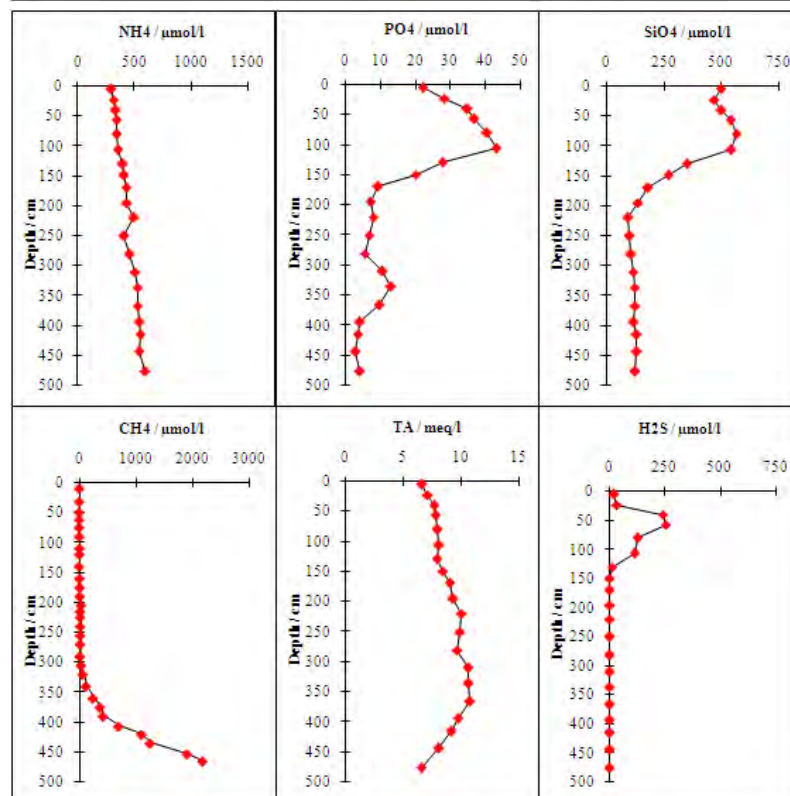


Figure 5.4.3.3: Measured concentrations of porewater constituents in the channel (39-1 GC3, top) and the levee (40-1 GC4, bottom).

5.4.3.4 SW channel-levee system / multiple BSRs

3 sites were sampled in the southwestern channel-levee system that exhibits multiple BSR reflections at depth and a strong seismic reflector within the shallowest channel-fill (see chapter 5.3). As indicated by TA values of less than 10-12 meq/l and broad peaks (Fig. 5.4.3.3), AOM appears to be less intensive than typical, i.e. lower methane flux from below.

In the channel (26-1-MIC2, 39-1 GC3) the upward methane flux and, hence, the AOM activity is slightly higher than at the levee site (27-1 MIC3, 40-1 GC4).

5.4.3.5 NE channel-levee system / upward bending BSR

In total 9 cores were sampled at the northeastern channel-levee system, where the 2-D seismic data (see chapter 5.3) indicated an upward bending BSR. At this site the limit of the gas hydrate stability is approached, i.e. at a water depth of 665 m. Fig. 5.4.3.4 shows the methane–seawater phase diagram for bottom water salinities of 22.3 and porewater salinities of ~3 in relevant sediment depths of 25–300 m and regional geothermal gradients.

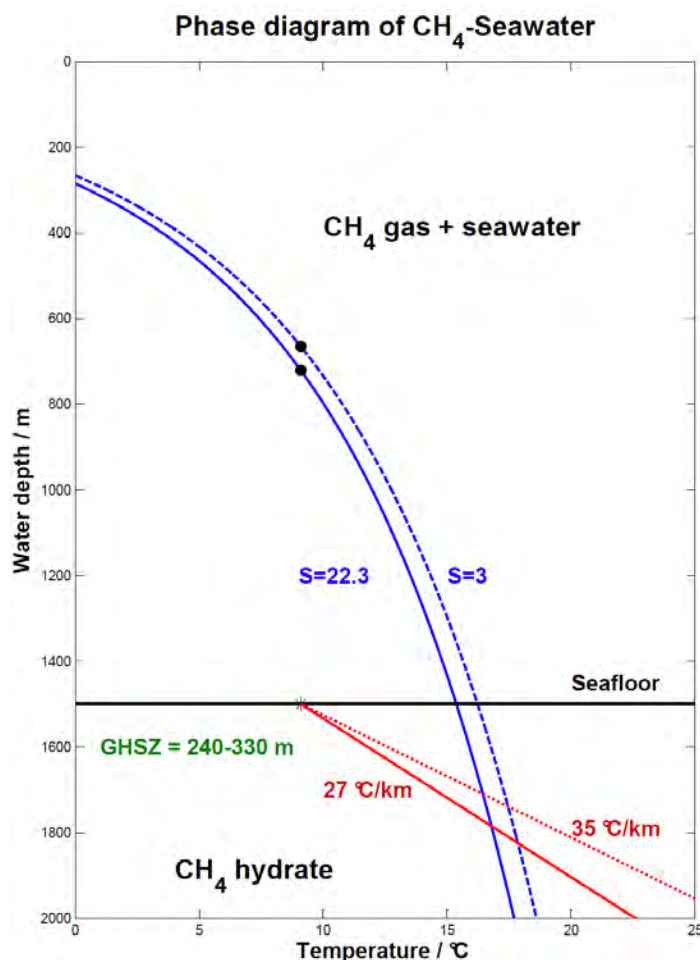


Figure 5.4.3.4: Gas hydrate stability for pure s-I methane hydrate for porewater (S=3; in 25–300 m sediment depth) and bottom water (S=22.3) salinities.

The minimum water depths, where gas hydrates are stable under ambient bottom water temperatures of 9.1 °C are indicated by black dots: 665 m for S=22.3 and 721 m for S=3.

For the regional observed geothermal gradients of 27–35 °C/km (see chapter 6.4) a gas hydrate stability zone (GHSZ) of 240–330 m (relevant salinity is S=3) results.

The upward bending BSR coincided with a sediment slump at the seafloor, located above the levee west of the channel. We took sediment cores at the eastern flank of the slide and its eastern head wall, where gas seepage was detected with the Parasound system. As expected, the methane flux and respectively the AOM rate are highest at the gas seep (66-1 MIC7; Fig. 5.4.3.5) with maximum TA and H₂S values at ~30 cm sediment depth and a strong methane increase in the same depth.

Generally, the methane flux seems to correlate with the observed geothermal gradient (see chapter 5.5), respectively heat flow, i.e. the higher the heat flow, the more intense is the upward methane flux and corresponding AOM. The geothermal gradient and the methane flux appear to be lowest, exactly where the water depth matches the upper limit of the GHSZ (around 670 m). This may potentially indicate that here, gas hydrates are dissociating and thereby cool down the heat flow. The highest heat flow and correspondingly a high methane flux were observed in the channel itself (89-1 GC9; Fig. 5.4.3.5).

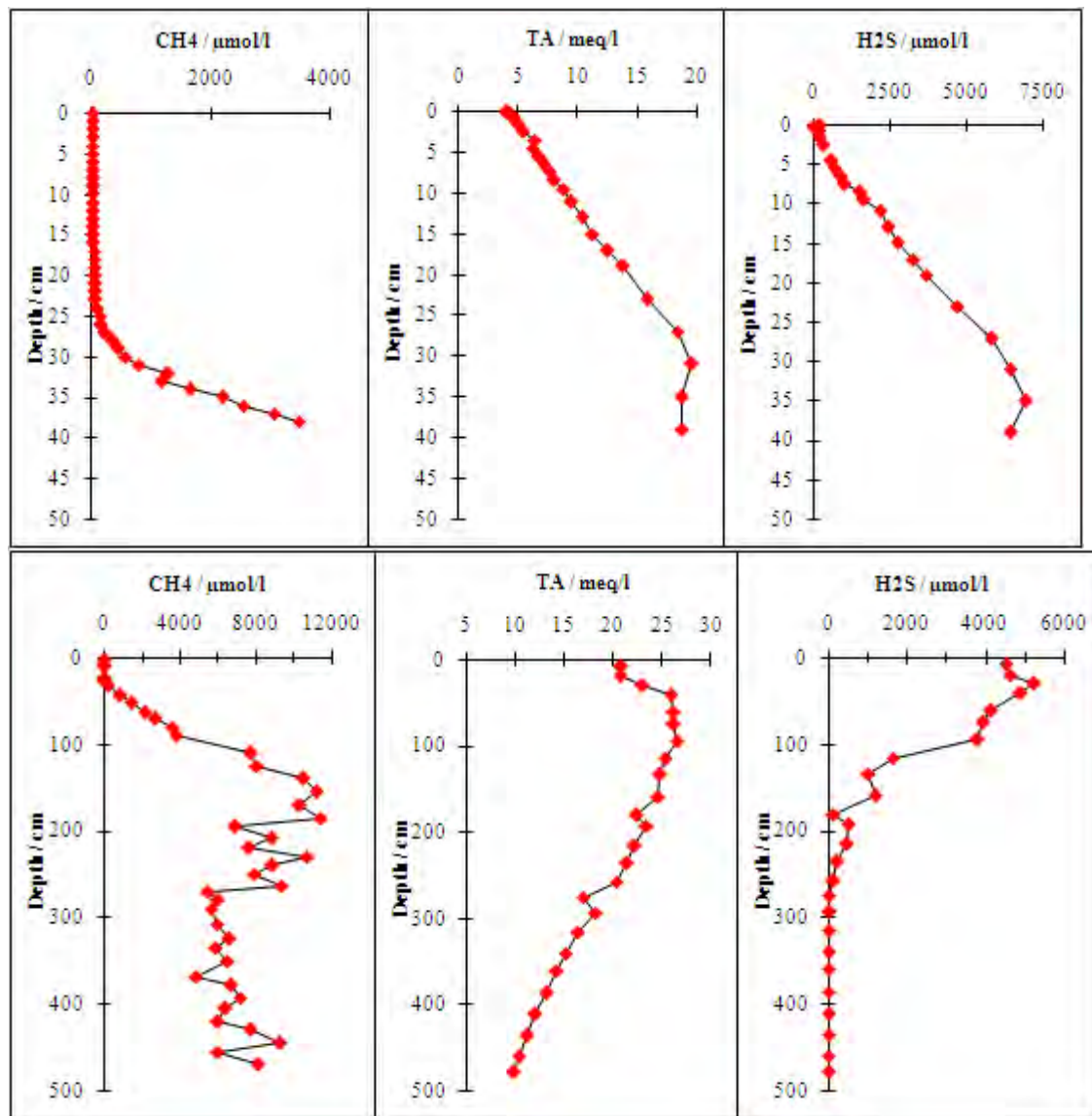


Figure 5.4.3.5: Measured porewater TA, H₂S, and CH₄ concentrations at the seep site at the slump head wall (66-1 MIC7; top) and in the channel (89-1 GC9; bottom).

5.5 Heatflow measurements

Jörg Bialas, Gero Wetzel

Heatflow operations started with a single deployment next to piezometer station PR1FG in 418 m water depth. After decline of the temperature pulse induced from the penetration a heat pulse was released. From the heat pulse decay a temperature conduction coefficient of 1.05 W/m K was calculated. The corresponding temperature gradient was calculated with 26.6 K/m (Table 5.5.1).

A calibration deployment in about 1.500 m water depth was undertaken. A temperature measurement in the water column was used to achieve deviation values for the single temperature sensors of the string.

5.5.1 Working area 1

The second deployment of the heatflow probe was used to achieve a profile across the buried canyon system, which was investigated with the first 3D data set. 11 sampling points were distributed starting at the foot of the western wall of the most recent canyon (Fig. 5.2). On the 2D seismic image of profile MSM34-1_07 (fig. 5.3.12 and P1107, fig. 5.3.2.3) two

buried canyon systems were identified, which terminate eastwards into well stratified parallel sediment layers. The heatflow profile was terminated with sampling station HF2-11 in this regime (Table 5.5.2).

Station	No.	Latitude N	Longitude E	Water depth EM122 (m)	Temperature gradient (K/m)	Thermal Conductivity W/m K HP = heat pulse
HF1-1	3-1	43:48.355	30:24.797	418	26.6	1.3 HP

Table 5.5.1: Seafloor positions of heatflow probe during deployment 1

Deduced from the heat pulse test at station HF1 the temperature gradient was calculated with a conductive coefficient of 1.05 W/m K

Station	No.	Latitude N	Longitude E	Water depth EM122 (m)	Temperature gradient (K/m)	Thermal Conductivity W/m K HP = heat pulse
HF2-1	28-1	43°28.216	30°26.256	1430	29.2	1.06 HP
HF2-2	29-1	43°28.092	30°26.021	1468	29.5	0.98 HP
HF2-3	30-1	43°27.956	30°25.782	1466	32.2	0.98 HP
HF2-4	31-1	43°27.863	30°25.607	1470	32.0	1.35
HF2-5	32-1	43°27.760	30°25.430	1478	29.1	1.35
HF2-6	33-1	43°27.660	30°25.253	1475	29.8	1.35
HF2-7	34-1	43°27.547	30°25.045	1478	27.3	1.35
HF2-8	35-1	43°27.471	30°24.905	1495	33.0	1.35
HF2-9	36-1	43°27.373	30°24.729	1500	37.3	1.35
HF2-10	37-1	43°27.276	30°24.550		37.1	1.35
HF2-11	38-1	43°27.189	30°24.372	1500	34.4	1.35

Table 5.5.2: Seafloor positions of heatflow probe during deployment 2

5.5.2 Working area 2

Major interest of working area 2 was the observation of an upward bending BSR in the seismic data of profile 15 recorded during leg 1. Seven heatflow locations were planned along profile 15 with a distance of about 300 m between the sample points. Two were located in larger water depth than the BSR projection to the seafloor, one right on top and four in shallower water depth (Fig. 5.3).

At the first deployment site a heat pulse was generated after decline of the penetration temperature signal. From this measurement heat conduction k was calculated to be 0.93 W/m K. The residual of the temperature gradient was found to be 0.038 K/m. From this measurement a value of 1 W/m K has been deduced and used to calculate the temperature gradient of the remaining stations for which the decline of the penetration pulse has been observed only.

Heatflow values were found to be in general in the range of 27 K/km to 36.8 K/km (Table 5.5.3). Increased values were found in the centre of the channel system to the east of the slump area for the stations HF4-18 and following (Table 5.5.3). The Reduced temperature gradients of 27 K/km were calculated for stations HF3-3 and HF3-4 both at a seafloor depth of 670 m. HF3-3 is located at the interpolated cross point location for BSR and seafloor of seismic profile MSM34-15. Moreover the profile is located at the foot of the eastern headwall of a slump area. It is suggested that recent slumping has caused a deviation from steady state conditions for gas hydrates with continuous dissolution and cooling.

A second deployment of the heatflow probe was used for intermediate sampling stations. A small region of reduced temperature gradients clusters around stations HF3-3 and HF3-4. The

location of HF3-4 was chosen for a gravity core and a Mini MUC.

In the bathymetric map a small fault is visible, which cuts through the middle of the failed area. Therefore a third heatflow deployment was carried out to provide a regional picture on temperature gradients crossing that fault. With respect to the model of gas migration along the canyon centre further measurements provide a link into the centre of the nearby canyon depression. HF4-18 sampled the canyon floor. Here the probe sunk into the sediment without a clear sign of tension release. At the same time the temperature values increased for all sensors of the device. The deepest sensor recorded about 9.5 °C. Additional measurements indicate that the area of increased temperature is limited by the canyon walls (HF4-20 and HF4-24), while along the trench temperature values remain anomalously high (HF4-20 to HF4-23). Although seismic and Parasound data do not show any anomaly for this area a gravity core was taken at the site.

Station	No.	Latitude N	Longitude E	Water depth EM122 (m)	Temperature gradient (K/km)	Thermal Conductivity W/m K HP = heat pulse
HF3-1	44-1	43:57.0580	30:46.9120	752	36.8	0.93 HP
HF3-2	45-1	43:57.1860	30:46.7710	726	34.4	1.35
HF3-3	46-1	43:57.3080	30:46.6430	700	27	1.35
HF3-4	47-1	43:57.4400	30:46.5120	670	28	1.35
HF3-5	48-1	43:57.5600	30:46.3770	670	33.6	1.35
HF3-6	49-1	43:57.6850	30:46.2430	650	35.6	1.35
HF3-7	50-1	43:57.8110	30:46.1150	636	32.5	1.35
HF4-1	67-1	43°57.231	30°46.727	713	32	0.91 HP
HF4-2	68-1	43°57.273	30°46.679	703	28.6	0.94 HP
HF4-3	69-1	43°57.313	30°46.498	696	30.5	0.97 HP
HF4-4	70-1	43°57.363	30°46.587	703	33.1	0.89 HP
HF4-5	71-1	43°57.411	30°46.680	696	34.4	0.9 HP
HF4-6	72-2	43°57.406	30°46.538	688	29.8	0.97 HP
HF4-7	73-1	43°57.485	30°46.457	674	28.4	0.98 HP
HF4-12	76-1	43°57.023	30°46.005	700	32.9	0.92 HP
HF4-13	77-1	43°57.201	30°46.299	710	34.5	0.93 HP
HF4-10	78-1	43°57.567	30°46.502	650	27.7	0.96 HP
HF4-Flare1	79-1	43°57.627	30°46.533	620	20	1.33 HP
HF4-15	80-1	43°57.506	30°46.869	630	17.6	0.96 HP
HF4-17	81-1	43°57.591	30°47.293	760	31.7	0.97 HP
HF4-18	82-1	43°57.684	30°47.749	830	53.7	0.68 HP
HF4-19	83-1	43°57.684	30°47.740	830	55.6	1.35
HF4-20	84-1	43°57.682	30°47.535	816	43.8	0.85 HP
HF4-21	85-1	43°57.827	30°47.721	816	50.1	0.79 HP
HF4-22	86-1	43°57.592	30°47.726	832	65.4	0.69 HP
HF4-23	87-1	43°57.393	30°47.733	838	47.3	0.93 HP
HF4-24	88-1	43°57.693	30°47.941	801	36.7	1.35

Table 5.5.3: Seafloor positions of heatflow probe during deployments 3, 4 and 5

5.6 Piezometer installation

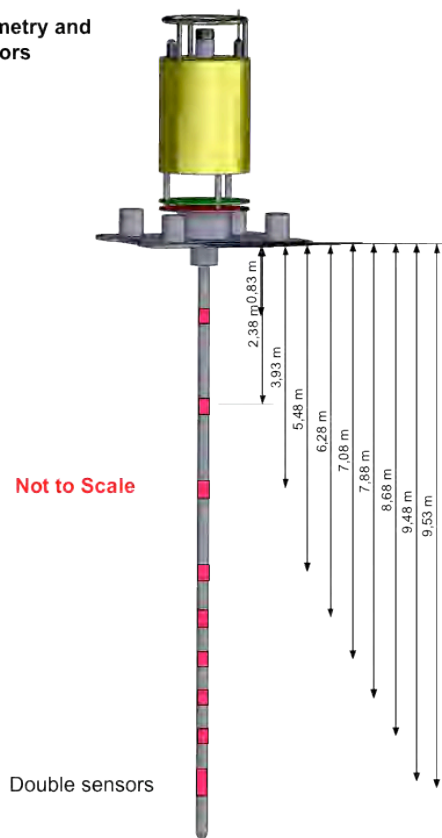
Mickael Roudaut, Anthony Ferrant

During cruise MSM34 Leg-1 two piezometers were assembled and deployed for long-term measurements. Both instruments were left in the ground for recovery during the French GHASS project. The instruments are expected to achieve a minimum of 6 month of observation time and can operate for up to 3 years.

	Latitude	Longitude	Depth	# sensors	Lenght lance
PR1FG	43° 48.396' N	30° 24.92' E	394 m	10	10 m
PR1HS	43° 34.981' N	31° 07.949' E	1645 m	11	10.8 m

Piezometrer – Priority 1 – Free gas (10 sensors)

Geometry and sensors



Piezometrer – Priority 1 – Hydrate system (11 sensors)

Geometry and sensors

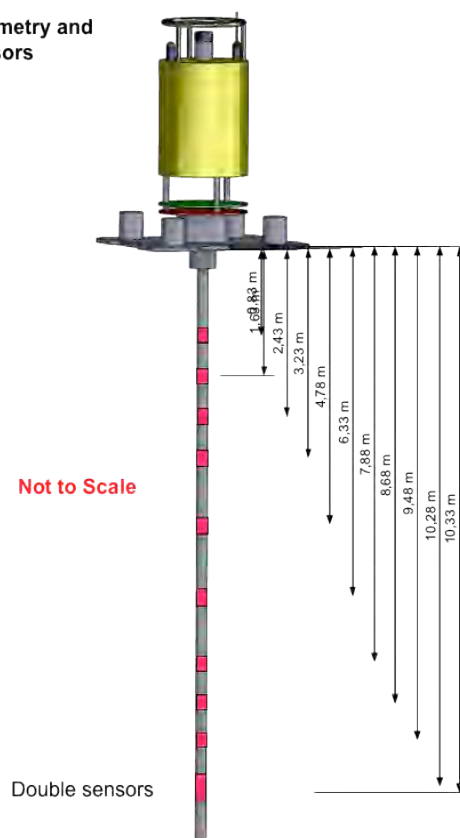


Figure 5.6.1: Measures of the pressure sensor distribution selected for the two long-term installations.

6 Ship's Metrological Station

n.a.

2 Station List

2.1 Stationsliste MSM34-1

Station	Name	Date	Time	PositionLat	PositionLon	Depth [m]	Gear
MSM34/894-1		10.12.2013	03:08	43° 14.76' N	30° 41.89' E	1893.9	Schallprofilsonde
MSM34/895-1		10.12.2013	04:52	43° 14.76' N	30° 41.89' E	1897.8	MB und ParaSound Start
MSM34/895-1		10.12.2013	06:10	43° 21.09' N	30° 38.75' E	1767.3	MB und ParaSound End
MSM34/896-1		11.12.2013	10:09	43° 48.39' N	30° 24.91' E	391.9	Piezometer_Probe
MSM34/896-1		11.12.2013	16:24	43° 48.40' N	30° 24.92' E	397	Piezometer
MSM34/897-1	Profile-01	11.12.2013	22:57	43° 34.24' N	29° 58.16' E	688.8	Seismic reflection profile
MSM34/897-1		12.12.2013	12:00	44° 9.81' N	31° 2.86' E	519.5	Seismic reflection profile
MSM34/897-1	Profile-02	12.12.2013	13:12	44° 7.79' N	31° 5.58' E	620.9	Seismic reflection profile
MSM34/897-1		13.12.2013	02:22	43° 32.53' N	30° 0.92' E	850.5	Seismic reflection profile
MSM34/897-1	Profile-03	13.12.2013	03:24	43° 30.37' N	30° 3.13' E	1028.4	Seismic reflection profile
MSM34/897-1		13.12.2013	16:43	44° 5.65' N	31° 7.77' E	780.1	Seismic reflection profile
MSM34/897-1	Profile-04	13.12.2013	18:13	44° 3.60' N	31° 10.17' E	922.8	Seismic reflection profile
MSM34/897-1		14.12.2013	07:15	43° 28.30' N	30° 5.55' E	1187.1	Seismic reflection profile
MSM34/897-1	Profile-05	14.12.2013	08:24	43° 26.33' N	30° 8.15' E	1275.1	Seismic reflection profile
MSM34/897-1		14.12.2013	21:26	44° 1.57' N	31° 12.71' E	989.9	Seismic reflection profile
MSM34/897-1	Profile-06	14.12.2013	22:34	43° 59.33' N	31° 14.79' E	1146.5	Seismic reflection profile
MSM34/897-1		15.12.2013	11:40	43° 23.63' N	30° 9.81' E	1386.2	Seismic reflection profile
MSM34/897-1	Profile-07	15.12.2013	12:50	43° 21.42' N	30° 11.94' E	1474.2	Seismic reflection profile
MSM34/897-1		16.12.2013	02:00	43° 56.98' N	31° 17.02' E	1170.9	Seismic reflection profile
MSM34/897-1	Profile-08	16.12.2013	02:57	43° 54.86' N	31° 19.46' E	1273.3	Seismic reflection profile
MSM34/897-1		16.12.2013	10:26	43° 34.72' N	30° 42.43' E	1185.2	Seismic reflection profile
MSM34/897-1	Profile-08b	16.12.2013	14:26	43° 36.48' N	30° 45.61' E	990.3	Seismic reflection profile
MSM34/897-1		16.12.2013	20:54	43° 19.23' N	30° 14.49' E	1569.1	Seismic reflection profile
MSM34/897-1	Profile-09	16.12.2013	22:00	43° 17.05' N	30° 16.66' E	1624.5	Seismic reflection profile
MSM34/897-1		17.12.2013	10:09	43° 49.25' N	31° 15.46' E	1612.1	Seismic reflection profile
MSM34/897-1	Profile-10	17.12.2013	11:14	43° 47.14' N	31° 17.72' E	1661.7	Seismic reflection profile
MSM34/897-1		17.12.2013	23:36	43° 14.34' N	30° 18.02' E	1700.1	Seismic reflection profile
MSM34/897-1	Profile-11	18.12.2013	00:39	43° 12.40' N	30° 20.61' E	1778.8	Seismic reflection profile
MSM34/897-1		18.12.2013	12:08	43° 42.83' N	31° 16.07' E	1738.8	Seismic reflection profile
MSM34/897-1	Profile-12	18.12.2013	13:14	43° 40.99' N	31° 18.85' E	1743.8	Seismic reflection profile
MSM34/897-1		18.12.2013	13:25	43° 40.51' N	31° 17.95' E	1731.6	Seismic reflection profile
MSM34/897-1		18.12.2013	15:32	43° 40.81' N	31° 18.49' E	1730.6	Seismic reflection profile

MSM34/897-1		19.12.2013	02:42	43° 10.41' N	30° 23.38' E	1820.6	Seismic reflection profile
MSM34/897-1	Profile-13	19.12.2013	03:39	43° 8.34' N	30° 25.74' E	1858	Seismic reflection profile
MSM34/897-1		19.12.2013	14:10	43° 36.71' N	31° 17.29' E	1666.1	Seismic reflection profile
MSM34/897-1	Profile-14	19.12.2013	14:30	43° 38.03' N	31° 17.27' E	1673	Seismic reflection profile
MSM34/897-1		19.12.2013	21:45	44° 3.99' N	30° 50.12' E	343.9	Seismic reflection profile
MSM34/897-1		19.12.2013	22:07	44° 4.25' N	30° 48.16' E	254.3	MB und ParaSound Start
MSM34/897-1		19.12.2013	23:03	44° 1.75' N	30° 43.49' E	188.2	MB und ParaSound End
MSM34/897-1	Profile-15	19.12.2013	23:30	44° 0.09' N	30° 43.70' E	337.2	Seismic reflection profile
MSM34/897-1		20.12.2013	05:35	43° 38.18' N	31° 6.64' E	1642.1	Seismic reflection profile
MSM34/897-1	Profile-15b	20.12.2013	08:31	43° 37.85' N	31° 6.98' E	1650.7	Seismic reflection profile
MSM34/897-1		20.12.2013	10:42	43° 30.07' N	31° 15.04' E	1624.1	Seismic reflection profile
MSM34/898-1		20.12.2013	13:19	43° 34.98' N	31° 7.95' E	1648.5	Piezometer_Probe
MSM34/898-1		20.12.2013	20:05	43° 34.98' N	31° 7.95' E	1648.1	Piezometer
MSM34/899-1		20.12.2013	23:54	43° 55.75' N	30° 46.44' E	687.5	MB und ParaSound Start
MSM34/899-1		21.12.2013	10:30	43° 7.23' N	30° 36.50' E	1934.2	MB und ParaSound End
MSM34/900-1	Profile-20	21.12.2013	12:05	43° 8.53' N	30° 34.83' E	1912.9	Seismic reflection profile
MSM34/900-1		21.12.2013	13:14	43° 12.66' N	30° 30.58' E	1848.6	Seismic reflection profile
MSM34/900-1		21.12.2013	15:36	43° 8.64' N	30° 34.71' E	1910.5	Seismic reflection profile
MSM34/900-1		22.12.2013	00:00	43° 38.88' N	30° 3.52' E	529.7	Seismic reflection profile
MSM34/900-1	Profile-19	22.12.2013	01:27	43° 42.08' N	30° 10.32' E	458.3	Seismic reflection profile
MSM34/900-1		22.12.2013	09:49	43° 11.91' N	30° 41.41' E	1891.1	Seismic reflection profile
MSM34/900-1	Profile-21	22.12.2013	11:17	43° 15.77' N	30° 47.36' E	1879.3	Seismic reflection profile
MSM34/900-1		22.12.2013	19:38	43° 45.71' N	30° 16.01' E	379.3	Seismic reflection profile
MSM34/900-1	Profile-18	22.12.2013	21:01	43° 48.55' N	30° 22.87' E	200.4	Seismic reflection profile
MSM34/900-1		23.12.2013	05:11	43° 19.14' N	30° 53.39' E	1611.1	Seismic reflection profile
MSM34/900-1	Profile-22	23.12.2013	06:20	43° 21.49' N	30° 57.88' E	1480.7	Seismic reflection profile
MSM34/900-1		23.12.2013	14:33	43° 50.79' N	30° 27.13' E	551.9	Seismic reflection profile
MSM34/900-1	Profile-17	23.12.2013	15:46	43° 53.28' N	30° 31.52' E	833.8	Seismic reflection profile
MSM34/900-1		24.12.2013	00:05	43° 23.39' N	31° 2.56' E	1369.4	Seismic reflection profile
MSM34/900-1	Profile-16	24.12.2013	01:22	43° 26.96' N	31° 8.06' E	1510.8	Seismic reflection profile
MSM34/900-1		24.12.2013	09:42	43° 57.03' N	30° 36.88' E	409.3	Seismic reflection profile
MSM34/900-1	Profile-23	24.12.2013	11:32	43° 52.63' N	30° 40.79' E	893.7	Seismic reflection profile
MSM34/900-1		24.12.2013	16:44	44° 6.72' N	31° 6.66' E	701.2	Seismic reflection profile
MSM34/900-1	Profile-24	24.12.2013	18:45	44° 4.31' N	30° 59.19' E	679.4	Seismic reflection profile
MSM34/900-1		24.12.2013	23:41	43° 46.81' N	31° 17.91' E	1673.8	Seismic reflection profile
MSM34/900-1	Profile-25	24.12.2013	23:53	43° 45.95' N	31° 18.16' E	1705	Seismic reflection profile

MSM34/900-1		25.12.2013	02:44	43° 33.14' N	31° 16.59' E	1639.6	Seismic reflection profile
MSM34/900-1	Profile-26	25.12.2013	02:56	43° 32.42' N	31° 15.89' E	1661.7	Seismic reflection profile
MSM34/900-1		25.12.2013	11:38	43° 8.94' N	30° 33.08' E	1893.6	Seismic reflection profile
MSM34/900-1	Profile-27	25.12.2013	12:36	43° 7.16' N	30° 35.65' E	1936.2	Seismic reflection profile
MSM34/900-1		25.12.2013	21:11	43° 30.37' N	31° 17.70' E	1685.1	Seismic reflection profile
MSM34/900-1	Profile-28	25.12.2013	21:31	43° 31.71' N	31° 18.11' E	1665.3	Seismic reflection profile
MSM34/900-1		26.12.2013	05:59	44° 2.01' N	30° 47.08' E	448.2	Seismic reflection profile
MSM34/901-1		26.12.2013	08:47	44° 1.09' N	31° 2.15' E	784.6	MB und ParaSound Start
MSM34/901-1		26.12.2013	20:00	43°41.18' N	30° 10.73' E	522.2	MB und ParaSound End

2.2 Stationsliste MSM34-2

Station No.	Date	Time [UTC]	Position Lat	Position Lon	Depth [m]	Gear
MSM34/001-1	30.12.13	00:40	43° 5.87' N	29° 58.26' E	1648.3	Multibeam und ParaSound
MSM34/001-1	30.12.13	00:56	43° 6.51' N	29° 59.43' E	1626.3	Multibeam und ParaSound
MSM34/001-2	30.12.13	01:16	43° 6.59' N	29° 58.58' E	1622.6	Multibeam und ParaSound
MSM34/001-2	30.12.13	01:31	43° 5.89' N	29° 59.57' E	1643.9	Multibeam und ParaSound
MSM34/002-1	30.12.13	05:59	43° 51.91' N	30° 31.15' E	700.1	Multibeam und ParaSound
MSM34/002-1	30.12.13	07:52	43° 45.07' N	30° 18.79' E	393.3	Multibeam und ParaSound
MSM34/003-1	30.12.13	09:33	43° 48.35' N	30° 24.79' E	425.5	Heat Flow
MSM34/003-2	30.12.13	10:29	43° 48.35' N	30° 24.78' E	417	Multi corer
MSM34/003-3	30.12.13	11:17	43° 48.35' N	30° 24.78' E	419.2	Gravity corer
MSM34/003-3	30.12.13	11:19	43° 48.35' N	30° 24.79' E	419.4	Gravity corer
MSM34/004-1	30.12.13	15:14	43° 20.80' N	30° 32.99' E	1735	Schallprofilsonde
MSM34/004-2	30.12.13	17:07	43° 20.80' N	30° 32.99' E	1745.2	Heat Flow
MSM34/005-1	30.12.13	19:07	43° 29.18' N	30° 24.31' E	1424.8	Ocean Bottom Seismometer
MSM34/006-1	30.12.13	19:31	43° 28.74' N	30° 24.75' E	1443	Ocean Bottom Seismometer
MSM34/007-1	30.12.13	19:48	43° 28.31' N	30° 25.20' E	1459.4	Ocean Bottom Seismometer
MSM34/008-1	30.12.13	20:02	43° 27.88' N	30° 25.64' E	1465	Ocean Bottom Seismometer
MSM34/009-1	30.12.13	20:16	43° 27.45' N	30° 26.09' E	1494	Ocean Bottom Seismometer
MSM34/010-1	30.12.13	20:38	43° 27.13' N	30° 25.50' E	1497.1	Ocean Bottom Seismometer

MSM34/011-1	30.12.13	20:57	43° 27.57' N	30° 25.06' E	1474.8	Ocean Bottom Seismometer
MSM34/012-1	30.12.13	21:14	43° 28.00' N	30° 24.62' E	1443.3	Ocean Bottom Seismometer
MSM34/013-1	30.12.13	21:29	43° 28.43' N	30° 24.16' E	1466.8	Ocean Bottom Seismometer
MSM34/014-1	30.12.13	21:44	43° 28.86' N	30° 23.72' E	1453.1	Ocean Bottom Seismometer
MSM34/015-1	30.12.13	22:02	43° 28.53' N	30° 23.13' E	1449.6	Ocean Bottom Seismometer
MSM34/016-1	30.12.13	22:27	43° 28.10' N	30° 23.58' E	1470.2	Ocean Bottom Seismometer
MSM34/017-1	30.12.13	22:44	43° 27.67' N	30° 24.02' E	1480.8	Ocean Bottom Seismometer
MSM34/018-1	30.12.13	23:01	43° 27.24' N	30° 24.47' E	1501.2	Ocean Bottom Seismometer
MSM34/019-1	30.12.13	23:27	43° 26.82' N	30° 24.91' E	1514.7	Ocean Bottom Seismometer
MSM34/020-1	31.12.13	02:09	43° 43.16' N	30° 18.86' E	527.8	Multibeam und ParaSound
MSM34/020-1	31.12.13	02:47	43° 45.80' N	30° 22.55' E	443.1	Multibeam und ParaSound
MSM34/020-1	31.12.13	04:13	43° 51.01' N	30° 31.98' E	683.4	Multibeam und ParaSound
MSM34/021-1	31.12.13	05:25	43° 45.73' N	30° 17.98' E	365.8	Multibeam und ParaSound
MSM34/021-1	31.12.13	07:19	43° 52.63' N	30° 30.40' E	739.9	Multibeam und ParaSound
MSM34/022-1	31.12.13	10:32	43° 25.68' N	30° 26.05' E	1551.2	Gravity corer
MSM34/024-1	31.12.13	17:41	43° 25.40' N	30° 28.16' E	1549.9	Seismic reflection profile
MSM34/024-1	31.12.13	19:28	43° 31.07' N	30° 22.34' E	1348.4	Seismic reflection profile
MSM34/024-1	31.12.13	22:17	43° 24.98' N	30° 27.71' E	1617.1	Seismic reflection profile
MSM34/024-1	01.01.14	01:46	43° 27.03' N	30° 20.33' E	1429.9	Seismic reflection profile
MSM34/024-1	01.01.14	03:14	43° 30.57' N	30° 26.83' E	1244.5	Seismic reflection profile
MSM34/024-1	01.01.14	05:23	43° 26.62' N	30° 20.89' E	1466.2	Seismic reflection profile
MSM34/024-1	01.01.14	07:26	43° 29.90' N	30° 27.97' E	1257.8	Seismic reflection profile
MSM34/024-1	01.01.14	09:20	43° 25.81' N	30° 21.89' E	1490.3	Seismic reflection profile
MSM34/024-1	01.01.14	11:16	43° 28.88' N	30° 28.75' E	1315.5	Seismic reflection profile
MSM34/025-1	01.01.14	18:55	43° 25.81' N	30° 25.00' E	1463.4	Seismic reflection profile
MSM34/025-1	01.01.14	20:16	43° 29.14' N	30° 21.54' E	1406.6	Seismic reflection profile
MSM34/025-1	01.01.14	22:11	43° 26.10' N	30° 26.49' E	1537.1	Seismic reflection profile
MSM34/025-1	02.01.14	00:11	43° 29.40' N	30° 21.34' E	1405.9	Seismic reflection profile
MSM34/025-1	02.01.14	02:09	43° 26.43' N	30° 26.25' E	1522.3	Seismic reflection profile

MSM34/025-1	02.01.14	03:58	43° 29.14' N	30° 21.67' E	1407.1	Seismic reflection profile
MSM34/025-1	02.01.14	05:45	43° 26.63' N	30° 26.10' E	1523.6	Seismic reflection profile
MSM34/025-1	02.01.14	07:39	43° 29.15' N	30° 21.73' E	1409.8	Seismic reflection profile
MSM34/025-1	02.01.14	09:32	43° 26.35' N	30° 26.44' E	1529.5	Seismic reflection profile
MSM34/025-1	02.01.14	11:31	43° 29.40' N	30° 21.54' E	1410.5	Seismic reflection profile
MSM34/025-1	02.01.14	13:26	43° 26.44' N	30° 26.43' E	1551.2	Seismic reflection profile
MSM34/025-1	02.01.14	15:26	43° 29.29' N	30° 21.70' E	1413.9	Seismic reflection profile
MSM34/025-1	02.01.14	17:13	43° 26.61' N	30° 26.31' E	1521	Seismic reflection profile
MSM34/025-1	02.01.14	19:05	43° 29.28' N	30° 21.79' E	1417.6	Seismic reflection profile
MSM34/025-1	02.01.14	21:00	43° 26.50' N	30° 26.49' E	1529	Seismic reflection profile
MSM34/025-1	02.01.14	22:58	43° 29.44' N	30° 21.68' E	1411.6	Seismic reflection profile
MSM34/025-1	03.01.14	00:57	43° 26.36' N	30° 26.70' E	1535.8	Seismic reflection profile
MSM34/025-1	03.01.14	02:56	43° 29.33' N	30° 21.86' E	1415.6	Seismic reflection profile
MSM34/025-1	03.01.14	04:44	43° 26.65' N	30° 26.46' E	1524.4	Seismic reflection profile
MSM34/025-1	03.01.14	06:39	43° 29.38' N	30° 21.88' E	1424.5	Seismic reflection profile
MSM34/025-1	03.01.14	08:32	43° 26.56' N	30° 26.62' E	1527.5	Seismic reflection profile
MSM34/025-1	03.01.14	10:33	43° 29.58' N	30° 21.73' E	1405.6	Seismic reflection profile
MSM34/025-1	03.01.14	12:27	43° 26.74' N	30° 26.50' E	1529.2	Seismic reflection profile
MSM34/025-1	03.01.14	14:32	43° 29.37' N	30° 22.02' E	1426.3	Seismic reflection profile
MSM34/025-1	03.01.14	16:29	43° 26.70' N	30° 26.59' E	1530.1	Seismic reflection profile
MSM34/025-1	03.01.14	18:26	43° 29.51' N	30° 21.94' E	1410.3	Seismic reflection profile
MSM34/025-1	03.01.14	20:23	43° 26.52' N	30° 26.89' E	1536.3	Seismic reflection profile
MSM34/025-1	03.01.14	22:26	43° 29.69' N	30° 21.83' E	1399.4	Seismic reflection profile
MSM34/025-1	04.01.14	00:30	43° 26.43' N	30° 27.01' E	1535.5	Seismic reflection profile
MSM34/025-1	04.01.14	02:30	43° 29.48' N	30° 22.10' E	1417.9	Seismic reflection profile
MSM34/025-1	04.01.14	04:19	43° 26.72' N	30° 26.78' E	1526.1	Seismic reflection profile
MSM34/025-1	04.01.14	06:12	43° 29.59' N	30° 22.05' E	1416.4	Seismic reflection profile
MSM34/025-1	04.01.14	08:04	43° 26.63' N	30° 26.95' E	1535.8	Seismic reflection profile
MSM34/025-1	04.01.14	10:01	43° 29.67' N	30° 22.05' E	1402.7	Seismic reflection profile

MSM34/025-1	04.01.14	11:06	43° 28.76' N	30° 24.79' E	1427.4	Seismic reflection profile
MSM34/025-1	04.01.14	11:09	43° 28.64' N	30° 24.91' E	1429.6	Seismic reflection profile
MSM34/026-1	04.01.14	13:48	43° 27.23' N	30° 24.47' E	1498.4	Multi corer
MSM34/027-1	04.01.14	15:20	43° 28.10' N	30° 26.04' E	1465.8	Multi corer
MSM34/028-1	04.01.14	16:57	43° 28.22' N	30° 26.25' E	1438.4	Heat Flow
MSM34/029-1	04.01.14	17:52	43° 28.09' N	30° 26.03' E	1458.2	Heat Flow
MSM34/030-1	04.01.14	18:38	43° 27.95' N	30° 25.79' E	1471.1	Heat Flow
MSM34/031-1	04.01.14	19:19	43° 27.86' N	30° 25.62' E	1471	Heat Flow
MSM34/032-1	04.01.14	19:52	43° 27.75' N	30° 25.44' E	1485.4	Heat Flow
MSM34/033-1	04.01.14	20:24	43° 27.67' N	30° 25.26' E	1473	Heat Flow
MSM34/034-1	04.01.14	20:54	43° 27.55' N	30° 25.05' E	1473.5	Heat Flow
MSM34/035-1	04.01.14	21:21	43° 27.47' N	30° 24.91' E	1506.1	Heat Flow
MSM34/036-1	04.01.14	21:49	43° 27.37' N	30° 24.73' E	1501.8	Heat Flow
MSM34/037-1	04.01.14	22:22	43° 27.27' N	30° 24.56' E	1504.3	Heat Flow
MSM34/038-1	04.01.14	22:53	43° 27.18' N	30° 24.37' E	1499.3	Heat Flow
MSM34/018-1	04.01.14	23:56	43° 27.23' N	30° 24.20' E	0	Ocean Bottom Seismometer
MSM34/017-1	05.01.14	00:41	43° 27.55' N	30° 23.90' E	0	Ocean Bottom Seismometer
MSM34/016-1	05.01.14	01:16	43° 27.99' N	30° 23.44' E	0	Ocean Bottom Seismometer
MSM34/015-1	05.01.14	01:51	43° 28.39' N	30° 23.00' E	0	Ocean Bottom Seismometer
MSM34/014-1	05.01.14	02:19	43° 28.76' N	30° 23.65' E	0	Ocean Bottom Seismometer
MSM34/013-1	05.01.14	02:51	43° 28.30' N	30° 24.00' E	0	Ocean Bottom Seismometer
MSM34/012-1	05.01.14	03:22	43° 27.82' N	30° 24.50' E	0	Ocean Bottom Seismometer
MSM34/011-1	05.01.14	03:48	43° 27.40' N	30° 24.94' E	0	Ocean Bottom Seismometer
MSM34/010-1	05.01.14	04:16	43° 27.04' N	30° 25.41' E	0	Ocean Bottom Seismometer
MSM34/019-1	05.01.14	04:46	43° 26.72' N	30° 24.81' E	0	Ocean Bottom Seismometer
MSM34/009-1	05.01.14	05:14	43° 27.40' N	30° 25.96' E	0	Ocean Bottom Seismometer
MSM34/008-1	05.01.14	05:42	43° 27.85' N	30° 25.48' E	0	Ocean Bottom Seismometer
MSM34/007-1	05.01.14	06:13	43° 28.30' N	30° 24.90' E	0	Ocean Bottom Seismometer
MSM34/006-1	05.01.14	06:40	43° 28.73' N	30° 24.51' E	0	Ocean Bottom Seismometer
MSM34/005-1	05.01.14	07:11	43° 29.17' N	30° 24.06' E	0	Ocean Bottom Seismometer
MSM34/039-1	05.01.14	08:45	43° 27.25' N	30° 24.48' E	1498.8	Gravity corer
MSM34/040-1	05.01.14	10:43	43° 28.10' N	30° 26.04' E	1462.3	Gravity corer
MSM34/041-1	05.01.14	14:39	43° 30.12' N	30° 23.47' E	1381.3	Seismic reflection profile

MSM34/041-1	05.01.14	16:03	43° 26.66' N	30° 27.05' E	1533.9	Seismic reflection profile
MSM34/041-1	05.01.14	17:57	43° 29.65' N	30° 22.12' E	1401.5	Seismic reflection profile
MSM34/041-1	05.01.14	19:51	43° 26.70' N	30° 27.07' E	1528.1	Seismic reflection profile
MSM34/041-1	05.01.14	21:47	43° 29.65' N	30° 22.19' E	1404.9	Seismic reflection profile
MSM34/041-1	05.01.14	23:45	43° 26.65' N	30° 27.13' E	1528.6	Seismic reflection profile
MSM34/041-1	06.01.14	01:50	43° 29.80' N	30° 22.04' E	1350.8	Seismic reflection profile
MSM34/041-1	06.01.14	03:45	43° 26.74' N	30° 27.11' E	1526.4	Seismic reflection profile
MSM34/041-1	06.01.14	05:40	43° 29.68' N	30° 22.24' E	1381.8	Seismic reflection profile
MSM34/041-1	06.01.14	07:35	43° 26.69' N	30° 27.19' E	1531	Seismic reflection profile
MSM34/042-1	06.01.14	16:20	43° 25.68' N	30° 26.07' E	1549.7	Multi corer
MSM34/041-1	06.01.14	21:10	43° 28.19' N	30° 23.84' E	1462.2	Seismic reflection profile
MSM34/041-1	06.01.14	21:47	43° 29.67' N	30° 22.31' E	1377.6	Seismic reflection profile
MSM34/041-1	06.01.14	23:54	43° 26.30' N	30° 27.55' E	1533.4	Seismic reflection profile
MSM34/041-1	07.01.14	01:58	43° 29.82' N	30° 22.16' E	1351.7	Seismic reflection profile
MSM34/041-1	07.01.14	03:52	43° 26.79' N	30° 27.16' E	1508.4	Seismic reflection profile
MSM34/041-1	07.01.14	05:52	43° 29.77' N	30° 22.26' E	1375.2	Seismic reflection profile
MSM34/041-1	07.01.14	07:51	43° 26.73' N	30° 27.29' E	1517.3	Seismic reflection profile
MSM34/041-1	07.01.14	09:48	43° 29.80' N	30° 22.33' E	1368.2	Seismic reflection profile
MSM34/041-1	07.01.14	11:43	43° 26.76' N	30° 27.30' E	1518.3	Seismic reflection profile
MSM34/041-1	07.01.14	13:47	43° 29.87' N	30° 22.28' E	1353.5	Seismic reflection profile
MSM34/041-1	07.01.14	15:39	43° 26.93' N	30° 27.19' E	1502.1	Seismic reflection profile
MSM34/041-1	07.01.14	17:35	43° 29.73' N	30° 22.49' E	1373.5	Seismic reflection profile
MSM34/041-1	07.01.14	19:31	43° 26.80' N	30° 27.37' E	1506.5	Seismic reflection profile
MSM34/041-1	07.01.14	21:28	43° 29.79' N	30° 22.50' E	1363.2	Seismic reflection profile
MSM34/041-1	07.01.14	23:26	43° 26.83' N	30° 27.42' E	1509.3	Seismic reflection profile
MSM34/041-1	08.01.14	01:29	43° 29.95' N	30° 22.38' E	1361.7	Seismic reflection profile
MSM34/041-1	08.01.14	03:25	43° 26.95' N	30° 27.36' E	1494.5	Seismic reflection profile
MSM34/041-1	08.01.14	05:18	43° 29.74' N	30° 22.64' E	1370.3	Seismic reflection profile
MSM34/041-1	08.01.14	07:28	43° 26.65' N	30° 27.01' E	1529.8	Seismic reflection profile
MSM34/041-1	08.01.14	09:24	43° 29.68' N	30° 22.04' E	1380.5	Seismic reflection profile
MSM34/041-1	08.01.14	11:23	43° 26.57' N	30° 27.04' E	1531.1	Seismic reflection profile
MSM34/041-1	08.01.14	11:46	43° 25.36' N	30° 26.60' E	1563.9	Seismic reflection profile
MSM34/041-1	08.01.14	12:54	43° 27.73' N	30° 23.27' E	1390.6	Seismic reflection profile
MSM34/041-1	08.01.14	13:11	43° 28.39' N	30° 22.60' E	1380.7	Seismic reflection profile

MSM34/041-1	08.01.14	13:18	43° 28.68' N	30° 22.35' E	1367.9	Seismic reflection profile
MSM34/041-1	08.01.14	13:32	43° 29.25' N	30° 21.76' E	1411.4	Seismic reflection profile
MSM34/041-1	08.01.14	15:42	43° 26.49' N	30° 26.04' E	1516.7	Seismic reflection profile
MSM34/041-1	08.01.14	17:18	43° 28.19' N	30° 23.12' E	1418.5	Seismic reflection profile
MSM34/041-1	08.01.14	17:24	43° 28.42' N	30° 22.82' E	1395.1	Seismic reflection profile
MSM34/041-1	08.01.14	17:49	43° 29.47' N	30° 21.72' E	1409.5	Seismic reflection profile
MSM34/041-1	08.01.14	19:41	43° 26.58' N	30° 26.55' E	1527.7	Seismic reflection profile
MSM34/041-1	08.01.14	21:47	43° 29.67' N	30° 21.84' E	1391	Seismic reflection profile
MSM34/041-1	08.01.14	23:49	43° 26.41' N	30° 27.03' E	1533.8	Seismic reflection profile
MSM34/041-1	09.01.14	01:53	43° 29.52' N	30° 22.01' E	1413.7	Seismic reflection profile
MSM34/041-1	09.01.14	03:19	43° 28.35' N	30° 24.13' E	1467.6	Seismic reflection profile
MSM34/041-1	09.01.14	03:26	43° 28.09' N	30° 24.46' E	1471	Seismic reflection profile
MSM34/041-1	09.01.14	04:09	43° 26.29' N	30° 26.33' E	1524.7	Seismic reflection profile
MSM34/041-1	09.01.14	05:03	43° 26.95' N	30° 24.09' E	1406.8	Seismic reflection profile
MSM34/041-1	09.01.14	05:32	43° 28.23' N	30° 23.07' E	1408.8	Seismic reflection profile
MSM34/041-1	09.01.14	05:57	43° 29.26' N	30° 22.01' E	1421.7	Seismic reflection profile
MSM34/043-1	09.01.14	11:21	43° 57.43' N	30° 46.50' E	681	Gravity corer
MSM34/043-2	09.01.14	12:19	43° 57.44' N	30° 46.50' E	671.2	Multi corer
MSM34/044-1	09.01.14	13:16	43° 57.05' N	30° 46.90' E	751.6	Heat Flow
MSM34/045-1	09.01.14	14:05	43° 57.18' N	30° 46.76' E	722.9	Heat Flow
MSM34/046-1	09.01.14	14:29	43° 57.31' N	30° 46.63' E	695.3	Heat Flow
MSM34/047-1	09.01.14	14:57	43° 57.44' N	30° 46.50' E	674	Heat Flow
MSM34/048-1	09.01.14	15:21	43° 57.56' N	30° 46.37' E	680.1	Heat Flow
MSM34/049-1	09.01.14	15:46	43° 57.68' N	30° 46.23' E	655.8	Heat Flow
MSM34/050-1	09.01.14	16:12	43° 57.81' N	30° 46.10' E	636.3	Heat Flow
MSM34/051-1	09.01.14	17:42	43° 57.17' N	30° 46.76' E	723.1	Gravity corer
MSM34/051-1	09.01.14	18:09	43° 57.17' N	30° 46.76' E	730.5	Gravity corer
MSM34/052-1	09.01.14	18:44	43° 57.49' N	30° 45.41' E	654.3	Ocean Bottom Seismometer
MSM34/053-1	09.01.14	18:57	43° 57.17' N	30° 45.73' E	680.8	Ocean Bottom Seismometer
MSM34/054-1	09.01.14	19:08	43° 56.84' N	30° 46.08' E	704.2	Ocean Bottom Seismometer
MSM34/055-1	09.01.14	19:20	43° 56.52' N	30° 46.44' E	704.5	Ocean Bottom Seismometer
MSM34/056-1	09.01.14	19:35	43° 56.92' N	30° 47.15' E	792.2	Ocean Bottom Seismometer
MSM34/057-1	09.01.14	19:48	43° 57.23' N	30° 46.82' E	708.8	Ocean Bottom Seismometer
MSM34/058-1	09.01.14	19:58	43° 57.56' N	30° 46.49' E	656.4	Ocean Bottom Seismometer

MSM34/059-1	09.01.14	20:10	43° 57.86' N	30° 46.14' E	602.1	Ocean Bottom Seismometer
MSM34/060-1	09.01.14	20:32	43° 58.28' N	30° 46.83' E	594.6	Ocean Bottom Seismometer
MSM34/061-1	09.01.14	20:43	43° 57.96' N	30° 47.17' E	702	Ocean Bottom Seismometer
MSM34/062-1	09.01.14	20:53	43° 57.65' N	30° 47.51' E	806.3	Ocean Bottom Seismometer
MSM34/063-1	09.01.14	21:05	43° 57.32' N	30° 47.86' E	846.8	Ocean Bottom Seismometer
MSM34/064-1	09.01.14	23:32	43° 55.90' N	30° 47.11' E	712.7	Seismic reflection profile
MSM34/064-1	10.01.14	00:25	43° 58.35' N	30° 44.49' E	522.4	Seismic reflection profile
MSM34/064-1	10.01.14	01:51	43° 56.56' N	30° 48.66' E	830.3	Seismic reflection profile
MSM34/064-1	10.01.14	03:27	43° 57.74' N	30° 43.85' E	527	Seismic reflection profile
MSM34/064-1	10.01.14	04:48	43° 56.14' N	30° 47.99' E	892.8	Seismic reflection profile
MSM34/064-1	10.01.14	06:10	43° 57.81' N	30° 43.90' E	544.1	Seismic reflection profile
MSM34/064-1	10.01.14	07:35	43° 56.14' N	30° 48.11' E	902.3	Seismic reflection profile
MSM34/064-1	10.01.14	09:03	43° 58.02' N	30° 43.83' E	555.3	Seismic reflection profile
MSM34/064-1	10.01.14	10:30	43° 56.06' N	30° 48.32' E	908.9	Seismic reflection profile
MSM34/064-1	10.01.14	11:50	43° 58.19' N	30° 44.30' E	546.7	Seismic reflection profile
MSM34/064-1	10.01.14	13:14	43° 56.04' N	30° 48.40' E	913.2	Seismic reflection profile
MSM34/064-1	10.01.14	14:30	43° 58.25' N	30° 44.27' E	536.5	Seismic reflection profile
MSM34/064-1	10.01.14	15:50	43° 56.23' N	30° 48.29' E	902.8	Seismic reflection profile
MSM34/064-1	10.01.14	17:05	43° 58.19' N	30° 44.43' E	538	Seismic reflection profile
MSM34/064-1	10.01.14	18:23	43° 56.29' N	30° 48.32' E	912.5	Seismic reflection profile
MSM34/064-1	10.01.14	19:38	43° 58.20' N	30° 44.48' E	539.7	Seismic reflection profile
MSM34/064-1	10.01.14	20:53	43° 56.24' N	30° 48.40' E	912.7	Seismic reflection profile
MSM34/064-1	10.01.14	22:10	43° 58.24' N	30° 44.48' E	529.2	Seismic reflection profile
MSM34/064-1	10.01.14	23:28	43° 56.25' N	30° 48.44' E	906	Seismic reflection profile
MSM34/064-1	11.01.14	00:54	43° 58.37' N	30° 44.44' E	517.5	Seismic reflection profile
MSM34/064-1	11.01.14	02:05	43° 56.71' N	30° 48.10' E	869.3	Seismic reflection profile
MSM34/064-1	11.01.14	03:31	43° 58.21' N	30° 44.72' E	532.3	Seismic reflection profile
MSM34/064-1	11.01.14	04:53	43° 56.42' N	30° 48.48' E	865	Seismic reflection profile
MSM34/064-1	11.01.14	06:15	43° 58.30' N	30° 44.69' E	518.8	Seismic reflection profile
MSM34/064-1	11.01.14	07:35	43° 56.44' N	30° 48.52' E	850.7	Seismic reflection profile
MSM34/064-1	11.01.14	08:55	43° 58.32' N	30° 44.75' E	524.1	Seismic reflection profile
MSM34/064-1	11.01.14	10:14	43° 56.26' N	30° 48.75' E	858.8	Seismic reflection profile
MSM34/064-1	11.01.14	11:34	43° 58.44' N	30° 44.68' E	504.9	Seismic reflection profile
MSM34/064-1	11.01.14	12:55	43° 56.33' N	30° 48.75' E	856.6	Seismic reflection profile

MSM34/064-1	11.01.14	14:14	43° 58.32' N	30° 44.86' E	517.3	Seismic reflection profile
MSM34/064-1	11.01.14	15:27	43° 56.55' N	30° 48.59' E	831.2	Seismic reflection profile
MSM34/064-1	11.01.14	16:44	43° 58.26' N	30° 45.00' E	530.9	Seismic reflection profile
MSM34/064-1	11.01.14	18:03	43° 56.58' N	30° 48.71' E	830.2	Seismic reflection profile
MSM34/064-1	11.01.14	19:21	43° 58.38' N	30° 44.94' E	531.6	Seismic reflection profile
MSM34/064-1	11.01.14	20:34	43° 56.59' N	30° 48.76' E	825.9	Seismic reflection profile
MSM34/064-1	11.01.14	21:49	43° 58.40' N	30° 44.97' E	531.3	Seismic reflection profile
MSM34/064-1	11.01.14	23:09	43° 56.46' N	30° 48.93' E	844	Seismic reflection profile
MSM34/064-1	12.01.14	00:27	43° 58.51' N	30° 44.94' E	519.8	Seismic reflection profile
MSM34/064-1	12.01.14	01:47	43° 56.56' N	30° 48.87' E	838.5	Seismic reflection profile
MSM34/064-1	12.01.14	03:05	43° 58.50' N	30° 45.00' E	523.1	Seismic reflection profile
MSM34/064-1	12.01.14	04:24	43° 56.63' N	30° 48.91' E	831.9	Seismic reflection profile
MSM34/064-1	12.01.14	05:40	43° 58.51' N	30° 45.07' E	522.2	Seismic reflection profile
MSM34/064-1	12.01.14	06:59	43° 56.71' N	30° 48.90' E	839.8	Seismic reflection profile
MSM34/064-1	12.01.14	08:06	43° 58.06' N	30° 45.61' E	562.4	Seismic reflection profile
MSM34/064-1	12.01.14	09:37	43° 56.60' N	30° 49.08' E	836.3	Seismic reflection profile
MSM34/064-1	12.01.14	10:57	43° 58.63' N	30° 45.07' E	519.1	Seismic reflection profile
MSM34/064-1	12.01.14	12:14	43° 56.64' N	30° 49.11' E	845.9	Seismic reflection profile
MSM34/064-1	12.01.14	13:31	43° 58.70' N	30° 45.06' E	513	Seismic reflection profile
MSM34/064-1	12.01.14	14:47	43° 56.68' N	30° 49.12' E	823.8	Seismic reflection profile
MSM34/064-1	12.01.14	16:00	43° 58.62' N	30° 45.20' E	520.2	Seismic reflection profile
MSM34/064-1	12.01.14	17:18	43° 56.66' N	30° 49.23' E	841.9	Seismic reflection profile
MSM34/064-1	12.01.14	18:40	43° 58.65' N	30° 45.26' E	520.4	Seismic reflection profile
MSM34/064-1	12.01.14	19:12	43° 57.52' N	30° 45.10' E	631.8	Seismic reflection profile
MSM34/064-1	12.01.14	19:51	43° 55.59' N	30° 47.10' E	690.5	Seismic reflection profile
MSM34/064-1	12.01.14	21:09	43° 58.70' N	30° 45.32' E	514.2	Seismic reflection profile
MSM34/064-1	12.01.14	22:29	43° 56.67' N	30° 49.26' E	848.8	Seismic reflection profile
MSM34/064-1	12.01.14	23:50	43° 58.82' N	30° 45.44' E	495.4	Seismic reflection profile
MSM34/064-1	13.01.14	00:34	43° 57.44' N	30° 45.55' E	673.7	Seismic reflection profile
MSM34/064-1	13.01.14	00:40	43° 57.11' N	30° 45.80' E	690.2	Seismic reflection profile
MSM34/064-1	13.01.14	01:09	43° 55.68' N	30° 47.29' E	727.1	Seismic reflection profile
MSM34/064-1	13.01.14	02:24	43° 58.84' N	30° 45.75' E	494.4	Seismic reflection profile
MSM34/064-1	13.01.14	03:40	43° 56.75' N	30° 49.25' E	834.1	Seismic reflection profile
MSM34/064-1	13.01.14	04:16	43° 56.70' N	30° 47.64' E	859.5	Seismic reflection profile

MSM34/064-1	13.01.14	04:25	43° 57.15' N	30° 47.20' E	758.4	Seismic reflection profile
MSM34/064-1	13.01.14	04:29	43° 57.35' N	30° 46.99' E	664.1	Seismic reflection profile
MSM34/064-1	13.01.14	04:37	43° 57.77' N	30° 46.61' E	605.1	Seismic reflection profile
MSM34/064-1	13.01.14	04:42	43° 58.02' N	30° 46.34' E	580.5	Seismic reflection profile
MSM34/064-1	13.01.14	04:47	43° 58.31' N	30° 46.16' E	555.2	Seismic reflection profile
MSM34/064-1	13.01.14	04:52	43° 58.58' N	30° 45.91' E	510.3	Seismic reflection profile
MSM34/064-1	13.01.14	05:45	43° 58.33' N	30° 45.75' E	543.2	Seismic reflection profile
MSM34/064-1	13.01.14	05:52	43° 57.97' N	30° 46.13' E	583.5	Seismic reflection profile
MSM34/064-1	13.01.14	06:02	43° 57.45' N	30° 46.67' E	673.9	Seismic reflection profile
MSM34/064-1	13.01.14	06:04	43° 57.34' N	30° 46.78' E	686	Seismic reflection profile
MSM34/064-1	13.01.14	06:22	43° 56.42' N	30° 47.76' E	876.8	Seismic reflection profile
MSM34/064-1	13.01.14	07:23	43° 56.33' N	30° 47.99' E	886.3	Seismic reflection profile
MSM34/064-1	13.01.14	07:30	43° 56.66' N	30° 47.65' E	863.3	Seismic reflection profile
MSM34/064-1	13.01.14	07:41	43° 57.16' N	30° 47.11' E	711.6	Seismic reflection profile
MSM34/064-1	13.01.14	08:13	43° 58.69' N	30° 45.51' E	495.7	Seismic reflection profile
MSM34/065-1	13.01.14	12:41	43° 57.17' N	30° 46.77' E	720.5	Multi corer
MSM34/066-1	13.01.14	13:44	43° 57.62' N	30° 46.53' E	638	Multi corer
MSM34/066-2	13.01.14	14:38	43° 57.62' N	30° 46.53' E	633.3	Gravity corer
MSM34/067-1	13.01.14	15:56	43° 57.22' N	30° 46.72' E	713.5	Heat Flow
MSM34/068-1	13.01.14	16:25	43° 57.27' N	30° 46.67' E	707.1	Heat Flow
MSM34/069-1	13.01.14	16:54	43° 57.31' N	30° 46.49' E	697.4	Heat Flow
MSM34/070-1	13.01.14	17:29	43° 57.36' N	30° 46.58' E	680.8	Heat Flow
MSM34/071-1	13.01.14	18:00	43° 57.40' N	30° 46.68' E	676.7	Heat Flow
MSM34/072-1	13.01.14	18:32	43° 57.40' N	30° 46.54' E	686	Heat Flow
MSM34/073-1	13.01.14	19:06	43° 57.48' N	30° 46.44' E	674.2	Heat Flow
MSM34/073-1	13.01.14	19:12	43° 57.48' N	30° 46.45' E	678	Heat Flow
MSM34/072-2	13.01.14	19:44	43° 57.40' N	30° 46.53' E	688.2	Heat Flow
MSM34/074-1	13.01.14	22:22	43° 57.44' N	30° 46.50' E	678.4	Multi corer
MSM34/074-2	13.01.14	23:07	43° 57.44' N	30° 46.50' E	671.9	Gravity corer
MSM34/075-1	14.01.14	01:28	43° 58.00' N	30° 44.01' E	558.4	Seismic reflection profile
MSM34/075-1	14.01.14	03:27	43° 53.09' N	30° 49.14' E	950.4	Seismic reflection profile
MSM34/075-1	14.01.14	06:08	43° 58.42' N	30° 44.46' E	508.1	Seismic reflection profile
MSM34/075-1	14.01.14	08:47	43° 53.74' N	30° 50.47' E	1092.8	Seismic reflection profile
MSM34/075-1	14.01.14	11:20	43° 58.81' N	30° 46.26' E	529.6	Seismic reflection profile

MSM34/075-1	14.01.14	11:40	43° 59.63' N	30° 45.37' E	456.7	Seismic reflection profile
MSM34/075-1	14.01.14	12:05	44° 0.58' N	30° 44.30' E	296.5	Seismic reflection profile
MSM34/075-1	14.01.14	13:02	43° 59.65' N	30° 47.12' E	499.3	Seismic reflection profile
MSM34/075-1	14.01.14	14:59	43° 54.83' N	30° 52.14' E	953.8	Seismic reflection profile
MSM34/075-1	14.01.14	16:57	43° 53.87' N	30° 47.76' E	845.3	Seismic reflection profile
MSM34/075-1	14.01.14	17:50	43° 55.79' N	30° 44.39' E	647.3	Seismic reflection profile
MSM34/075-1	14.01.14	18:58	43° 58.70' N	30° 48.58' E	609.4	Seismic reflection profile
MSM34/052-1	14.01.14	21:24	43° 57.47' N	30° 45.19' E	661.5	Ocean Bottom Seismometer
MSM34/053-1	14.01.14	21:48	43° 57.17' N	30° 45.58' E	686.5	Ocean Bottom Seismometer
MSM34/054-1	14.01.14	22:10	43° 56.84' N	30° 45.88' E	698.5	Ocean Bottom Seismometer
MSM34/055-1	14.01.14	22:36	43° 56.52' N	30° 46.29' E	691.3	Ocean Bottom Seismometer
MSM34/056-1	14.01.14	22:57	43° 56.92' N	30° 46.99' E	799.7	Ocean Bottom Seismometer
MSM34/057-1	14.01.14	23:14	43° 57.21' N	30° 46.62' E	721.4	Ocean Bottom Seismometer
MSM34/058-1	14.01.14	23:33	43° 57.54' N	30° 46.41' E	681.7	Ocean Bottom Seismometer
MSM34/059-1	14.01.14	23:47	43° 57.88' N	30° 46.04' E	604	Ocean Bottom Seismometer
MSM34/060-1	15.01.14	00:08	43° 58.22' N	30° 46.72' E	607.6	Ocean Bottom Seismometer
MSM34/061-1	15.01.14	00:22	43° 57.91' N	30° 47.06' E	697.3	Ocean Bottom Seismometer
MSM34/062-1	15.01.14	00:42	43° 57.60' N	30° 47.41' E	794.3	Ocean Bottom Seismometer
MSM34/063-1	15.01.14	01:00	43° 57.32' N	30° 47.80' E	858.6	Ocean Bottom Seismometer
MSM34/076-1	15.01.14	01:51	43° 57.03' N	30° 46.02' E	698.2	Heat Flow
MSM34/077-1	15.01.14	02:35	43° 57.21' N	30° 46.31' E	706.6	Heat Flow
MSM34/078-1	15.01.14	03:23	43° 57.57' N	30° 46.51' E	641.4	Heat Flow
MSM34/079-1	15.01.14	03:49	43° 57.63' N	30° 46.54' E	615.1	Heat Flow
MSM34/080-1	15.01.14	04:28	43° 57.51' N	30° 46.88' E	626.8	Heat Flow
MSM34/081-1	15.01.14	05:15	43° 57.60' N	30° 47.30' E	752.9	Heat Flow
MSM34/082-1	15.01.14	06:01	43° 57.69' N	30° 47.76' E	827.1	Heat Flow
MSM34/083-1	15.01.14	06:26	43° 57.69' N	30° 47.75' E	819.4	Heat Flow
MSM34/084-1	15.01.14	06:54	43° 57.69' N	30° 47.54' E	816.5	Heat Flow
MSM34/085-1	15.01.14	07:42	43° 57.83' N	30° 47.74' E	827.6	Heat Flow
MSM34/086-1	15.01.14	08:22	43° 57.60' N	30° 47.74' E	819.1	Heat Flow
MSM34/086-1	15.01.14	08:48	43° 57.60' N	30° 47.74' E	834.4	Heat Flow
MSM34/087-1	15.01.14	09:13	43° 57.40' N	30° 47.75' E	845.5	Heat Flow
MSM34/088-1	15.01.14	10:03	43° 57.69' N	30° 47.94' E	794.8	Heat Flow
MSM34/089-1	15.01.14	11:33	43° 57.69' N	30° 47.76' E	818.1	Gravity corer

MSM34/090-1	15.01.14	15:24	43° 37.72' N	30° 38.61' E	1072.5	Seismic reflection profile
MSM34/090-1	15.01.14	16:42	43° 34.63' N	30° 32.94' E	1196.8	Seismic reflection profile
MSM34/090-1	15.01.14	18:00	43° 38.34' N	30° 28.39' E	1042.8	Seismic reflection profile
MSM34/090-1	15.01.14	19:31	43° 42.22' N	30° 34.06' E	967.3	Seismic reflection profile
MSM34/090-1	15.01.14	21:08	43° 47.55' N	30° 29.74' E	612	Seismic reflection profile
MSM34/090-1	15.01.14	22:43	43° 44.45' N	30° 22.74' E	525	Seismic reflection profile
MSM34/090-1	16.01.14	00:06	43° 49.40' N	30° 22.50' E	1064.3	Seismic reflection profile
MSM34/090-1	16.01.14	04:58	43° 35.01' N	30° 38.82' E	1188.5	Seismic reflection profile
MSM34/090-1	16.01.14	05:25	43° 33.79' N	30° 37.19' E	1226.3	Seismic reflection profile
MSM34/090-1	16.01.14	06:15	43° 36.10' N	30° 34.19' E	1172.3	Seismic reflection profile
MSM34/091-1	16.01.14	09:18	43° 13.72' N	30° 10.93' E	1604.5	Multibeam und ParaSound
MSM34/091-1	16.01.14	11:06	43° 4.51' N	29° 55.80' E	1731.8	Multibeam und ParaSound
MSM34/091-1	16.01.14	11:24	43° 6.09' N	29° 53.49' E	1669.2	Multibeam und ParaSound
MSM34/091-1	16.01.14	12:17	43° 10.68' N	30° 0.51' E	1604.2	Multibeam und ParaSound
MSM34/091-1	16.01.14	12:36	43° 12.69' N	29° 58.84' E	1525.9	Multibeam und ParaSound
MSM34/091-1	16.01.14	13:22	43° 9.20' N	29° 52.17' E	1611	Multibeam und ParaSound
MSM34/091-1	16.01.14	13:49	43° 10.47' N	29° 49.23' E	1597.8	Multibeam und ParaSound
MSM34/091-1	16.01.14	14:10	43° 12.57' N	29° 51.76' E	1560.3	Multibeam und ParaSound
MSM34/091-1	16.01.14	15:50	43° 20.97' N	30° 5.93' E	1415.6	Multibeam und ParaSound
MSM34/091-1	16.01.14	16:11	43° 23.20' N	30° 4.38' E	1281.5	Multibeam und ParaSound
MSM34/091-1	16.01.14	17:47	43° 15.29' N	29° 50.60' E	1512.1	Multibeam und ParaSound
MSM34/091-1	16.01.14	18:08	43° 16.99' N	29° 48.05' E	1476.6	Multibeam und ParaSound
MSM34/091-1	16.01.14	19:46	43° 25.04' N	30° 2.09' E	1175.8	Multibeam und ParaSound
MSM34/091-1	16.01.14	20:06	43° 27.18' N	30° 0.39' E	1079.9	Multibeam und ParaSound
MSM34/091-1	16.01.14	21:43	43° 19.84' N	29° 46.61' E	1407.7	Multibeam und ParaSound
MSM34/091-1	16.01.14	22:00	43° 21.19' N	29° 44.47' E	1314.7	Multibeam und ParaSound

8 Data and Sample Storage and Availability

Data processing and archiving was prepared on board already. Station lists were submitted to the online database PANGAEA, the German Oceanographic Data Centre DOD and the GEOMAR Data Management Portal. Archiving of digital data will be supported by the automatic backup system in GEOMAR. All data will be made available to public upon request through the named data portals.

Station lists have been submitted to the PANGAEA and DOD databases.

[PANGAEA Data Archiving & Publication](#)

[PDI-7246](#)

Data submission 2014-03-10T12:03:28Z (Dr. Jörg Bialas, GEOMAR)

9 Acknowledgements

The cruise MSM34 SUGAR Site Leg 1 and 2 was supported by the German Federal Ministry for Education and Research (Bundesministerium für Bildung und Forschung, BMBF) under project No. 03G0819A (SUGAR-II A) and by the European Union Seventh Framework Programme (FP7/2007-2013) under the MIDAS project, grant agreement n° 603418.

The authors wish to express their gratitude to all the colleagues who have supported the work before, during and after the cruise. Much of the work done during the cruise was only made possible by the scientists', technicians' and the crews' experience.

Particular thanks are directed to the masters (Björn Maaß and Ralf Schmidt) and their entire crew of R/V MARIA S. MERIAN for the excellent support throughout the cruise.

10 References

- Bahr A, Lamy F, Arz HW, Major C, Kwiecien O, Wefer G (2008) Abrupt changes of temperature and water chemistry in the late Pleistocene and early Holocene Black Sea. *Geochemistry Geophysics Geosystems* 9, doi:10.1029/2007GC001683.
- Bahr A, Pape T, Abegg F, Bohrmann G, van Weering TCE, Ivanov MK (2010) Authigenic carbonates from the eastern Black Sea as an archive for shallow gas hydrate dynamics – Results from the combination of CT imaging with mineralogical and stable isotope analyses. *Marine and Petroleum Geology* 27(9), 1819-1829.
- Baristean, N. (2006), Seismische Fazies, Tektonik und Gashydratvorkommen im nordwestlichen Schwarzen Meer, Diploma thesis, 110 pp, Hamburg, Hamburg.
- Berndt, C., Bünz, S., Clayton, T. et al., 2004. Seismic character of bottom-simulating reflections: examples from the mid-Norwegian margin. *Mar. Pet. Geol.*, 21, 723–733.
- Bohrmann G, Schenck S (2002) GEOMAR Cruise Report M52/1, MARGASCH, RV Meteor, marine gas hydrates of the Black Sea. GEOMAR, Kiel.
- Bohrmann G., Greinert J., Suess E., Torres M., 1998. Authigenic carbonates from Cascadia subduction zone and their relation to gas hydrate stability. *Geology*. 26, 647–650.
- Bohrmann G, Ivanov I, Foucher J-P, Spiess V, Bialas J, Greinert J, Weinrebe W, Abegg F, Aloisi G, Artemov Y, Blinova V, Broser A, Drews M, Heidersdorf F, Krabbenhoft A, Klauke I, Krastel S, Leder T, Polikarpov I, Saburova M, Schmale O, Seifert R, Volkonskaya A, Zillmer M (2003) MVs and gas hydrates in the Black Sea –new data from Dvurechenskii and Odessa mud volcanoes. *Geo-Mar Lett* 23 (3/4) <http://dx.doi.org/10.1007/s00367-003-0157-7>.
- Campbell, K. J., 1991, Deepwater geohazards: an engineering challenge: *Offshore*, 51, 10, 46-51.

- Degens ET, Ross DA (1974) The Black Sea - Geology, Chemistry, and Biology. The American Association of Petroleum Geologists, Tulsa, USA.
- Dickas A.B., Payne J.L. Epper Paleocene Buried channel in Sacramento valley, California. Bull. Am. Assoc. Petrol. Geolog., N 51, 1967, p. 873-882.
- Egorov V. N., Artemov Y. G., Gulin S. B. (Ed. G. G. Polikarpov), 2011. Methane seeps in the Black Sea Environment - forming and ecological role. Sevastopol: ECOSEA, Hydrophysics, 405 p. (Figs 156, Tables 21)
- Finetti I., G. Bricchi, A. Del Ben, M. Pipan, Z. Xuan. Geophysical Study of the Black Sea. In: Monograph on the Black Sea, Bullettino di Geophysica Teorica ed Applicata, 30, 1988, 117-118, 197-324.
- Геолого-геофизические исследования Болгарского сектора Черного моря. София, изд-во БАН, 1980, 318 с.
- Gevorkyan, B., V. Burakov, U. Isagulova, D. Semenov, V. Malahov, F. Olepnik, A. Gryazanov, A. Shevchenko, 1991. Gas venting buildups on the seafloor of the North-Western Black Sea part. (in Russian), Docladi Ac. Nauck Ukraina, Geology, 4: 80-85.
- Ginsburg GD, Ivanov VL, Soloviev VA (1984) Natural gas hydrates of the World's Oceans. In: Oil and gas content of the World's Oceans. PGO Sevmorgeologia, pp 141–158 (in Russian).
- Gornitz V., I. Fung. Potential distribution of methane hydrates in the world's oceans. Global Biogeochemical Cycles, 1994, 8, 335-347.
- Grasshoff K, Ehrhardt M, Kremling K (1999) Methods of Seawater Analysis. Wiley-VCH, Weinheim.
- Hein, J. R., Scholl, D. W., Barron, J. A. et al., 1978. Diagenesis of Late Cenozoic diatomaceous deposits and formation of the bottom simulating reflector in southern Bering Sea. Sedimentology 25, 155–181.
- Henriet J. P., J. Mieneret (Editors) Gas Hydrates - Relevance to word margin stability and climatic change, England, Special Publ. No 137, 1998.
- Holbrook, W. S., Hoskins, H., Wood, W. T. et al., 1996. Methane hydrate and free gas on the Blake Ridge from vertical seismic profiling. Science 273, 1840–1843.
- Hovland, M., 2000. Are there commercial deposits of marine hydrates in ocean sediments? Energy Explor. Exploit. 18, 339–347.
- Jones GA, Gagnon AR (1994) Radiocarbon chronology of Black Sea sediments. Deep-Sea Research 41, 531–557.
- Калинин А.В., Калинин В.В., Пивоваров Б.Л. Сейсмоакустические исследования на акваториях. М., Недра, 1983, 204 с.
- Kessler J. D., W. S. Reeburgh, J. Southon, R. Seifert, W. Michaelis, S. C. Tyler. Basin-wide estimates of the input of methane from seeps and clathrates to the Black Sea. Earth and Planet. Sci. Lett., 2006, doi:10.1016/j.epsl.2006.01.006.
- Кобелев В. П., 2003. Геодинамическая модель Черноморской мегавпадины. Геофизический журнал, 25/2, 15-35.
- Korsakov O. D., Yu. A. Byakov, S. N. Stupak. Gas hydrates of the Black Sea Basin (in Russian). (Gasovie gidrati Chernomorskoi vpadini). Sov. geologia, 1989, 12, 3-10.
- Krasen J., M. Ciesnik. Basin analysis, formation, and 'stability in the Black Sea; Geological Evolution and Analysis of Confirmed or Suspected Gas Hydrate Localities, 11, 1988, US Department of Energy, DOE/MC/21181-1950 (DE80001057), 88 p.
- Krastel S, Spiess V, Ivanov M, Weiirebe W, Bohrmann G, Shaskin P, Heidorsdorf F (2003) Acoustic investigations of mud volcanoes in the Sorokin Trough. Geo-Mar Lett 23 (3/4) <http://dx.doi.org/10.1007/s00367-003-0143-0>.
- Kutas R, Kobolev V, Bevzyuk M, Kravchuk O (2003) New heat flow determinations in the

- NE Black Sea (In Russian). Ukr Geophys J, 25 (2): 48-53.
- Kutas R. I., V. A. Tsvashchenko, V. P. Kobolev, O. P. Kravchuk, M. I. Bevzyuk. Geothermal aspects of gas hydrate formation in the Black Sea Basin. Geophys. J., 16, 1997, 337-350.
- Kvenvolden, K. A., 1993. Gas hydrates – Geological perspective and global change. Rev. Geophys., 31, 173–187.
- Lachenbruch A. H., J. H. Sass. The stress heat-flow paradox and thermal results from Cajon Pass. Geophys. Res. Lett., 15, 1988, 9, 981-984.
- Lamy F, Arz HW, Bond G, Bahr A, Pätzold J (2006) Multicentennial-scale hydrological changes in the Black Sea and northern Red Sea during the Holocene and the Arctic/North Atlantic Oscillation, Paleoclimatology 2, PA1008.
- Lericolais, G., C. Bulois, H. Gillet, and F. Guichard (2009), High frequency sea level fluctuations recorded in the Black Sea since the LGM, *Global Planet Change*, 66(1-2), 65-75.
- Лейн А. Ю., Иванов М. В. Крупнейший на Земле метановый водоем // Природа. – 2005. – №2 – С. 18 – 26.
- Лейн А. Ю., Иванов М. В. Биогеохимический цикл метана в океане. – М.: Наука. – 2009. – 575 С.
- Limonov AF, Woodside JM, Ivanov MK (1994) Mud volcanism in the Mediterranean and Black seas and shallow structure of the Eratosthenes Seamount. UNESCO reports in marine science 64, 173 pp.
- Lüdmann T. H., H. K. Wong, P. H. Konerding, M. Zillmer, J. Petersen, E. Flüh. Heat Flow and Quantity of Methane Deduced from a Gas Hydrate Field in the Vicinity of the Dnieper Canyon, Northwestern Black Sea. Geo-Mar. Lett., 24, 2004, 3-4, 180-193.
- Mackay, M. E., Jarrard, R. D., Westbrook, G. K. et al., 1994. Origin of bottom-simulating reflectors: geophysical evidence from the Cascadia accretionary prism. Geology 22, 459–462.
- Маев Е.Г., Козлов В.Б., Крыстев Т.Н., Лимонов А.Ф., Мысливец В.И., Пырличев Д.Г., Чистяков А.А. Структурно-геоморфологическая характеристика континентальной террасы. В сб.: "Геолого-геофизические исследования Болгарского сектора Черного моря". София, БАН, 1980, с. 145-156.
- Manheim FT, Schug DM (1978) Interstitial waters of Black Sea cores. In: Ross DA, Neprochnov YP (Eds.), Initial Reports of the Deep-Sea Drilling Project. U.S. Government Printing Office, Washington.
- Major CO, Goldstein SL, Ryan WBF, Lericolais G, Piotrowski AM, Hajdas I (2006) The coevolution of Black Sea level and composition through the last deglaciation and its paleoclimatic significance. Quaternary Science Reviews 25, 2031-2047.
- Makarenko I.B., V.I. Starostenko, O.M. Rusakov, I.K. Pashkevich, R.I. Kutas, O.V. Legostaeva, 2008. Proceedings: Petroleum Geology & Hydrocarbon Potential of Caspian and Black Sea Regions, Baku, Azerbaijan, 271-275. Marine Slides and other mass movements. NATO Conf. series. Series IV: Marine Sciences. Plenum Press, New York and London, 1:982, p. 350.
- McGinnis D. F., A. Wüest, J. Greinert, A. Lorke, C. J. Schubert. Vertical pathways of methane in the Black Sea. Geophysical Research Abstracts, 7, 00077, 2005, SRef-ID: 1607-7962/gra/EGU05-A-00077.
- Milkov A. V., R. Sassen, T. V. Apanasovich, F. G. Dadashev. Geophys. Res. Lett., 30, 2003, 2, 1037, DOI:10.1029/2002GL016358.
- Neretin LN, Böttcher ME, Jørgensen BB, Volkov II, Lüschen H, Hilgenfeld K (2004) Pyritization processes and greigite formation in the advancing sulfidization front in the Upper Pleistocene sediments of the Black Sea. Geochimica et Cosmochimica Acta 68(9),

2081-2093.

- Poort J., A. Vassilev, L. Dimitrov. Did postglacial catastrophic flooding trigger massive changes in the Black Sea gas hydrate reservoir? *Terra Nova*, 17, 2005, 135-140.
- Popescu, I., G. Lericolais, N. Panin, M. De Batist, and H. Gillet (2007), Seismic expression of gas and gas hydrates across the western Black Sea, *Geo-Marine Letters*, 27(2), 173-183.
- Popescu I., M. Debatist, G. Lericolais, H. Nouzé, J. Poort, N. Panin, W. Versteeg, H. Gillet Multiple bottom-simulating reflections in the Black Sea, Potential proxies of past climate conditions. *Mar. Geol.*, 2006, doi:10.1016/j.margeo.2005.12.006.
- Posewang, J., Mienert, J., 1999. The enigma of double BSRs: indicators for changes in the hydrate stability field? *Geo Mar. Lett.* 19, 157–163.
- Reeburgh W., B. Ward, S. Whalen, K. Sandbeck, K. Kilpatrick, L. Kerkhof. Black Sea methane geochemistry. *Deep-Sea Research*, 38, 1991, Suppl. 2, S1189-S1210.
- Ross, D. A., 1978. Summary of results of Black Sea drilling. In: Ross, D.A., Neprochnov, Y.P., et al. (Eds.), *Initial Reports of the Deep Sea Drilling Project*, vol. 42/2. US Government Printing Office, Washington, pp. 1149–1178.
- Ryan W. B. F., C. W. Pitman III, C. O. Major, K. Shimkus, V. Moscalenko, G. Jones A., P. Dimitrov, N. Gorer, M. Sakinc, H. Y. Seyir. An abrupt drowning of the Black Sea shelf at 7.5 Kyr BP. *Geo-Eco-Marina*, 1997, 2, 115-126.
- Schmale O., J. Greinert, G. Rehder. Methane emission from high-intensity marine gas seeps in the Black Sea into the atmosphere. *Geophys. Res. Lett.* (in press), 32, 2005, L07609, doi:10.1029/2004GL021138.
- Sedimentation in Submarine canyons, fans and trenches, Stroudsburg, Pennsylvania, 1978, p. 395.
- Shnyukov E. F., A. P. Ziborov. Mineral resources of the Black Sea (in Russian). NASU, Kiev, 2004.
- Shnyukov EF, Pasinkov AA, Kleshchenko AS, Kutniy VA (2003) The biggest gas jet in the Black Sea depression (in Russian). *Geophysical journal*, NASU, Kiev, 25/2, 170-176.
- Sloan E. D. *Clathrate hydrates of natural gases*, CRC Press, Boca Raton, Fla., 1998, 705 p.
- Sloan E. D. Introductory overview: Hydrate knowledge development. *American Mineralogist*, 89, 2004, 1155-1161.
- Starovoitov A. V., 1985. Black Sea Pliocene-Quaternary sediments structure and gravitational processes on the continental slope and rise (PhD Thesis). Moscow State University M. V. Lomonosov, UDK 551.352:550.834.05(262.5), 185 p.
- Soulet G, Delaygue G, Vallet-Coulomb C, Böttcher ME, Sonzogni C, Lericolais G, Bard E (2010) Glacial hydrologic conditions in the Black Sea reconstructed using geochemical pore water profiles. *Earth and Planetary Science Letters* 296, 57-66.
- Taylor, M. H., Dillon, W. P., Pecher, I. A., 2000. Trapping and migration of methane associated with the gas hydrate stability zone at the Blake Ridge Diapir: new insights from seismic data. *Mar. Geol.* 164, 79–89.
- Чистяков А.А. Условия формирования и фациальная дифференциация дельт и глубоководных конусов. *Итоги науки и техники. Сер. "Общая геология"*, т. 10, М., ВИНТИ, 1980, 164 с.
- Vassilev A., L. Dimitrov. Spatial and qualitative evaluation of methane hydrates in the Black Sea (in English and Russian). *Russian Geology and Geophysics*, 43, 2002, 7, 637-649.
- Verzhbitsky E., I. Kuzin, L. Lobkovsky. *Turkish J. Earth Sci.*, 11, 2002, 231-242.
- Yefremova A. G., Zhizhchenko B. P., 1972. Occurrence of crystalline hydrates from gases in precipitates of present-day oceanic regions (in Russian). *Dokl. Akad. Nauk SSSR* 214, 5: 1179-1181.
- Woodside J, Ivanov M, Limonov A (eds.) (1997) *Neotectonics and fluid flow through*

seafloor sediments in the Eastern Mediterranean and Black Seas' Part II. IOC Technical Series No 48, UNESCO.

Woodside J. M., D. I. Modin, M. K. Ivanov. An enigmatic strong reflector on subbottom profiler records from the Black Sea – the top of shallow gas hydrate deposits. *Geo-Mar. Lett.*, 23, 2003, 269-277.

Zillmer M., E. R. Flueh, J. Petersen, 2005. Seismic investigation of a bottom simulating reflector and quantification of gas hydrate in the Black Sea. *Geophysical Journal International*, 161 (3), 662–678. doi:10.1111/j.1365-246X.2005.02635.x.

11 Appendix

11.1 Regional setting

Atanas Vasilev

11.1.1 Introduction

Gas hydrates (GHs) are one of the most important geological objects today. Only one percent of the methane trapped in them could solve the global energy problem for centuries (Sloan, 2004) or make the planet's climate unbearable (Henriet & Mienert, 1998). The global amount of methane in GHs is enormous, but estimates are speculative and range about $(30-7,500) \cdot 10^{15} \text{ m}^3$ (Sloan, 2004). The world deposits of organic carbon in GHs are 2 times higher than in recoverable and unrecoverable fossil fuels (Johnson, 2006).

The Black Sea deep waters (87% of the total volume) are the biggest anoxic, hydrogen sulphide and methane reservoirs of the world (Reeburgh et al. 1991). The amount of dissolved methane of 96 Tg is 2.4-6 times greater than the global annual geological methane contribution to the atmosphere. However, preliminary surface flux estimations are far too inaccurate ranging from less than 70 Mg/y (McGinnis, 2005) to 50-210 Gg/y (Kessler, 2006). GHs and their contribution to the methane budget are an important part of the problem.

The NW Black Sea margin is marked by deltaic deposits from major rivers with significant sediment supply - the Danube, the Dniepr and the Dniestr. The deep basin consists of large and thick organic-rich fan complexes and the periodical sea bottom anoxia created favourable conditions for gas generation.

11.1.2 Regional Geology of the Black Sea

11.1.2.1 Morphology

The morphology of the basin reflects this evolution: the continental shelf is narrow along the surrounding compressional belts (20–40 km), and considerably wider in the NW Black Sea (up to 190 km). A relatively steep slope (2.5%) lies between the shelfbreak (100–140 m water depth) and a flat abyssal plain (2,200 m) (Ross et al., 1974).

Three types of continental slopes are described in the first geomorphological zoning of the Black Sea (Goncharov et al., 1972):

- with steep slope angles of 6-10°, up to 20-30°, and numerous valleys - SW of the Crimea;
- with smoothed relief - bottom angles 1-3° and U- shape valleys in the upper part of the slope - Bulgarian sector and S of the Kerch Strait;
- both - flat and more steep areas - a wide area from cape Kaliakra to the Crimea.

MSM34&35 area is located in the NW continental slope of the Black Sea (fig. 11.1.1) and is diagonally crossed by the Viteaz Canyon. The area is restricted between water depths of 300 m at NW part to 2000 m at SE. The continental shelf is wide (50-100 km) but not exceptionally wide as the Ukrainian shelf. The shelf break occurs at a water depth of approximately 130 m.

11.1.2.2 Black Sea basin evolution

The Black Sea is a semi-isolated extensional basin with maximum water depth of 2212 m. At the level of the crystalline basement (fig. 11.1.2 & 3), the Black Sea consists of two basins - Western and Eastern, separated by the Mid-Black Sea ridge: Andrusov Ridge to the NW, and Arkhangelskiy Ridge to the SW. The area is part of the Alpine folded belt, including the Pontides-Balkanides, the Caucasus, the Crimea Mountains and the Moesian and Scythian platforms. They form the marginal part of the basin, shelf and continental slope of the Black Sea (Tugolesov et al., 1985; Finetti et al., 1988; Robinson et al., 1996; Nikishin et al., 2003).

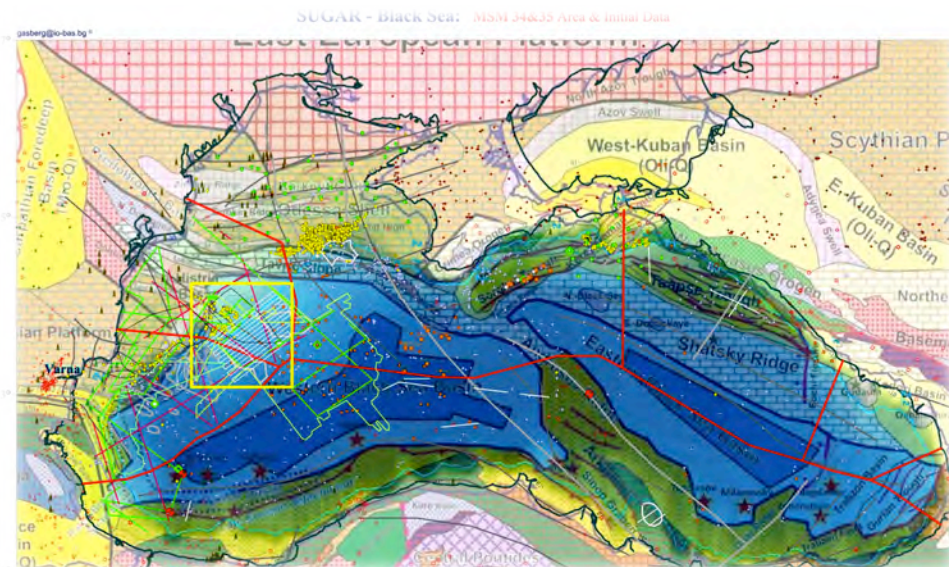


Figure 11.1.1 After Nikishn et al, 2013

The Black Sea depression formed from the Late Cretaceous to the Eocene (Dercourt et al. 1986; Zonenshain and Le Pichon 1986; Gorur, 1988, Rangin et al. 2002) as a marginal back-arc extension on a cold and thick lithosphere (Spadini et al., 1996) from the northward subduction of the Thetian plate (Tethys Ocean; African and Arabian plates) (e.g. Robinson et al. 1995) under the volcanic arc of the Balkanides and Pontides. The Western Black Sea is structurally distinct from the Eastern Black Sea, as these two basins have different ages and coalesced only in their post-rift phases. The western Black Sea opened in the Cretaceous (Upper Barremian to Cenomanian) (Finetti et al., 1988).

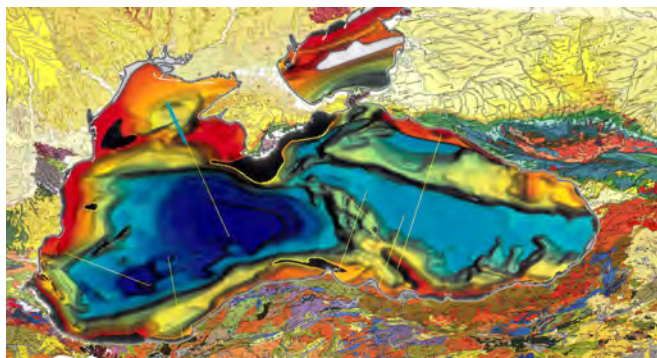


Figure 11.1.2 Robinson et al.,

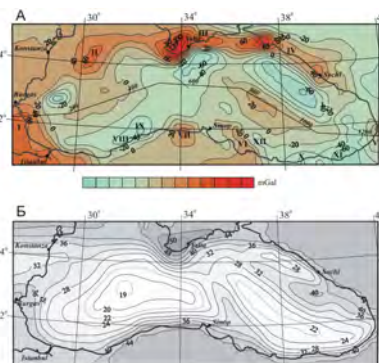


Figure 11.1.3 Starostenko et al. ,

Although the Black Sea is primarily of extensional origin, most of its margins are with compressive deformation. Until the Miocene, regional compression affected the margins of the basin to the south (in the Pontides), southwest (in the Balkanides) and northeast (in Crimea), but had only a minor effect on its north-western part (Robinson et al., 1995).

The Black Sea is widely recognized as a back-arc basin, but the details of its evolution are still discussed (Саваренский, Вольднер, 1960; Миндели и др., 1965; Сорский, 1966; Мелихов и др., 1971; Гончаров и др., 1972; Муратов, 1972; Адамия и др., 1974; Ross et al. 1974; The Black Sea, 1974; Маловицкий и др., 1975; Яншин и др., 1976, 77, 80; Letouzey et al., 1977; Intlat Reports, 1978; Геологическая история, 1980; Геолого-геофизические исследования, 1980; Тектоника и история развития, 1981; Лимонов, 1981; Sengor, Yilmaz, 1981; Туголесов и др., 1983, 85; Zonenshain & Le Pishon, Моргунов и др., 1983; 1986; Finetti et al, 1988; Okay et al., 1994; Милановский, 1996; Robinson et al., 1997; Ustaömer and Robertson, 1997; Копп, Щерба, 1998; Шлезингер,

1998; Короновский, Демина, 1999; Dercourt et al., 2000; Казьмин и др., 2000; Хаин, 2001; Лисицын, 2001; Nikishin et al., 2003; Besutiu & Zugravescu, 2003; Kutas, 2003; Коболев, 2003; Starostenko et al., 2004; Лобковский и др., 2004; Галушкин, 2007; Афанасенков и др., 2007).

The hypotheses about the Black Sea genesis and evolution in chronological order are:

- Suess (1909) named Tethys Sea the aquatory corresponding to marine sediments found all over in the belt of mountains from the Alps to the Himalayas;
- Alfred Wegener created the theory of continental drift (*Kontinentalverschiebung*) in 1912. His hypothesis was not widely accepted until the 1950s, when numerous discoveries such as paleomagnetism provided strong support for continental drift. In 1981 the modern model of plate tectonics was officially adopted in the USSR on a conference of the Institute of Oceanology in Moscow;



- The Black Sea is a giant graben arisen during the Neogene or even the Quaternary in the place of an extensive land - Pontides, which united the Crimea and Asia Minor (Dobrynin, 1922; Andrusov, 1965/Добрынин, 1922; Андрусов, 1965);
- The Black Sea is a geosynclines at the stage of deepening and widening by a system of faults parallel to the axes of the surrounding mountains from the late Pliocene or a little earlier (Archangel , Strakhov, 1938/Архангельский, Страхов, 1938);
- Geophysical investigations of the Black Sea discover basin area with lack of granite layer (Savarenskiy, Voldner, 1960; Mindeli et al., 1965; Neprochnov, 1976; Belousov et al., 1988/ Саваренский, Вольднер, 1960; Миндели и др., 1965; Непрочнов, 1976; Belousov et al., 1988) which gave rise to a number of new hypotheses;
- The Black Sea was formed by continental crust oceanisation converting the granite layer in the basalt (Belousov, 1962; Yanshin et al., 1980; Schlesinger , 1981/Белоусов, 1962; Яншин и др., 1980; Шлезингер, 1981);
- One explanation for the absence within the granitic layer of the Black Sea was the hypothesis of its oceanic origin (Milanovskiy, 1967/Милановский, 1967);
- Lack of granite layer within the Black Sea received an explanation in the ideas about the newly formed earth crust due to horizontal extension (Kropotkin, 1967 , Adam et al., 1974/ Кротопкин, 1967, Адамия и др., 1974). The Black Sea is a rift structure - extension of Adjara-Trialet trough, filled mainly with Paleogene and later volcanic-sediments. It appeared on the hard, long uplifted and intensively eroded up to the Late Cretaceous pre-Alpian fundament which actively sinks from the Paleogene;
- For a long time the Black Sea basin was considered very young - late Miocene or Pliocene-Quaternary (Muratov, 1972/Муратов, 1972);
- Accounting for the very thick sedimentary cover the age of the oceanic structure was estimated at 200 million years or more (Goncharov et al, 1972/Гончаров и др., 1972);
- The transformation of the basalt layer into denser rocks (garnet granulites and eclogite), leading to their subsidence into the mantle, is considered as a mechanism of the basin formation, too (Artyushkov et al, 1979 , 1993 , 2000/ Артюшков и др., 1979; 1993; 2000);
- Reconstructions of paleo-Tethys obtained quantitative characterization with the advent of the concept of plate tectonics (New global tectonics, 1974/ Новая глобальная тектоника, 1974). Most modern are reconstructions in the frame of the project

"Tethys" (History of ... , 1987/ История..., 1987) and their continuations (Dercourt, 1992; Dercourt et al., 2000). They consider that the Alpine-Himalayan fold belt was born from the collision of surrounding Tethys continents - Eurasia, Africa and India;

- The Black Sea crust without granite is a relict of the oceanic crust of the older (Late Palaeozoic-Triassic) ocean Thetis (Сорохтин, 1974; Вардапетян, 1981);
- Further is formulated the idea of the basin formation as a back-arc basin behind the Pontides volcanic island arc during spreading of the continental crust (Adamia et al , 1974 ; Letouzey et al., 1977/ Адамия и др., 1974; Letouzey et al., 1977). These studies were continued and developed in the works (Koronovskii, Demin, 1996; 1999; Lomize et al, 2001; Nikishin et al, 1997; 2001; 2005; Afanasenkov et al., 2007; Galushkin, 2007; Kopp, Szczerba, 1998; Kaz'min et al, 1998; 2000; Hain, 2001; Patalakha et al., 2003, Structure..., 1992; Shniukov, Ziborov, 2004; Lobkovskii et al., 2004; Dewey et al., 1973; Okay et al., 1994; Robinson et al., 1997/ Короновский, Демина, 1996; 1999; Ломизе и др., 2001; Никишин и др., 1997; 2001; 2005; Афанасенков и др., 2007; Галушкин, 2007; Копп, Щерба, 1998; Казьмин и др., 1998; 2000; Хаин, 2001; Паталаха и др., 2003; Строение..., 1992; Шнюков, Зиборов, 2004; Лобковский и др., 2004; Dewey et al., 1973; Okay et al., 1994; Robinson et al., 1997). Possible kinematics of the deep basin formation is associated with the change of the northern continental drift with southern and the emplacement of subduction zone (Ломизе, Панов, 2001);
- According to Nikishin et al.(2001, 2003), the Black Sea began to form as a back-arc basin in the Early Cretaceous. The earth crust began splitting at the end of Alb as a result of continental rifting along the axis of the Albian volcanic arc. In Cenomanian-Cognac rifting led to the disclosure of a deep-water trough with a highly thinned continental and/or oceanic crust, and synchronous formation of two depressions - West and East. The Black Sea region was in a compression phase from the late Santonian to late Paleocene and in the Eocene in the eastern depression manifested a new phase of extension that led to the formation of Adjara-Trialet rift. The region is in compressional environment beginning in the late Eocene to the present time. Prompt additional sink of the basin in the Pliocene-Quaternary is associated with regional compressive stresses;
- Some models suppose the formation of eastern and western parts in different times: Western - on early-late Cretaceous, Eastern - in the Late Cretaceous and Paleocene-Eocene (Okay et al., 1994; Robinson et al., 1995; Golonka, 2004), other - the simultaneously - in the Late Cretaceous (Nikishin et al., 1997, 2001; Wierzbicki et al, 2003/Никишин и др., 1997, 2001; Вержбицкий и др., 2003);
- The age of the deep depressions in the History... (1987/История..., 1987) is defined as the Late Cretaceous-Early Paleocene and to the 130-95 million years in the works (Golmshtok , fancy man, 1987; Golmshtok et al., 1992/Гольмшток, Хахалев, 1987; Golmshtok et al., 1992) with 110 Ma most likely for the eastern basin (Golmshtok et al., 1992). For Zonenshain & Le Pichon (1987) the age of disclosure of the Black Sea basins corresponds to the end of the Senonian (89.3-65.5 Ma). Schroeder et al. (1997) suggest the existence of a short-term episode of spreading in the deep eastern part later 83.5 Ma ago. Similar result is obtained from the interpretation of heat flow data (Wierzbicki et al., 2003/Вержбицкий и др., 2003); CHECK KOSTYANEV CALCS!
- Tectonic disturbances are not depicted uniform in the literature. Finetti et al. (1988) traced a fault - continuation of the Pecheneg-Kamena (Banks, Robinson, 1997; Kaz'min et al, 1998; Hauser et al., 2001/Казьмин и др., 1998) from the north of Constanta south-east to the latitude of Varna. This fault is the most important link of the transcontinental Tornquist tectonic line (or Tornquist-Teyssere (Hippolyte, 2002). For Kopp (1996/Копп, 1996) this fault takes a different position. On Fig. 1 from his

work the Tornquist line goes from Odessa to the Crimea and continues in the eastern basin, while on Fig. 3 of the same work, she goes to the south and partly crosses the West Crimean fault from the work of Finetti et al. (1988). West Crimean fault for Finetti et al. (1988) cannot be traced to the south of 43°N, while in the works (Okay et al., 1994; Okay, Sahinturk, 1997), it crosses the basin and continues further south within the Turkish coast;

- Scythian plate has a late Hercynian foundation in the north of that experienced deformation in the Late Triassic-Early Jurassic, in the South Crimean orogen main phases of deformation occurred in pre-Bajocian, pre-Callovian and Berriasian time. Orogen Greater Caucasus was formed in the late Cenozoic. To the west of the Black Sea basin is located Moesian platform which has Precambrian basement. Between the Scythian and Moesian plates is located North Dobrogea area, which has a Hercynian basement.

11.1.3 Regional Geology of the NW Black Sea

11.1.3.1 Tectonic

Structurally, this part of the Black Sea forms the transition zone between the Moesian Platform in the west, Scythian Platform in the north and the Western Black Sea Basin in the southeast (Nikishin et al., 2003). Structural styles of the Moesian and Scythian Platforms are significantly different (Fig. 11.1.4).

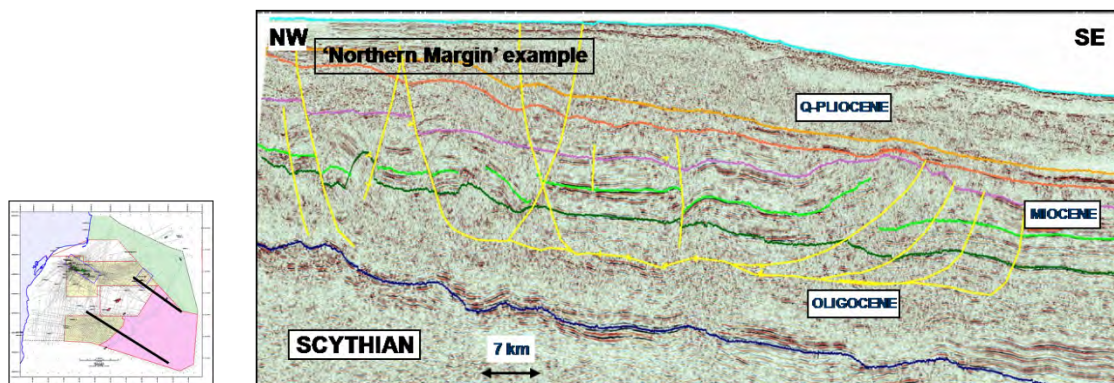


Fig 11.1.4 A mosaic of structural styles; thrusting, folding, toe-thrust and growth. All tectonic deformations are due to gravity-driven tectonics; mainly Miocene timing (Bega et al., 2012)

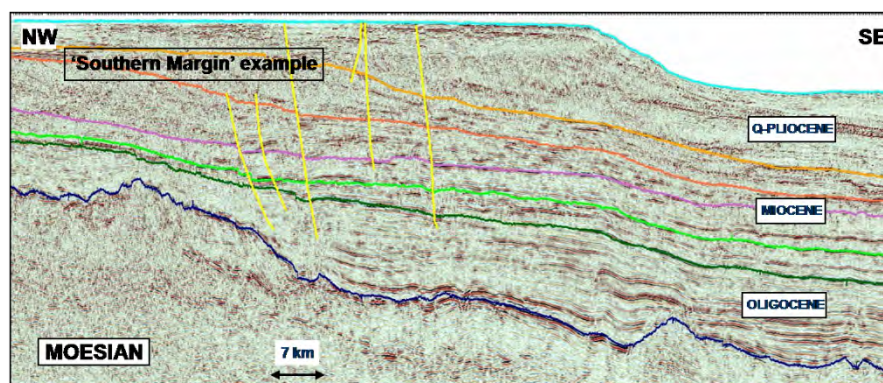


Fig 11.1.5 Rather quite area regarding structuration; mainly normal faults (tilted blocks), associated with growth, with some surface expression (Bega et al., 2012).

The area is bounded on north and west by fault systems (Fig. 11.1.5). To the northeast the area is bounded by the present shelf break which has been associated with the East Moesian fault zone. The East Moesian trough and the Polshkov ridge (syn-rift Polshkov High) are located eastern from the East Moesian fault (most western in the MAM34&35 area).

The Polshkov High is the deepest exploration target with a trap defined by several fault

blocks in which the assumed Jurassic/Lower Cretaceous carbonate platform sequence may have a reservoir facies suitable for deepwater gas production (Tari, 2009). The target of this play is analogous to the ones targeted over the Andrusov Ridge offshore Turkey or over the Tetyaev High off shore Ukraine.

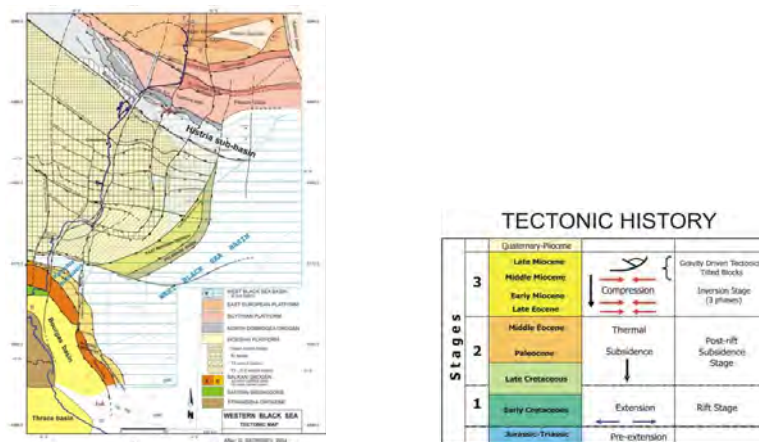


Figure 11.1.6 Georgiev, 2004

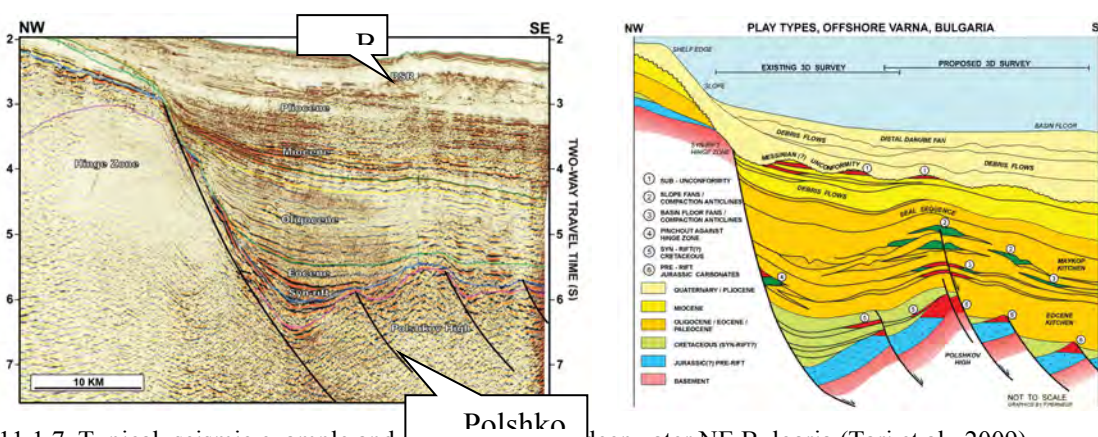


Fig 11.1.7 Typical seismic example and play types from deepwater NE Bulgaria (Tari et al., 2009)

Two faults starting from the area of the present Danube delta reach the northeastern and the southwestern corner of the area. Axis of the area, bounded of these faults, is the marine Peceneaga-Camena fault, which generally follows the last (main modern) levee-channel. The Peceneaga-Camena fault and the marine continuation of the Sinoe fault bounded the Histria Sub-basin on shelf and Babadag basin onshore.

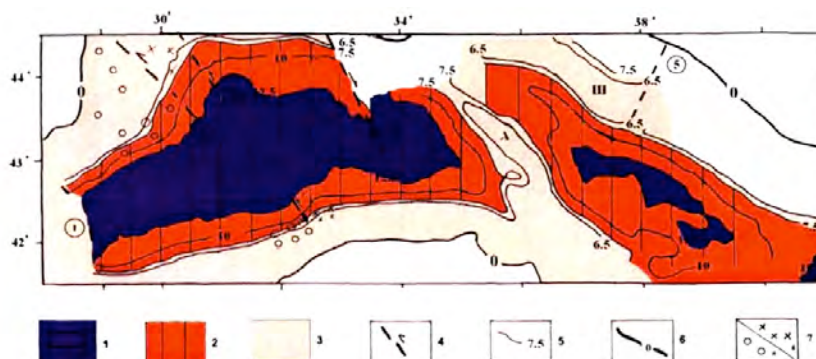


Figure 11.1.8. Sreider, 2008)

In Shreider (2008) the superimposition of 12.5 km depth contours in the Black Sea allows (Ris.4.13) to restore the configuration of the major rupture of continental lithosphere under

stretching and dock (within the error of 6 km) the fault on the northern shelf and continental slope (sea continuation of the Pecheneg-Kamen fault) and the fault on the southern continental slope of Western depression, known from the work of Finetti et al. (1988). Pechenenga-Kamen fault is the north-eastern boundary of the Moesian plate separating it from North Dobrogea Orogen (Nikishin et al., 2001; Kaz'min et al, 2000/Никишин и др., 2001; Казьмин и др., 2000). St. George fault divides the North Dobrogea orogen and Scythian plate (Hippolyte, 2002). It seems logical to associate marine continuation of Pechenenga-Kamena and St. George faults (Ris.4.15) such as marking the limits of maritime extensions of the Moesian plate, North Dobrogea Orogen and the Scythian plate. According to Shreider (2008) superimposition the Pechenga-Kamena fault is traced on the Turkish slope and thus indicates that after the split a part of Moesian plate moved south and now is a part of the Turkish continental slope. This conclusion is in agreement with the position (Hain, 2001; Nikishin et al., 2001; Nikishin et al., 2003) that Western Pontides have a foundation similar to the foundation of the Moesian plate.

It is known that in the Pliocene-Anthropogene Black Sea depression has experienced uncompensated sinking (Nikolaev, 1970; Muratov, 1972). At the same time in the peripheral fold areas of the Crimea, the Caucasus, the Balkans and the Pontides has undergone substantial uplifts (late orogenic stage by E.E. Milanovskomu, 1970/Е.Е.Милановскому, 1970).

Thus, the available data show that at the periphery of the Black Sea basin from the late Pliocene, there were significant uplift with a tendency to strengthen in the late Pleistocene and Holocene.

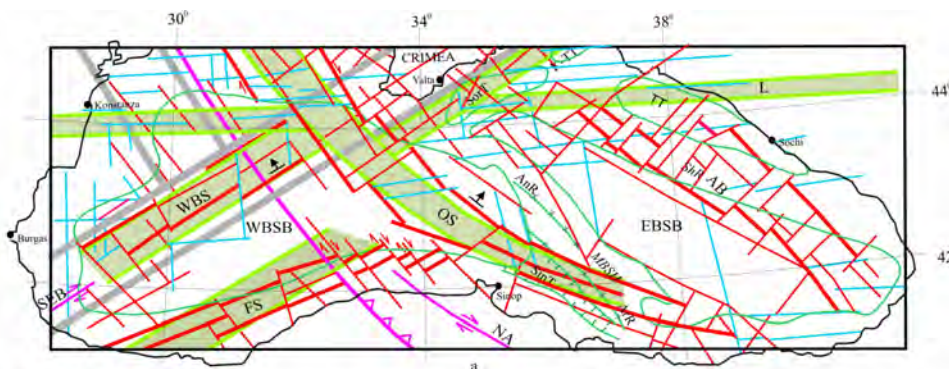


Figure 11.1.9 Fault systems in the Black Sea basin consolidated crust by geophysical data (Makarenko et al., 2008)

11.1.3.2 Sediment structure

Two deep basins are underlain by oceanic or thinned continental crust. The under-lying basaltic crust of the deep basins does not exceed 5–15 km in thickness (Tugolesov et al. 1985; Finetti et al. 1988). On the basin periphery, however, the continental crustal thickness reaches up to 40–50 km.

They are filled with Meso-Cenozoic sediments with a total thickness of 16–18 km in the Western basin and 12–14 km in the Eastern basin (Tugolesov et al. 1985). Sediments in the western part including 4–5 km of folded Maikopian deposits (Oligocene-Lower Micene) and 2–3 km of Cenozoic deposits (Tugolesov et al., 1983; Finetti et al., 1988). Cenozoic stratigraphic complexes become thinner or completely disappear on the basin periphery. The Andrusov Ridge is with continental crust and is overlain by only 5–6 km of sediment. In the central part of the basin, the sedimentary cover is characterized by subhorizontal stratification, whereas its offshore parts contain asymmetric folds and thrusts.

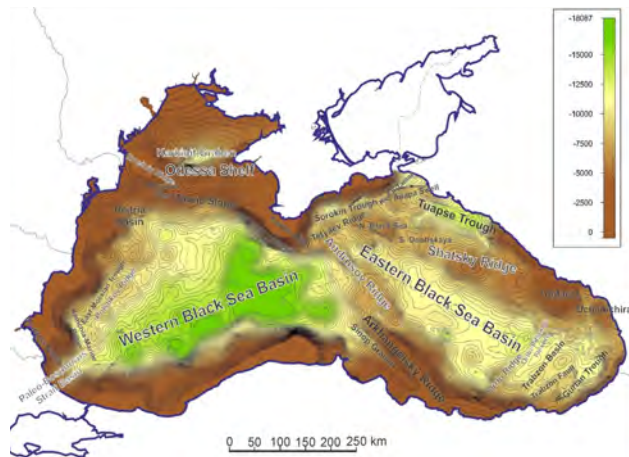


Figure 11.1.10 Basement topography of the Black Sea Basin. This map is based mainly on data of new seismic lines (Nikishin et al., 2013)

Stress field observations show that the region is still in a dominantly compressional environment (Reilinger et al. 1997; Nishishin et al. 2003). The compressional environment resulted from the collision between the Arabian, Anatolian, and the Eurasian Plates. The tectonic evolution of the basin is nevertheless characterized by alternations of extensional and compressional phases and by different stages of subsidence (Nikishin et al., 2003).

11.1.3.3 The Messinian event in the Black Sea

The Messinian event in the Black Sea, i.e. a sudden sea level drop and then its fast rise, was well substantiated [2]. We have available additional data on the scale of this event. On Line BS-050 on the Odessa Shelf, a thick wedge of sediments is distinctly singled out, which is overlain by Pliocene deposits. This wedge corresponds to a fast drop of the sea level in Messinian (Pontian) and high-rate clastic sedimentation and then a fast recovery of the sea level in Pliocene.

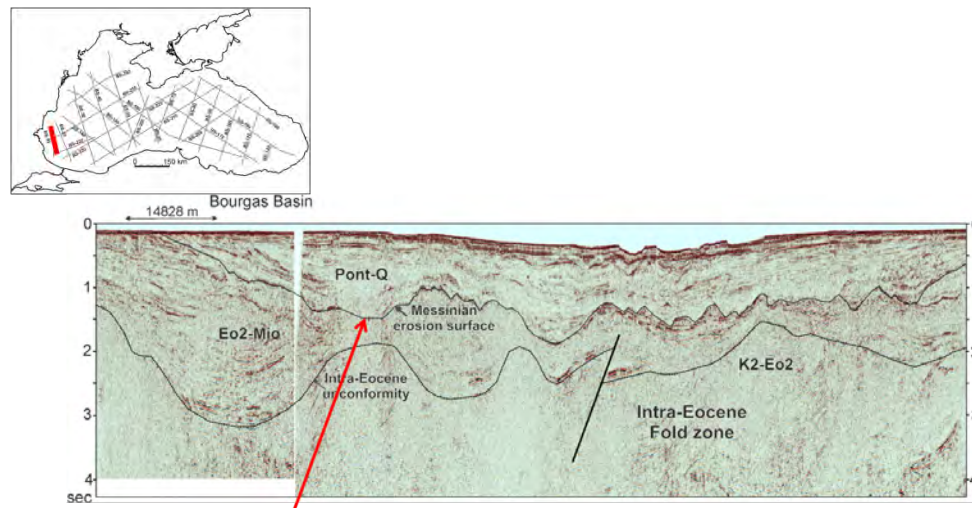


Figure 11.1.11 Geological interpretation of seismic line BS-10. An erosional surface is well recognized in this profile. We interpret this surface as Messinian erosion surface which originated due to rapid sea level fall. This Messinian event was discussed in a number of publications (Sac et al., 2011; Munteanu et al., 2011, 2012; Barche et al., 2012).

On Line BS-10 (Fig. 11.1.11), an erosional boundary is distinctly seen approximately at the level of the boundary of the Neogene and Quaternary. This boundary may be the Messinian (Intra-Pontian) erosional boundary proper, which shows the phase of a considerable drop of the sea level. Exact correlation of stratigraphy and events in the

Messinian in the Mediterranean and the Black seas still remain a problem.

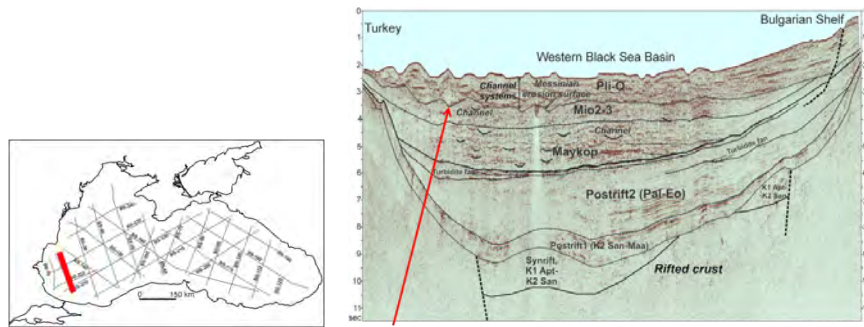


Figure 11.1.12 Geological interpretation of seismic line BS-20. Messinian erosion surface is well recognized

11.1.3.4 Danube levee system

The adjacent continental areas are drained mainly from Danube and Dnieper. Sedimentation in the northwestern Black Sea large deep-sea fan complexes is controlled by climate and sea-level change (e.g., Wong et al. 1994; Ryan et al. 1997; Aksu et al. 1999; Winguth et al. 2000; Gorur et al. 2001).

In the Pliocene Danube unloaded its waters in an outer Carpathian Lake (present Carpathian Trough) and flows into the Black Sea from the Anthropogene (Trimonis, 1980; Tugolesov, Meisner, 2002/ Тримонис, 1980; Туголесов, Мейснер, 2002).

Glacial periods are characterized by high sedimentation rates, because in the Pleistocene, simultaneously with the Black Sea bottom lowering, Russian plate, Central Europe and Scandinavia are uplifted. This contributed to the widespread of turbidities, which are more and thicker at the bottom of the formation, which is probably due to the high energy and youth of the drainage system.

In the northern part of the Bulgarian aquatory is located the south part of Danube underwater fan (Maev et al., 1980; Starovoytov et al., 1986/ Маев и др., 1980; Старовойтов и др., 1986), which is clearly visible in the morphology of the continental rise with a relative height of 120-150 m. Seismo-acoustic profiling identified on the fan surface several valleys with erosion origin. They have a width of 1-2 km and are filled with thin-layered sediments with a total thickness up to 200 m (Fig. 11.1.13). In the first works Danube alluvial fans includes all flat northwestern continental slope of the Black Sea and the age of the cone was dated as Pleistocene (Ross et al., 1974).

Modern valleys on the Bulgarian continental slope also apply to the Middle Pleistocene-Holocene - they are embedded in sediments of this age. Exception is the valley of Rezovska (on the boundary Bulgaria-Turkey), which partially eroded early Pleistocene sediments. Filling of some valleys with sediments indicates some attenuation of the erosion processes.

The most intense phase of the gravitational movements, resulted in a huge landslide body at the base of the continental slope (sediments with irregular stratification), timed to the Dnieper glacial epoch. All younger sediments that overlie this body have a simple parallel-layered structure with no signs of landslides.

The sedimentary architecture of this zone is dominantly determined of the turbidite system of the Danube deep-sea fan. This is the largest mud-rich fan in the basin, composed of a of stacked channel–levee systems that are emplaced during sea-level lowstands (Wong et al., 1994; Popescu et al., 2001). Channel–levee systems in mud-rich fans are lenticular sedimentary units with coarse-grained sediments at the channel axis, and fine grained, alternations of sand and mud in the lateral levees (Manley et al., 1997; Normark et al., 1997).

Fig 11.1.13 Lericolas et al., 2007, 2010

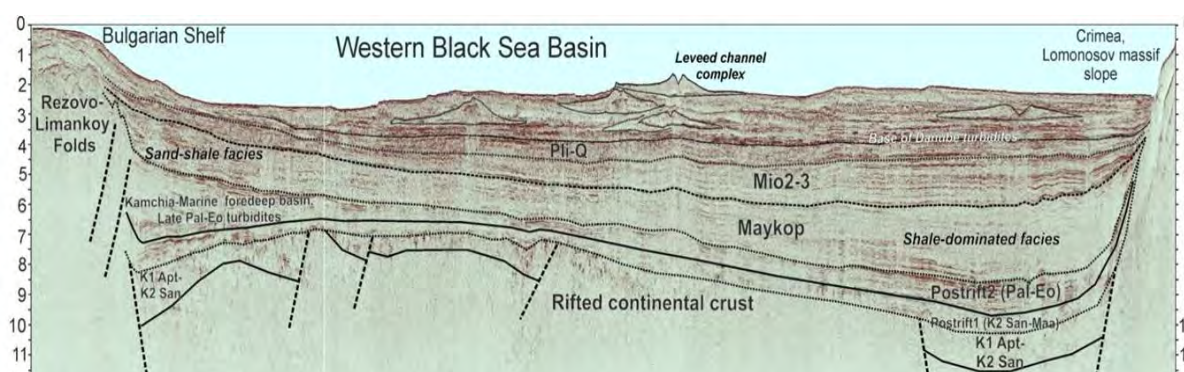


Figure 11.1.14 BS-230: Geological interpretation of seismic line BS-230. Large channel-levee complexes are seen between Bulgarian and Crimea continental slopes. A bottom of this complex is close to Miocene/Pliocene boundary. Danube delta origin is close to Messinian erosion event according to interpretation of this seismic line.

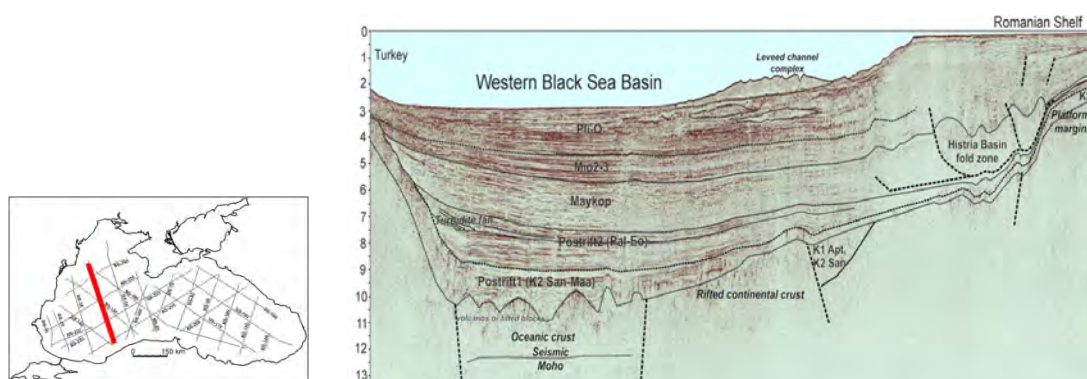


Figure 11.1.15 BS-40: Geological interpretation of seismic line BS-40. Channel-levee complex of Danube distal delta part is well presented. This complex was known before (Lericolais et al., 2010; Munteanu et al., 2012). Data show a big thickness of this unit.

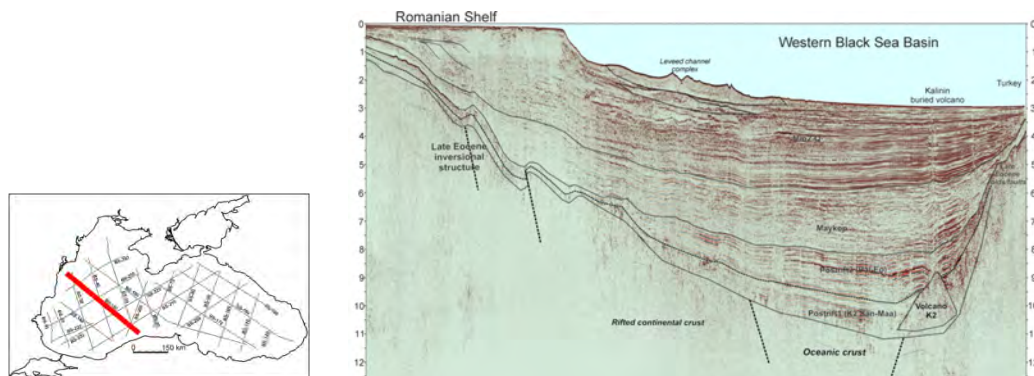


Figure 11.1.16 BS-150: Geological interpretation of seismic line BS-150. leveed channel complex are well seen on this line.

Only one channel–levee system in the Danube fan was active at a time (Popescu et al., 2006). The most recent system is the Danube channel overlays older channel–levee systems and is directly connected to the Danube canyon (Popescu et al., 2001). Fan growth is interrupted since the last sea-level rise (Popescu et al., 2001). It is seen on lines BS-40, BS-50, BS-150, BS-230 (Fig. 11.1.14 & 15 & 16) that such depositional systems are formed all over the Pliocene-Quaternary time. This system formed probably coeval with the Danube Delta (Nikishin et al., 2013).

At the same location is found one of the cones of the Danube (Moiseev Ridge) previously accepted for a fundament raise (Kazantsev and Shayyaurov, 1978). Sediment thickness in the central part of the cone is 600 m, and the age is estimated as late Pleistocene-Holocene.

As a rule, the main processes with a significant impact on the amount of sediments, are changes in sea level and tectonic regime (Damuth and Kumar, 1975; WatKer, 1978; Curray, Moore, 1971; Leontiev Safyanov, 1973; Damuth and Kumar, 1975; WatKer, 1978; Curray, Moore, 1971; Леонтьев, Сафьянов, 1973). At low sea level standing during glacial periods sediments were transported directly on the slope and the intensity of gravitational processes sharply increased. At this time often occurred over-deepening of channels in the canyons and cone valleys. Pelagic or hemipelagic sedimentation dominated in interglacial epochs and their strata is characterized by well-defined stratification.

Due to high freshwater supply from several rivers (e.g. Danube, Dnepr, Dniester, Don), surface waters have low salinities (17–18 psu), while deep waters are affected by the inflow of highly saline Mediterranean waters via the Bosphorus (~22.5 psu). As a result of different salinities, a persistently stratified water column with limited vertical mixing evolved, which caused permanently anoxic conditions at depths exceeding approximately 150 m (Uszöy and Ünülat, 1997).

In the Black Sea gas plumes in the water column have also been recorded at around 5000 locations (Bohrmann, 2002). In the Danube paleo-delta the deposition of organic-rich sediments and the subsequent microbial degradation has led to the formation of shallow gas in the sub-bottom and also prolific gas seepage into the water column (Naudts et al., 2006). The area is characterized by active seepage up to water depths of 800 m.

11.1.4 Additional References

BSR

Dondurur D., G. Cifci, 2009. Anomalous Strong Reflections on High Resolution Seismic Data from the Turkish Shelf of the Eastern Black Sea: Possible Indicators of Shallow Hydrogen Sulphide-Rich Gas Hydrate Layers. Turkish J. Earth Sci., Vol. 18, 2009, 299–313. doi:10.3906/yer-0801-1.

Tari G., J. Davies, R. Dellmour, E. Larratt, B. Novotny, E. Kozhuharov, 2009. Play types

and hydrocarbon potential of the deepwater Black Sea, NE Bulgaria. The Leading Edge, SEG, Special section: The Black Sea Region, 1076-1081.

Kruglyakova R. P., A. Byakov, L. A. Chalenko, N. T. Shevtsova, 2004. Natural oil and gas seeps on the Black Sea floor. *Geo-Mar Lett* (2004) 24: 150–162. DOI 10.1007/s00367-004-0171-4

Minshull T. A., N. J. White, R. A. Edwards, D. J. Shillington, C. L. Scott, A. Demirer, M. Shaw-Champion, S. M. Jones, M. Erduran, T. Besevli, G. Coskun, K. Raven, A. Price & B. Peterson, 2005. Seismic Data Reveal Eastern Black Sea Basin Structure. *Eos*, Vol. 86, No. 43, 413-428.

Minshull, T., Keddie, A., 2009. Measuring the Geotherm with Gas Hydrate Reflectors: A Novel Approach Using Three-Dimensional Seismic Data from the Eastern Black Sea. *Terra Nova*, Draft, 11 p.

Vasilev, A., 2010. First Bulgarian Gas Hydrates: Assessment from Probable BSRs. *Geology & Mineral Resources of the World Ocean*, 2, 22-26.

Black Sea Methane

Barkan, Y.S., Voronov, A.N., 1983. Ocienka resursov gaza v zonah vozmozhnogo gidratoobrazovania (Evaluation of gas reserves in zones of possible hydrate formation): *Sovietskaia Geologiya*, 7, 37 - 41.

Bolshakov, A.M., Trotsyuk, V.Y., Lapin, Svinarenko, V.G., 1984. Uglevodorodnie gazi v pridonnoi vode i donnih osadkah (Hydrocarbon gases in the nearbottom water column and bottom sediments) in A. Geodekyan, Y. Trotsyuk, I.V. Monahov eds., *Investigations of oil and gas potential in Bulgarian sector of the Black Sea*, 191-201.

Bryan, G.M., 1974. In situ indications of gas hydrates, in *Natural gases in marine sediments: Marine Sci.*, v. 3, 299-308.

Deuser, W.G., 1971. Organic budget of the Black Sea: *Deep Sea Research*, v. 18, 995-1004.

Deuser, W.G., 1974. Evolution of anoxic conditions in the Black Sea during the Holocene, in E.T. Degens and D.A. Ross, eds., *The Black Sea-- geology, chemistry and biology: Am. Assoc. Petroleum Geologists Mem.* 20, 133-136.

Faber, E., Schmitt, M., Stahl, W., 1978. Carbon isotope analyses of head space methane from samples of Leg 42B, sites 379, 380 and 381, in J.L. Usher and P. Supko, eds., *Initial reports of the Deep Sea Drilling Project*, v. 42, Part 2, 667-672.

Hunt, J.M., and Whelan, J.K., 1978. Dissolved gases in Black Sea sediments, in J.L. Usher and P. Supko; eds., *Initial reports of the Deep Sea Drilling Project*, v. 42, Part 2, 661-665.

Black Sea Tectonic

Adamiya, Sh.A., Gamkrelidze, I.P., Zakaridze, G.S., and Lordkipanidze, M.B., 1974. Adzhar-Trialet trough and the problem of the Black Sea deep water trough: *Geotectonics*, v. 1, 39-47.

Apostoloskiy, O.P., 1974. Origin of the Black Sea and S Caspian Sea troughs: *Geotectonics*, v. 3, 310-321.

Degens, ET, Stoffers, P., Golubic, S., Dickman, M.D., 1978. Varve chronology: estimated rates of sedimentation in the Black Sea deep basin, in J.L. Usher and P. Supko, eds., *Initial Reports of the Deep Sea Drilling Project*, v. 42, Part 2, 499-507.

Malinovskiy, Y.Y., 1967. Problem of origin of Black Sea depression and its position, in *Structure of the Alpine belt: Internet. Geology. Rev.*, v. 9, no. 9, 1237- 1249.

Muratov, M.V., 1975. Geolbical history of the Black Sea depression and the surrounding areas, in *The Earth's crust and the history of development of the Black Sea basin*, Nauka, Moscow.

Neprochov, Y.P., 1962. The results of the deep seismic sounding in the Black Sea, in *Deep*

seismic sounding of the Earth's crust, in the USSR: Gostochizdat, Leningrad, 25-38.

Neprochov, Y.P., Kosminskaya, I.P., and Malovitsky, Y.P., 1970. Structure of the crust and upper mantle of the Black and Caspian seas: Tectonophysics, v. 10, 517-538.

Schrader, H.J., 1978. Quaternary through Neogene history of the Black Sea deduced from the paleoecology of diatoms, silicoflagellates, ebridians, and chrysomonads, in Y.L. Usher and P. Supko, eds. Initial Reports of the Deep Sea Drilling Project, v. 42, Part 2, 789-902.

Data

Erickson, A. J., Von Herzen, R.P., 1978. Downhole temperature measurements and heat flow data in the Black Sea - DSDP Leg 42B, in J.L. Usher and P. Supko, eds., Initial reports of the Deep Sea Drilling Project, v. 42, Part 2, 1085-1101.

Goncharov, V.P., 1958. New data on topography of bottom of Black Sea: Dokladi Akad. Nauk SSSR, v. 121, no. 5, 830-833.

11.2 Equipment of the scientific party

11.2.1 GI-gun

Joerg Bialas, Torge Matthiessen

For the high-resolution seismic acquisition a GI-gun manufactured by *Sercel Marine Sources Division* was used with 45 in³ / 45 in³ volume (Fig. 11.2.1.1). The compressed air was supplied by one of the compressors of R/V MERIAN with a pressure of 200 bar. The GI-gun was attached with chains to a steel frame and towed either from a centre point between the trawl wires or at the port side at 25 m behind the stern in a depth of 2.3 m. A drawing with measures of the gun position is given in chapter 11.2.3.

The profiles were acquired with a shot interval of 3 s. Aiming point of the generator was 95 ms during the first acquisitions. After gun service at the start of line P2400 (07.01.2014 – 00:50 UTC) it was set to 80 ms and remained until the end of the cruise. The injector was fired at a delay of 45 ms.



Figure 11.2.1.1: GI-gun mounted below the carrier to which a Polyform floatation is attached.

11.2.1.1 External trigger

With the development of the 3-D P-Cable system GEOMAR has build its own GPS based trigger system. A GARMIN GPS receiver delivers GGA and PPS to a timing box. The timing box allows selecting the shot interval by a wheel switch in full second intervals. The TTL trigger pulse is delivered to a distribution box, from which the LongShot gun controller and

the Geometrics streamer system receive the signal. Together with the trigger generation a time stamp is written to an internal SD memory card with shot coordinates. GGA and RMC strings are sent out via TCP/IP and serial port from the trigger box for time stamp information of the GeoEel and the shot log files. RMC time stamp information of the shot trigger and the GPS values from the trawl doors are transmitted from a navigation laptop via telnet to the processing linux computer.

To ensure all systems trigger with the same reference all trigger circuits were adjusted to work on the uprising flank (TTL+). The LongShot gun controller was set to 80 ms aim point. The automatic adjustment based on the received shot signal from the gun hydrophone usually was within ± 1 ms.

11.2.2 Seismic navigation MSM-34/2

Joerg Bialas, Stephanie Koch, Gero Wetzel

Several Garmin GPS receivers were set up to provide position information for the various systems. Onboard a GPS antenna was mounted on the winch control cabin (Fig. 11.2.3.1 & 2).

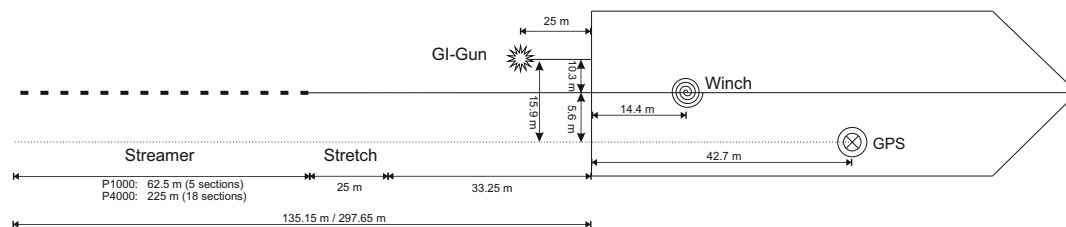


Figure 11.2.3.1: Measures used for the positioning of gun and streamers during the 2D seismic surveys of MSM34 leg-2

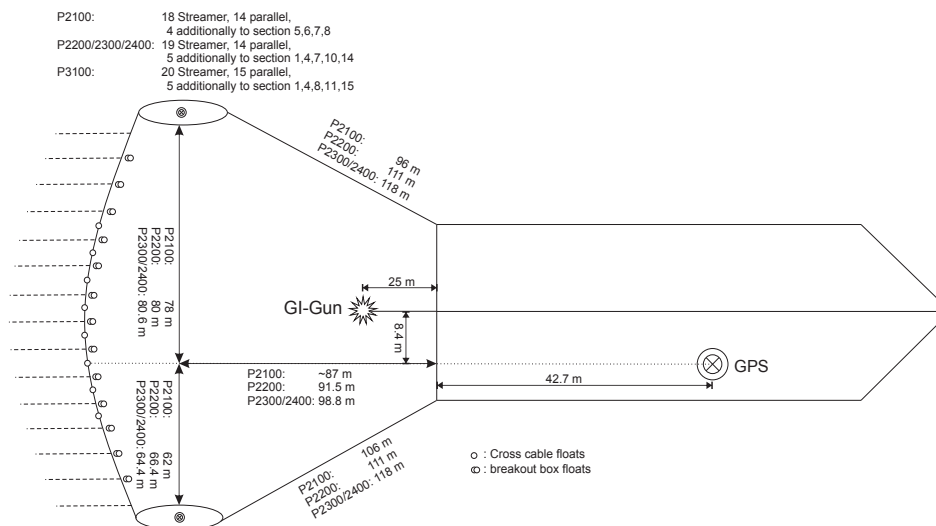


Figure 11.2.3.2: Measures used for the positioning of gun and streamers during the 3D seismic surveys of MSM34 leg-2

Additional Garmin GPS receivers were mounted on the two trawl doors for the 3-D P-Cable system. NMEA strings from the remote GPS were transmitted via radio link onboard R/V MERIAN. RS232 links submitted the position information to the OFOP PC (Fig 11.2.3.3). OFOP was used to display the ships and trawl doors positions on top of a bathymetric map. Track keeping accuracy could be controlled by the display of the waypoints. In addition offsets between trawl doors and trawl door – ship were displayed. A connecting line between the trawl doors is drawn in user-selected intervals. Its width can be adjusted to the expected CDP coverage. Storage of the coverage lines enables to redraw the achieved coverage any time. At the same time the GPS navigation data is processed already for calculation of the real streamer positions. Even in the case one of the trawl door GPS

receivers is lost the cross cable position can be estimated and a true CDP coverage map is provided. At a later stage of the survey the coverage map is used to identify remaining gaps. Additional profiles will then be used to fill the gaps (Fig. 11.2.3.4).

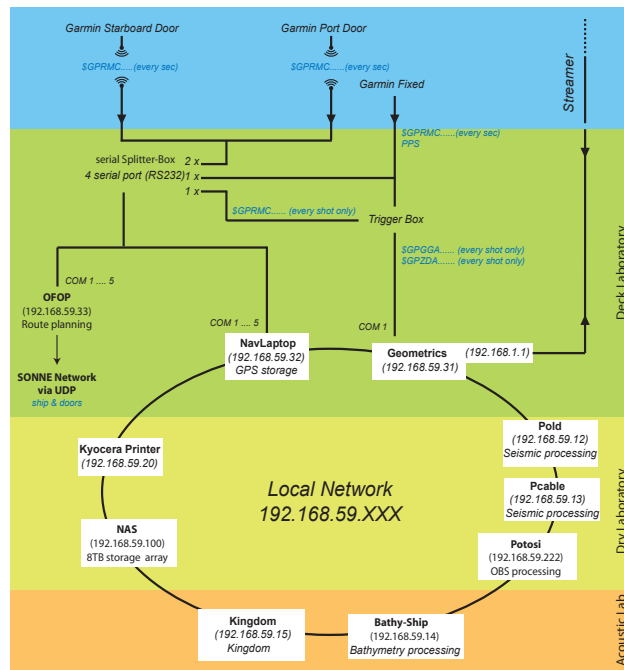


Figure 11.2.3.3: Local Area Network set up for the seismic data handling

With the P-Cable system the streamer sections are not distributed along a straight line. Due to drag forces in the water the cross cable can best be described forming a shape somewhere between a triangular and a half circle. Navigation processing sets out to calculate the exact shape by using the GPS positions of the trawl doors and the first arrival time of the direct wave from the airgun signal. During the course of profiling the trawl doors were affected by water currents and sea state. Therefore offsets between starboard and port side door and the airgun in the centre are varying depending on the heading of the sail line. Based on GPS positions of the trawl doors and the first arrival of the airgun shots at the front most streamer hydrophone the position of each streamer segment is calculated. Triangulation is applied and provides coordinates for the streamer groups within a range of less than 5 m. The assumption of a catenary-shaped outline for the cross cable provides best results (Fig. 11.2.3.5). Based on the resulting shot table interpolation, stacking and migration of the entire data cube can be done.

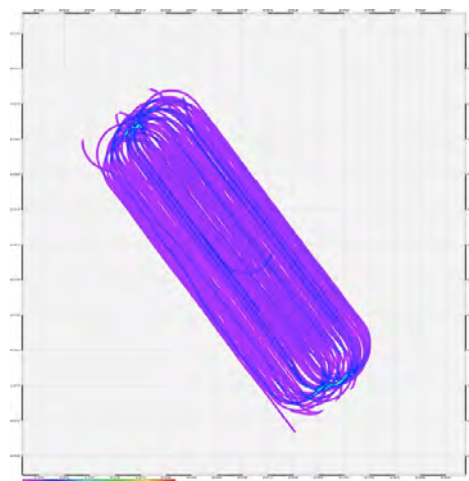


Figure 11.2.3.5: Coverage map from a 3D area. Colours indicate fold on a 3 m by 3 m grid

11.3 Streamer systems

11.3.1 SeisLab 2D streamer

Derman Dondurur, Gunay Cifci

During the MSM-034 seismic survey, the following equipment and systems have been mobilized from SeisLab of Dokuz Eylul University, Institute of Marine Sciences and Technology to onboard of Maria S. Merian for 2D seismic data acquisition:

- NTRS2 multichannel seismic recorder
- Seamux digital streamer
- ION Digibird system
- EIVA NaviPAC navigation system

The block diagram of mobilized equipment as well as communications and the data flow among the systems are given in Figure 11.3.1. The mobilized equipment will be described below in detail.

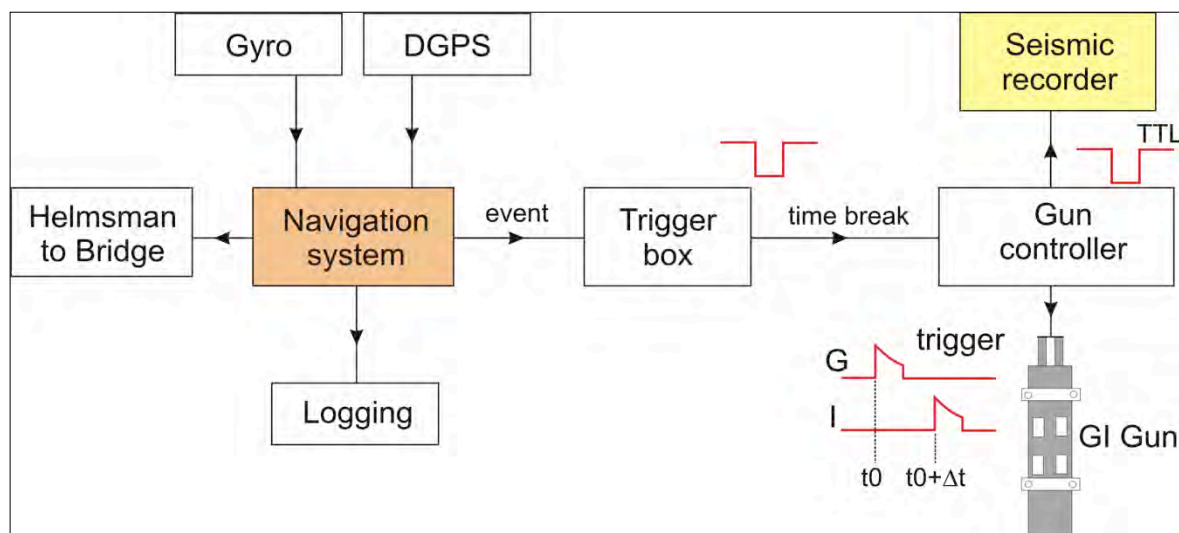


Figure 11.3.1. Block diagram of the systems used during the survey.

The seismic system works in synchronization with several different systems and modules. The components installed on the Maria S. Merian are shown in Figure 11.3.2. The technical specifications of each individual component mobilized from SeisLab are given in Table 11.3.1. The block diagram and streamer with bird configuration are shown in Figure 11.3.3 and Figure 11.3.4, respectively. Distance based shooting was used during the entire survey. Multichannel seismic data acquisition was performed as 7/24 basis. A QC reporting procedure was run immediately after the collection of each line and an onboard QC report was created for each seismic dataset.

When the vessel arrives at a shot point, the navigation system generates an "event" which is sent to the trigger box. This event is transformed into a "falling-edge trigger pulse" and sent to gun controller. The gun controller then triggers the gun solenoids and the seismic recorder simultaneously, and then recording starts. Data is received into one of the free 32 buffers, SegY IEEE header is generated, data is demultiplexed and recorded on the hard drive in a separate IEEE 32 bit SegY format. When the vessel arrives to the next shot point, this sequence starts all over again.

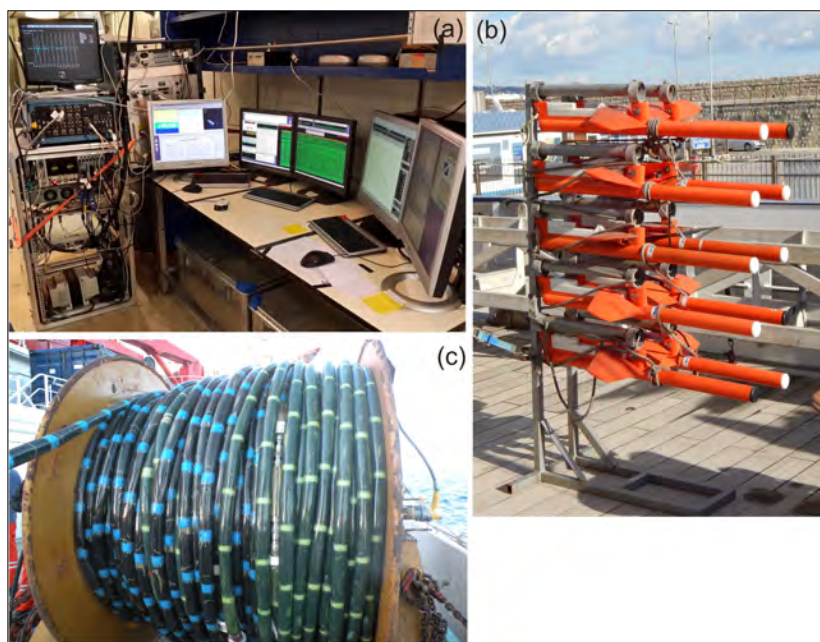


Figure 11.3.2. Photos of the multichannel seismic system installed on the Maria S. Merian. (a) Recording room and seismic recorder, (b) depth levellers (bird), (c) seismic streamer and its winch.

Table 11.3.1. Main specifications of the multichannel seismic system.

MULTI-CHANNEL SEISMIC SYSTEM	
Recorder	HydroScience NTRS–2 System
Number of channels	168
Sampling rates	0.25, 0.5, 1.0, 2.0, 4.0 ms
Record length	45 s max.
Trace summing	2:1, 3:1, 4:1
Max. no of channels	1920 @ 2 ms, 960 @ 1 ms
Data format	SegY 32 bit IEEE
DIGITAL SEISMIC STREAMER	
Model	HydroScience SeaMUX Digital-bidirectional
Number of channels	168
Streamer length	1050 m
Group interval	6.25 m
Cable diameter	51 mm
Number of sections	14x12 channel (14x75 m active sections)
Sampling type	24 bit delta-sigma
No of digitizer module	7 (1 for 2 active sections)
No of hydrophones	8 / group
STREAMER DEPTH CONTROL	
Model	I/O High Res. DMU
I/O 5010 DigiBird	7
I/O 5011 DigiBird	3

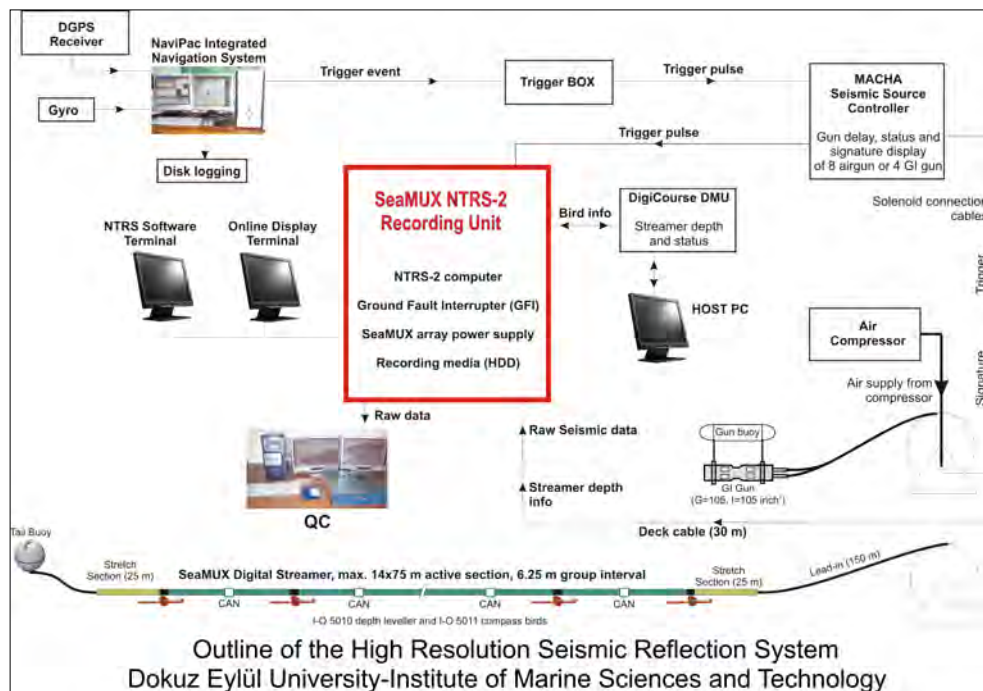


Figure 11.3.3. Block diagram of the entire 2D multichannel seismic system.

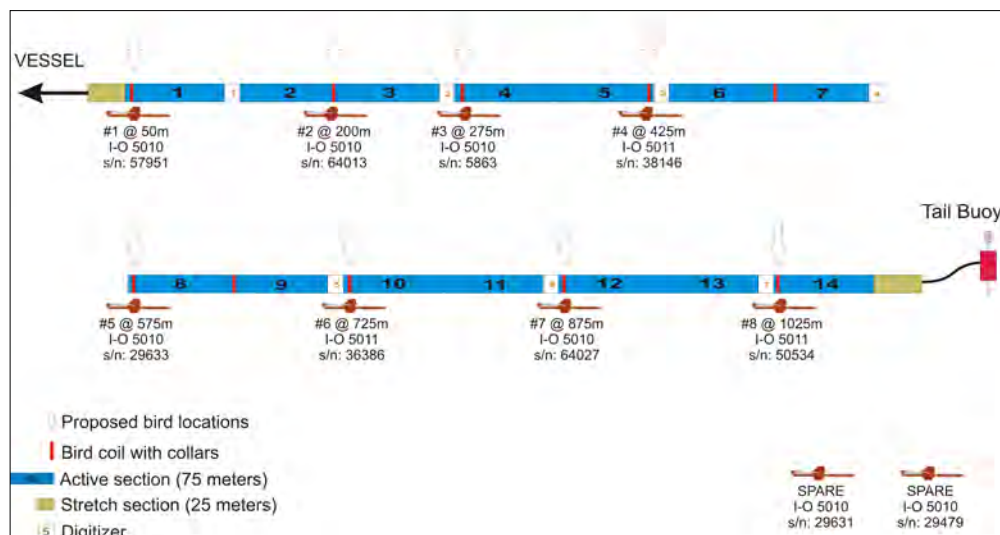


Figure 11.3.4. Streamer and bird configuration.

11.3.1.1 Definition of Navigation Data

The navigation parameters used along the entire survey are given in Table 11.3.2. Navigation logs have been created for each seismic line, and the locations of the sensors as well as some other information such as vessel speed and gyro have been logged at every shot location into the ASCII text files. Table 11.3.3 shows the data column definitions of the navigation log files. Additional log files in ASCII format for the easy definition of seismic line geometry during the seismic data processing were also prepared for each line. These logs contain only the shot number and shot locations in UTM35N projection, and are named seismic logs. Table 11.3.4 shows the data column definitions of the seismic log files.

Table 11.3.2. Navigation parameters used during the survey.

GPS	Global DGPS
Ellipsoid	WGS 84
Inverse Flattening	298.2572235630
Semi major axis	6378137.0000
Projection	UTM (north)
Scale Factor	0.999600000000
Eccentricity	0.081819190843
Central Meridian	027°00'0.0000"
Origin Latitude	000°00'0.0000"
False Easting	500000.0000
False Northing	0.0000
UTM zone	35

11.3.1.2 Definition of Multichannel Seismic Data

The seismic data have been collected in SegY Rev1.0 format and recorded into the hard drive as one separate SegY file for each individual shot. The data are in 32 bit IEEE floating point format. Sampling rate is 1.0 ms, which corresponds a 500 Hz Nyquist frequency. The data acquisition parameters for the multichannel seismic data are given in Table 11.3.5. Two noise records immediately before and after shooting were also recorded for each seismic line. Figure 11.3.5 shows the streamer layout and acquisition geometry used during the survey.

Table 11.3.3. Definitions of the columns in the navigation log files (xxxxxx.DAT).

Column	Header	Definition
1	event	Shot no (FFID)
2	time	Shot time (HH:MM:SS)
3	vessel-UTMx	Easting of vessel's reference position in UTM 35N
4	vessel-UTMy	Northing of vessel's reference position in UTM 35N
5	vessel-Lat	Lat. of vessel's reference position (DD.MMMMMM)
6	vessel-Long	Long. of vessel's reference position (DD.MMMMMM)
7	shot-UTMx	Easting of shot point position in UTM 35N
8	shot-UTMy	Northing of shot point position in UTM 35N
9	shot-Lat	Lat. of shot point position (DD.MMMMMM)
10	shot-Long	Long. of shot point position (DD.MMMMMM)
11	gyro	Gyro in degrees
12	speed	Vessel speed in m/s

Table 11.3.4. Definitions of the columns in the seismic log files (xxxxxx_PRONAV.DAT).

Column	Header	Definition
1	event	Shot no (FFID)
2	shot-UTMx	Easting of shot point position in UTM 35N
3	shot-UTMy	Northing of shot point position in UTM 35N

Table 11.3.5. Multi channel seismic reflection data acquisition parameters.

No of channels	168
Streamer length	1050 m
Record length	5000 ms
Group interval	6.25 m
Data format	SegY rev1.0 IEEE 32 bit Floating Point
Delay time	0 ms
Vessel speed	4.5 knots
Sampling rate	1.0 ms
Streamer depth	4 m
Shot interval	18.75 m (distance based)
Source	GI gun (105+105 inch ³ or 45+45 inch ³)
Source depth	2 m
Lateral offset	24 m
Source pressure	2000 psi
Gun injector delay	56 ms
Minimum offset	50 m
Birds	3x5011 and 5x5010 I/O DigiBird
Low cut / Slope	5 Hz / 12 dB / oct
High cut / Slope	412 Hz / 225 dB / oct

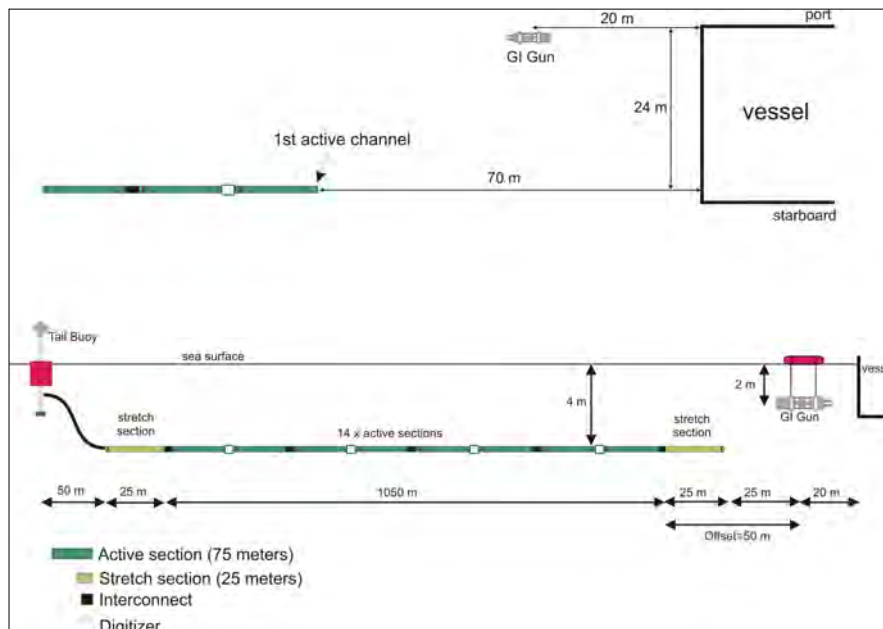


Figure 11.3.5. Streamer layout and data acquisition geometry.

11.3.1.3 Analyzing the Seismic Data and QC

QC analysis procedure for multichannel seismic and navigation data was run immediately after the completion of each seismic line. A standard onboard QC report was prepared for each seismic and navigation dataset. The basic purpose is to document the probable issues on the seismic and navigation data being collected and to take the necessary precautions.

The QC processes applied on the seismic data comprise:

- Virtual check of the all shot gathers along the line,
- RMS noise display at the beginning and end of the line,
- Amplitude spectra calculation of the selected shots from the beginning, middle and end parts of the line, before and after a 10-180 Hz band-pass filter,
- Common offset section calculation using 1st or 2nd channel (data loading, 10-180 Hz band-pass filter, 500 ms AGC),
- Calculation of the brute stack (data loading, geometry definition, 10-180 Hz band-pass filter, 500 ms AGC, CDP sort, constant velocity NMO correction, stack, constant velocity Stolt migration, 500 ms AGC),
- Fold number along the line and 2D stacking chart.

The QC processes applied on the navigation data comprise:

- Plot of line direction (the shot points) in UTM coordinates,
- Shot point - shot interval plot,
- Shot point - azimuth plot,
- Shot point - vessel speed plot,
- Shot point - water depth plot,
- Calculation of mean/min/max shot interval and total line length.

11.3.2 2D GEOMAR high resolution streamer

Joerg Bialas, Stephanie Koch, Sudipta Sarkar., Felix Gross, Timo Zander, Gero Wetzel, Torge Matthiessen, Mert Küçük, Orhan Atkin, Özkan Özel

For 2-D multichannel acquisition the streamer was deployed through the rear A-frame. The streamer was prepared in different settings. A first deployment composes of 5 sections (62.5 m active length) a vibration isolation section of 25 m and 55 m tow cable. Further deployments were done with a vibration isolation section of 25 m, 55 m tow cable and 19 active sections of 12.5 m length (237.5 m active length). Detailed measures are given in figure 11.2.3.1.

11.3.3 P-Cable

Joerg Bialas, Stephanie Koch, Sudipta Sarkar, Gero Wetzel, Torge Matthiessenn, Mert Küçük, Orhan Atkin, Özkan Özel

The P-Cable (VBPR patent of 2003) system is designed to high resolution imaging of shallow horizons. GEOMAR is holding an academic license of the P-Cable system and developed a custom made modular system in 2009.

Compared to standard reflection seismic applications in 2-D and 3-D the basic difference is that the P-Cable is build by a cross cable towed perpendicular to the ships heading (Fig. 11.2.3.2). Instead of a few single streamers the P-Cable uses a large number of short streamer sections towed parallel from the cross cable. Drawback is the limited depth penetration due to the short receiver offsets, which are not favourable for the removal of multiples. This is well compensated by the reduced costs of the system and the ability to operate it even from small multi purpose vessels, the usual academic platform for marine research.

Upon deployment the door next to the umbilical is released from its rest position while the ship sails at 1.5 kn through water against wind and waves. The door is lowered into the water while a 10 m long lead cable between door and connection point of cross cable is kept on board.. Next the data cable from the recording device to the door is hooked to the connection between lead wire and cross cable. Now trawl wire, data cable and cross cable are paid out

simultaneously. At the same time streamer sections are connected to the nodes of the cross cable. Floats were attached to the break outs and in centre of the cross cable segments (not on the outer three port and starboard side segments) help to keep the streamers at 2 m depth. When the entire cross cable is paid out a support rope on the support winch is used for secure transmit of the cross cable from the support winch to the lead wire of the second trawl door. Now both trawl wires are given out until the final length with sufficient stretch of the trawl doors is reached. The different measures during the MSM34 deployments are given in fig. 11.2.3.2.

MSM 34 2D Setup

192.168.1.1
GEOMETRICS PC
192.168.1.2
SPSU

Section	A/D	Streamer	Bird
Stretch	/	VR	x
1	DG01721	ARD1101	X
2	DG01281	AR01159	
3	DG01530	ARD1979	
4	DG01182	ARD1069	
5	DG01473	ARE01096	
6	DG01182	ARD1069	
7	DG01529	ARD1081	
8	DG01102	ARD1057	
9	DG01232	AR01102	
10	DG01183	ARE01122	
11	DG01235	ARE0111	
12	DG01530	ARD1979	
13	DG01267	AR01161	
14	DG01266	AR01153	X
15	DG1780	GS0247	
16	DG01774	GS0275	
17	DG01683	GS0274	
18	DG01685	GS0249	
19	DG01779	GS0284	

MSM 34 P-cable Setup P2100					
192.168.1.1 GEOMETRICS PC 192.168.1.2 SPSU					
Streamer Nr:	T - Switch	A/D	Streamer	A/D	Streamer
Starbord					
1	7	DG01102 ARD1057	/		/
2	1	DG01530 ARD1979	/		/
3	10	DG01473 ARE01096	/		/
4	16	DG01235 ARE0111	/		/
5	14	DG01112 ARE01073	DG01272	AR01155	
6	20	DG01182 ARE01122	DG01182	ARD1069	
7	2	DG01683 GS0274	DG01779	GS0284	
8	12	DG01721 ARD1101	DG01281	AR01159	
9	19	DG01241 AR01157	/		/
10	3	DG01232 AR01102	/		/
11	13	DG01267 AR01161	/		/
12	17	DG01266 AR01153	/		/
13	6	DG01529 ARD1081	/		/
14	18	DG01774 GS0275	/		/
Portside					

MSM 34 P-cable Setup P2200						
192.168.1.1 GEOMETRICS PC 192.168.1.2 SPSU						
Streamer	Position	T - Switch	A/D	Streamer	A/D	Streamer
Starbord						
6	1	7	DG01182	ARE01122	DG01182	ARD1069
3	2	1	DG01530	ARD1979	/	/
4	3	10	DG01473	ARE01096	/	/
7	4	16	DG01182	ARE01122	DG01182	ARD1069
OHNE Nummer	5	14	DG01102	ARD1057	/	/
11	6	20	DG01232	AR01102	/	/
8	7	2	DG01683	GS0274	DG01779	GS0284
2	8	12	DG01530	ARD1979	/	/
12	9	19	DG01267	AR01161	/	/
10	10	3	DG01721	ARD1101	DG01281	AR01159
5	11	13	DG01235	ARE0111	/	/
13	12	17	DG01266	AR01153	/	/
14	13	6	DG01529	ARD1081	/	/
					21	
15	14	18	DG01774	GS0275	DG1780	GS0247
Portside						

MSM 34 P-cable Setup P2400						
192.168.1.1 GEOMETRICS PC 192.168.1.2 SPSU						
Streamer	Position	T - Switch	A/D	Streamer	A/D	Streamer
Starbord						
6	1	7	DG01182	ARE01122	DG01182	ARD1069
3	2	1	DG01530	ARD1979	/	/
4	3	10	DG01473	ARE01096	/	/
7	4	16	DG01182	ARE01122	DG01182	ARD1069
OHNE Nummer	5	14	DG01102	ARD1057	/	/
11	6	20	DG01232	AR01102	/	/
8	7	2	DG01683	GS0274	DG01779	GS0284
2	8	12	DG01530	ARD1979	/	/
12	9	19	DG01267	AR01161	/	/
10	10	3	DG01721	ARD1101	DG01281	AR01159
5	11	13	DG01235	ARE0111	/	/
13	12	17	DG01266	AR01153	/	/
14	13	6	DG01529	ARD1081	/	/
15	14	18	DG01774	GS0275	DG1780	GS0247
Portside						

MSM 34 P-cable Setup P3100						
192.168.1.1 GEOMETRICS PC 192.168.1.2 SPSU						
All Streamer and T Switches Renamed!!!						
Streamer	Position	T - Switch	A/D	Streamer	A/D	Streamer
Starbord						
			3	4		
1	1	7	DG01182	ARE01122	DG01182	ARD1069
			5			
2	2	1	DG01530	ARD1979	/	/
			6			
3	3	10	DG01473	ARE01096	/	/
			7	8		
4	4	16	DG01182	ARD1069	DG01182	ARE01122
			9			
5	5	9	DG01685	GS0249	/	/
			10			
6	6	14	DG01102	ARD1057	/	/
			11			
7	7	20	DG01232	AR01102	/	/
			12	13		
8	8	2	DG01683	GS0274	DG01779	GS0284
			14			
9	9	12	DG01530	ARD1979	/	/
			15			
10	10	19	DG01267	AR01161	/	/
			16	17		
11	11	3	DG01721	ARD1101	DG01281	AR01159
			18			
12	12	13	DG01235	ARE0111	/	/
			19			
13	13	17	DG01266	AR01153	/	/
			20			
14	14	6	DG01529	ARD1081	/	/
			21	22		
15	15	18	DG01774	GS0275	DG1780	GS0247
Portside						

11.3.4 OBS-Instrumentation

Anke Dannowski, Isabel Sauermilch, Henning Schröder, Timo Zander

A total of 15 ocean bottom seismometers (OBS) were available for the MSM34-2 cruise. Altogether 27 sites were deployed to complement the seismic 2D streamer and 3D P-cable measurement. The principle design of the GEOMAR-OBS is described in detail by Flueh and Bialas (1996). Two types of OBS were used:

11.3.4.1 The GEOMAR three-leg Ocean Bottom Seismometers:



The system components are mounted on a steel tube, which holds the buoyancy body on its top (fig. 11.3.4.2). The buoyancy body is made of syntactic foam and is rated, as are all other components of the system, for a water depth of 6000 m. Attached to the buoyant body are a radio beacon, a flash light, a flag and a swimming line for retrieving from aboard the vessel. The release transponder for the acoustic release is also mounted here. The sensors are an *E-2PD* hydrophone from *OAS Inc.*, or a *HTI-01-PCA* hydrophone from *HIGH TECH*, and a three-component seismometer (*KUM*). The seismometer is only connected via a cable to the OBS and stands free on the seafloor after it was released from the OBS frame. As recording devices broadband seismocorders (*MBS*) of *SEND GmbH* were used, which are contained in their own pressure tubes. The recording sampling rate was chosen with 1000 Hz.

11.3.4.2 The GEOMAR Ocean Bottom Seismometer 2002 (OBS-2002):

This is the recent design based on experiences gained with three-leg GEOMAR Ocean Bottom Seismometer (OBS, Bialas and Flueh, 1999). Figure 11.3.4.1 shows the basic system. It is constructed to carry a hydrophone and a small seismometer for higher frequency active seismic profiling. However, due to the modular design of the front end it can be adapted to different seismometers and hydrophones or pressure sensors.

The sensitive seismometer is deployed between the anchor and the OBS frame, which allows good coupling with the sea floor. The three component seismometer (*KUM*), usually used for active seismic profiling, is housed in a titanium tube, modified from a package built by Tim Owen (Cambridge) earlier. Geophones of 4.5 Hz natural frequency were used during MSM34-2. While deployed to the sea floor the entire system rests horizontally on the anchor frame. After releasing its anchor weight the instrument turns 90° into the vertical and ascends to the surface with the floatation on top. This ensures a maximally reduced system height and water current sensibility at the ground (during measurement). On the other hand the sensors are well protected against damage during recovery and the transponder is kept under water, allowing permanent ranging, while the instrument floats at the surface.

During cruise MSM34-2 on RV Maria S. Merian tests on the position of the geophone were performed. One instrument was deployed for several times with two geophones and one hydrophone. One geophone was attached as described and seen on the picture. The second geophone was attached to an arm, thus, the geophone can stand free on the seafloor when released (Fig. 11.3.4.1).

	
<p>Fig. 11.3.4.1 – Modified OBS-2002 with an extra geophone.</p>	<p>Fig. 11.3.4.2 – Three-leg GEOMAR Ocean Bottom Seismometer. Geophone will be release from the arm when standing on the seafloor.</p>

11.3.4.3 Recording and processing of OBS-Data

The so-called *Marine Broadband Seismic recorder (MBS)* (Bialas and Flueh, 1999), manufactured by *SEND GmbH*, was developed based upon experience with the DAT-based recording unit *Methusalem* (Flueh and Bialas, 1996) over previous years. Redesign of the electronic layout enables decreased power consumption (1.5 W) of about 25% compared to the *Methusalem* system. Depending on the sampling rate, data output could be in 16 to 18 bit signed data. The bandwidth reaches from 0.1 Hz for seismological observations to the 50 Hz range for refraction seismic experiments and up to 10 kHz for high resolution seismic surveys. The basic system is adapted to the required frequency range by setting up the appropriate analogue front module. Alternatively, 1, 2, 3 or 4 analogue input channels may be processed. The instrument can be parameterised and programmed via a RS232 interface.

The time base is based on a DTCXO with a 0.05 ppm accuracy over temperature. Setting and synchronising the time as well as monitoring the drift is carried out automatically by synchronisation signals (DCF77 format) from a GPS-based coded time signal generator. Clock synchronisation and drift are checked after recovery and compared with the original GPS units. After recording, playback of the data is done by copying the flashcards to a PC workstation. During this transcription the data are decompressed and formatted according to the PASSCAL data scheme. This enables full compatibility with the established processing system and it can be easily transformed into standard seismological data formats.

A standard pre-processing of the active source seismic data was done following GEOMAR standard procedures. Raw data were first processed with software from the manufacturer of the seismic recorders (SEND GmbH) and internal time slips, etc. were corrected. Data were then stored in PASSCAL format. Later, dat2segy program was used to cut out shots by cutting the single SEG-Y trace (the ref2segy output) into traces with a defined time length based on the geometry and shooting time information in the ukooa file. In addition, a time offset of the trace and a reduction velocity was set (to determine the time of the first sample within a record). Also the clock drift of the recorder (skew) is taken into account and corrected for. The final SEG-Y format consists of the file header followed by the traces. Each trace is built up by a trace header followed by the data samples. The output of the dat2segy program can be used as input for further processing for example using Seismic Unix (SU).

11.4 Coring devices

Matthias Haeckel, Nikolaus Bigalke, Dirk Schroller (GEOMAR)

To carry out geological and geochemical sampling a gravity corer (GC) and a mini-multiple corer (MIC) were mobilized (Fig. 11.5.1). The GC, equipped with a weight of 1150 kg and a 5-m long core barrel, was operated by the large movebar, whereas the MIC (total weight of ~150 kg, including the 8 lead weights of ~10 kg each) was operated by the 5-t crane 1. Both, the GC and the MIC were lowered into the sediment with a rope speed of 0.3 m/s to minimize or avoid core overpenetration in the soft Black Sea sediments (see geochemistry chapter 6.3). After the retrieved GC was on deck the inner plastic liner (inner diameter of 110 mm) was pulled out, cut into 1-m long segments, which were each cut lengthwise into a sampling and an archive half using a special saw. The geological core description and sediment photography was followed by sediment sampling for geochemical analyses in the ship's hangar. Subsequently, the sampling and the archive half were transferred into D-tubes for long-term storage at GEOMAR's cooled core repository. The upper semi-liquid surface sediments were collected with the MIC retrieving up to 4 parallel cores with a diameter of 100 mm. The MIC allows sampling of an undisturbed sediment-water interface, typically including the uppermost 30-40 cm of the sediment together with the overlying bottom water. The MIC is considerably lighter than a regular multiple corer and hence, ideal for the soft Black Sea sediments as it does not sink in too far with the risk of overpenetration of the liners.



Figure 11.5.1: (Left) Mini-multiple corer (MIC) with 4 plastic liners and (right) gravity corer (GC) with 5-m barrel.

11.5 OBS station list

Profile 1000/2000 - Area 1 - 2D/3D

OBS	Date	Time	Lat	Long	Depth	Ch.	Release	Enable	Disable	released	surface	deck	Time Release	Rec Nr	Geophone	Hydr
1001	30.12.13	19:07	43°29.175	30°24.306	1422	D	533736	516006	516025	06:37	06:58	07:06	16.01.2014 06:00	980903	88	97
1002	30.12.13	19:31	43°28.743	30°24.75	1443	B	644421	656454	656477	06:08	06:29	06:38	16.01.2014 06:00	990712	85	91
1003	30.12.13	19:49	43°28.311	30°25.199	1464	D	450517	467743	467760	05:40	06:02	06:10	16.01.2014 06:01	980908	092	39
1004	30.12.13	20:02	43°27.883	30°25.638	1468	C	450704	470450	470473	05:13	05:33	05:41	16.01.2014 06:01	000616	83	93
1005	30.12.13	20:17	43°27.450	30°26.088	1492	B	447451	465213	465230	04:44	05:06	05:13	16.01.2014 06:02	980904	90	32
1006	30.12.13	20:37	43°27.134	30°25.500	1498	B	534123	516517	516534	03:47	03:07	04:15	16.01.2014 06:02	980907	1001-117	50
1007	30.12.13	20:57	43°27.568	30°25.061	1474	C	534224	516742	516761	03:19	03:39	03:48	16.01.2014 06:03	020504	89	64
1008	30.12.13	21:15	43°27.999	30°24.619	1448	D	5450551	470076	470107	02:49	03:10	03:21	16.01.2014 06:03	020507	57	38
1009	30.12.13	21:30	43°28.427	30°24.162	1469	B	450742	470567	470605	02:18	02:39	02:50	16.01.2014 06:04	971202	063	109
1010	30.12.13	21:44	43°28.858	30°23.725	1459	B	442102	440500	440523	01:49	02:09	02:19	16.01.2014 06:04	000611	11	76
1011	30.12.13	22:03	43°28.253	30°23.131	1428	B	451100	471153	471170	01:14	01:37	01:50	16.01.2014 06:05	980401	105	58
1012	30.12.13	22:27	43°28.100	30°23.578	1451	B	447604	465574	465616	00:40	01:02	01:15	16.01.2014 06:05	020503	87	28
1013	30.12.13	22:43	43°27.672	30°24.013	1481	A	447756	466147	466164	00:07	00:27	00:41	16.01.2014 06:06	001004	086	114
1014	30.12.13	23:01	43°27.241	30°24.450	1502	D	0397+0355			23:36	23:55	00:08	16.01.2014 06:06	990901	32	80
1015	30.12.13	23:26	43°26.817	30°24.912	1515	C	03B6+0355			04:14	04:38	05:13	16.01.2014 06:07	991292	14	108

Profile 3000/4000 - Area 2 - 3D/2D

OBS	Date	Time	Lat	Long	Depth	Ch.	Release	Enable	Disable	released	surface	deck	Time Release	Rec Nr	Geophone	Hydr
3001	09.01.14	18:43	43°57,491	30°45,410	656	B	450551	470076	470107	21:03	21:13	21:25	16.01.2014 06:00	020507	57	38
3002	09.01.14	18:56	43°57,14	30°45,734	689	B	447756	466147	466164	21:25	21:25	21:47	16.01.2014 06:00	001004	086	114
3003	09.01.14	19:08	43°56,842	30°46,079	708	B	451100	471153	471170	21:47	21:59	22:10	16.01.2014 06:00	980401	105	58
3004	09.01.14	19:20	43°56,525	30°46,441	704	D	534123	516517	516534	22:16	22:26	22:36	16.01.2014 06:00	980907	1001-117	50
3005	09.01.14	19:35	43°56,916	30°47,148	792	C	447451	465213	465230	22:29	22:40	22:56	16.01.2014 06:00	980904	90	32
3006	09.01.14	19:48	43°57,228	30°46,821	709	B	450517	467743	467760	22:45	23:00	23:14	16.01.2014 06:00	980908	092	39
3007	09.01.14	19:59	43°57,562	30°46,485	647	D	03B6+0355			23:09	23:19	23:33	16.01.2014 06:00	991292	14	108
3008	09.01.14	20:10	43°57,863	30°46,137	609	C	0397+0355			23:30	23:37	23:45	16.01.2014 06:00	990901	32	80
3009	09.01.14	20:32	43°58,284	30°46,833	596	B	644421	656454	656477	23:45	23:54	00:05	16.01.2014 06:00	990712	85	91
3010	09.01.14	20:43	43°57,954	30°47,163	704	D	533736	516006	516025	00:00	00:10	00:20	16.01.2014 06:00	980903	88	97
3011	09.01.14	20:53	43°57,646	30°47,51	807	B	450704	470450	470473	00:18	00:29	00:41	16.01.2014 06:00	000616	83	93
3012	09.01.14	21:05	43°57,321	30°47,857	859	B	534224	516742	516761	00:38	00:50	00:59	16.01.2014 06:00	020504	89	64

For precise locations of the coring gear at the seafloor, the ship's POSIDONIA underwater navigation system IXSEA was attached to the rod approximately 30 m above the MIC and GC.

During the cruise 9 gravity cores and 8 mini cores were taken (Table 5.3.2) in the 2 areas that were also investigated by 3-D seismic surveys, i.e. the channel-levee system southwest of the Viteaz canyon with shallow seismic reflections in the channel fill and the area with the upward bending BSR reflector north-east of the Viteaz canyon. In addition, a MIC and a GC core were also taken at the shallow piezometer location (see chapter 5.5).

11.15.1 Core descriptions

11.15.1.1 Site IFREMER Piezometer (in shallow water)

3-2 MIC1

0-49.5 cm



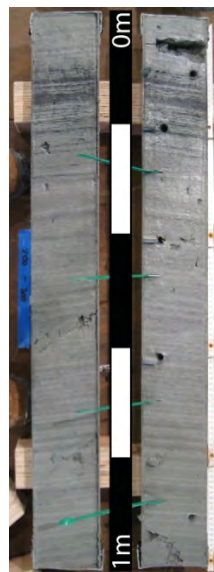
3-3 GC1



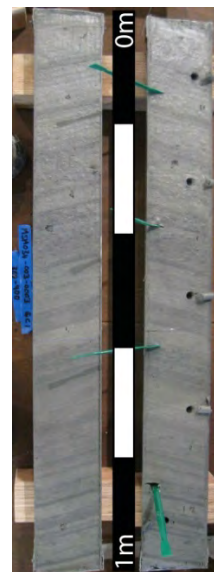
0-100 cm



100-200 cm



200-300 cm



300-400 cm



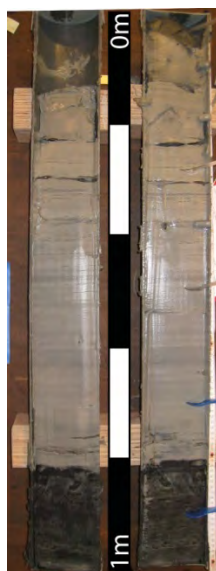
400-500 cm

11.5.1.2 Site SW channel-levee with multiple BSR (on seismic line 8b)

42-1
MIC4
0-42 cm



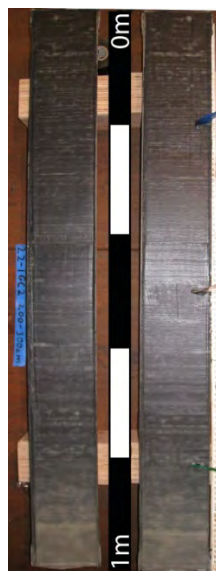
22-1 GC2



0-100 cm



100-200 cm



200-300 cm



300-400 cm



400-500 cm

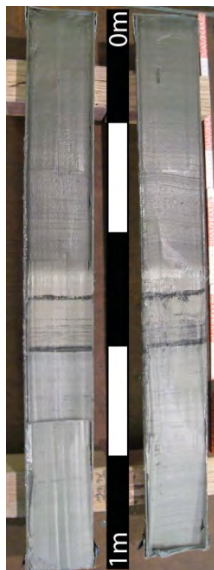
11.5.1.3 Site SW channel-levee with multiple BSR (channel)

26-1
MIC2

0-51 cm



39-1 GC3



0-100 cm



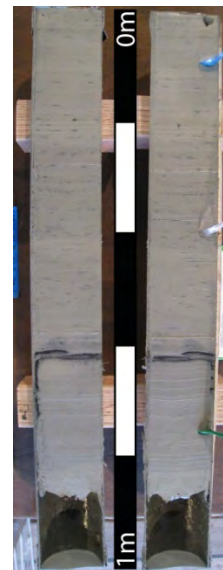
100-200 cm



200-300 cm



300-400 cm



400-500 cm

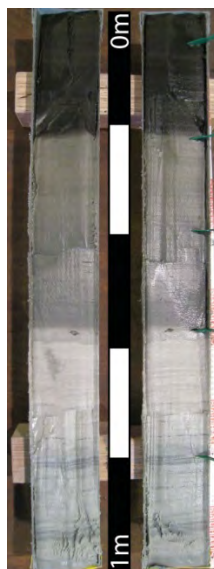
11.5.1.4 Site SW channel-levee with multiple BSR (levee)

27-1
MIC3

0-40 cm



40-1 GC4



0-100 cm



100-200 cm



200-300 cm



300-400 cm



400-500 cm

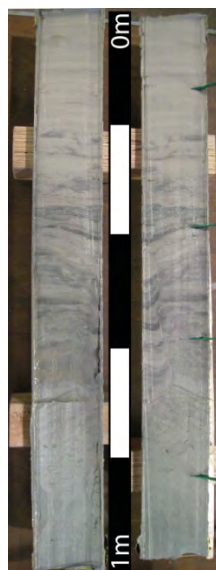
11.5.1.5 Site NE channel-levee with upward bending BSR (slump area)

43-2
MIC5

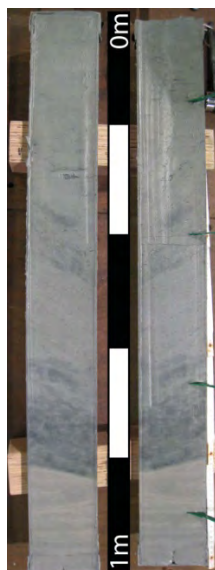
0-38 cm



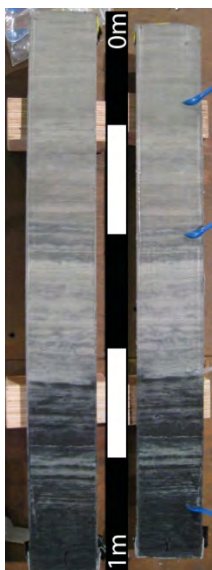
43-1 GC5



0-100 cm



100-200 cm



200-300 cm



300-400 cm



400-500 cm

11.5.1.6 Site NE channel-levee with upward bending BSR (slump area)

65-1
MIC6
0-41 cm



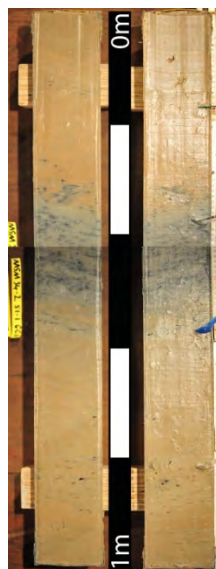
51-1 GC6



0-63 cm



63-163 cm



163-263 cm



263-363 cm



363-463 cm

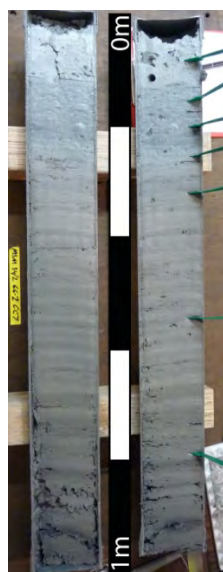
11.5.1.7 Site NE channel-levee with upward bending BSR (gas seep at slump head wall)

66-1
MIC7

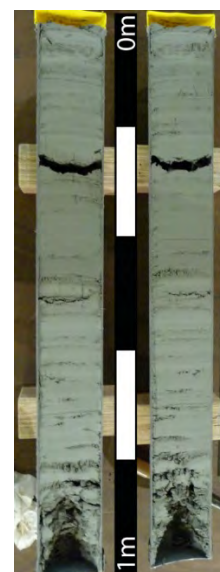
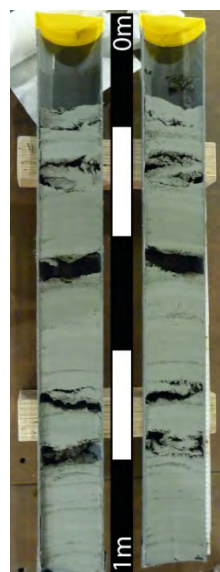
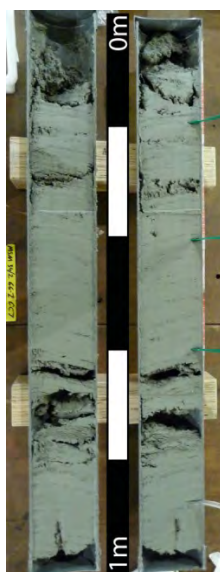
0-44 cm



66-2 GC7



Corrupted
Photo



0-100 cm

100-200 cm

200-300 cm

300-400 cm

400-500 cm

11.5.1.8 Site NE channel-levee with upward bending BSR (slump area)

74-1
MIC8

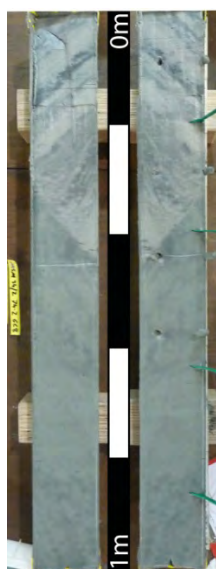
0-42 cm



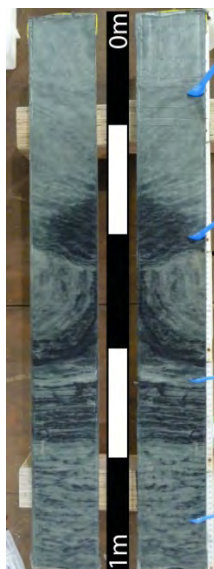
74-2 GC8



0-100 cm



100-200 cm



200-300 cm



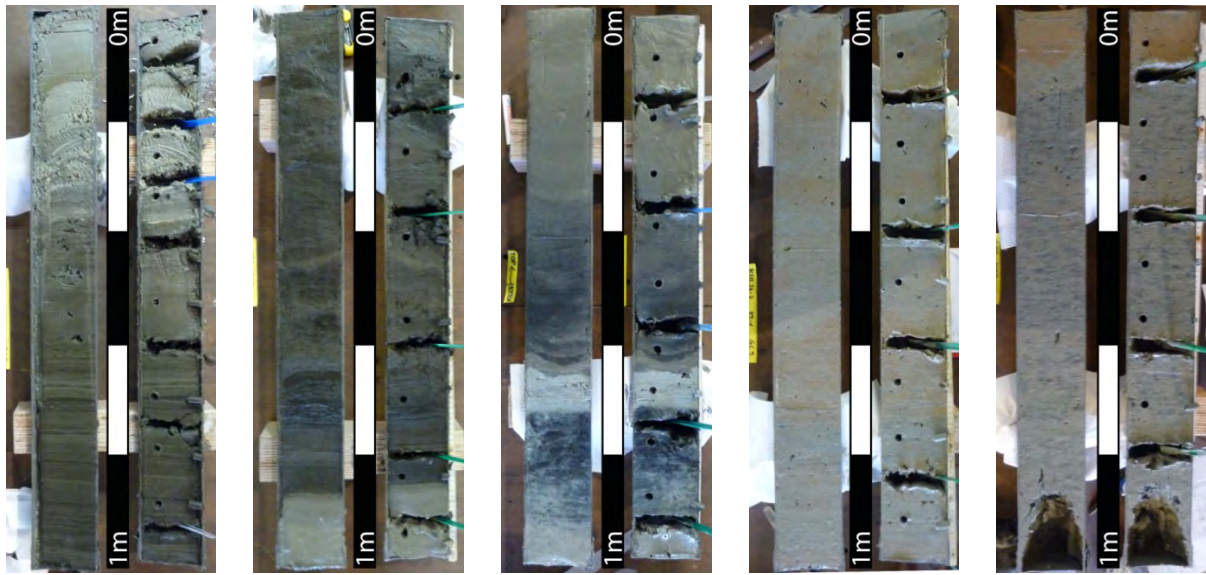
300-400 cm



400-500 cm

11.5.1.9 Site NE channel-levee with upward bending BSR (channel)

89-1 GC9



0-100 cm

100-200 cm

200-300 cm

300-400 cm

400-500 cm

11.6 Heatflow probe

Jörg Bialas, Gero Wetzel

A standard violin-bow-type heatflow probe was used to obtain in-situ sediment temperature and thermal conductivity measurements (Fig. 11.6.1). The active length of the probe is 5.67 m with 22 evenly spaced temperature sensors. Each sensor measures temperature at a resolution of less than 1 mK and is calibrated to an accuracy of better than 2 mK. In addition, sensors for tilt, pressure, absolute temperature, and acceleration are incorporated to provide detailed information about the state of the instrument during the measurement.

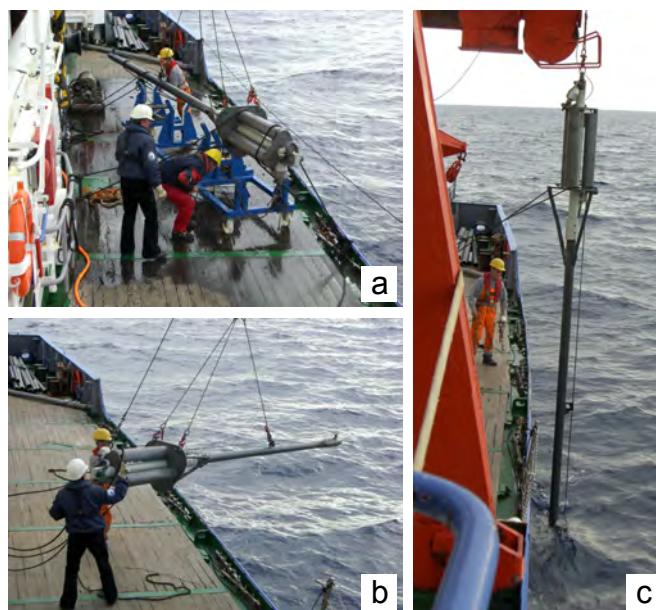


Figure 11.6.1: Deployment of the heatflow probe

On MERIAN the heatflow probe is operated from winch F2S2. Two cable floats were mounted about two meters above the probe to keep protecting the cable from bending and

damage. A POSIDONIA transponder is mounted 30 m above the probe. Online tracking allows manoeuvring the probe towards the foreseen sample position. For each measurement, the heatflow probe is lowered to the seafloor at a speed of around 0.3 m/s until it has entered the sediment. Display of tensile strength of the rope indicates the time of seafloor penetration. Additional four m of cable were allowed to compensate ships movement. Upon penetration, the probe is left in position for around 7 minutes to allow the temperature sensors to adjust to ambient sediment temperature. Temperature readings are recorded at a sampling rate of 1 s. Equilibrium temperatures may be calculated by extrapolation from the recorded temperature time series.

After recording the sediment temperature profile during the first seven minutes, an in-situ thermal conductivity measurement may be conducted by applying a controlled heat pulse to a heating wire along the sensor string of the probe. The depth-dependent thermal conductivity of the sediments may be calculated from the temperature time series recorded during the dissipation of the heat pulse for approximately 7 minutes following the heat pulse.

Several measurements may be conducted during one deployment by heaving the probe a few tens of meters while the ship approaches the position of the next measurements.

11.6.1 Heatflow probe station protocol

Expedition	MSM 34/2		remarks
Date	30.12.13		Mit HP 09:38:55 Transponder 296
Station no.	3-1 /HF1		
Position	43°48,355N	30°24,797 E	
Water depth	418 m		
Gear on bottom	09:31:50		
Gear out of bottom	09:48		
Gear on deck			

Expedition	MSM 34/2		remarks Mit HP 17:03:50 Transponder 296
Date	04.01.2014		
Station no.	28-1 /HF1		
Position	43°28,216N	30°26,256 E	
Water depth	1430 m		
Gear on bottom	16:56:30		
Gear out of bottom	17:13:30		
Gear on deck			

Expedition	MSM 34/2		remarks Mit HP 17:59:41 Transponder 296
Date	04.01.2014		
Station no.	29-01/HF2		
Position	43°28,092N	30°26,021 E	
Water depth	1468 m		
Gear on bottom	17:51:40		
Gear out of bottom	18:09:00		
Gear on deck			

Expedition	MSM 34/2		remarks
Date	04.01.2014		Mit HP 18:45:30
Station no.	30-1 /HF3		
Position	43°27,956N	30°25,782 E	Transponder 296
Water depth	1466 m		
Gear on bottom	18:37:20		
Gear out of bottom	18:53:30		
Gear on deck			

Expedition	MSM 34/2		remarks
Date	04.01.2014		:: Transponder 296
Station no.	31-1 /HF4		
Position	43°27,863N	30°25,607 E	
Water depth	1470 m		
Gear on bottom	19:19:10		
Gear out of bottom	19:26:30		
Gear on deck			

Expedition	MSM 34/2		remarks
Date	04.01.2014		Transponder 296
Station no.	32-1 /HF5		
Position	43°27,760N	30°25,430 E	
Water depth	1478 m		
Gear on bottom	19:51:20		
Gear out of bottom	20:00:00		
Gear on deck			

Expedition	MSM 34/2		remarks
Date	04.01.2014		
Station no.	33-1 /HF6		
Position	43°27,660N	30°25,253 E	
Water depth	1475 m		
Gear on bottom	20:23:30		
Gear out of bottom	20:31:00		
Gear on deck			

Expedition	MSM 34/2		remarks
Date	04.01.2014		
Station no.	34-1 /HF7		
Position	43°27,547N	30°25,045 E	
Water depth	1478 m		
Gear on bottom	20:53:20		
Gear out of bottom	21:01:00		
Gear on deck			

Expedition	MSM 34/2		remarks
Date	04.01.2014		
Station no.	35-1 /HF8		
Position	43°27,471N	30°24,905 E	
Water depth	1495 m		
Gear on bottom	21:20:40		
Gear out of bottom	21:28:00		
Gear on deck			

Expedition	MSM 34/2		remarks
Date	04.01.2014		
Station no.	36-1 /HF9		
Position	43°27,373N	30°24,729 E	
Water depth	1500 m		
Gear on bottom	21:48:55		
Gear out of bottom	21:57:00		
Gear on deck			

Expedition	MSM 34/2		remarks
Date	04.01.2014		
Station no.	37-1 /HF10		
Position	43°27,276N	30°24,550 E	
Water depth	418 m		
Gear on bottom	22:22:00		
Gear out of bottom	22:29		
Gear on deck			

Expedition	MSM 34/2		remarks
Date	04.01.2014		
Station no.	38-1 /HF11		
Position	43°27,189N	30°24,372 E	
Water depth	1500 m		
Gear on bottom	22:52:50		
Gear out of bottom	23:00		
Gear on deck			

Expedition	MSM 34/2		remarks Mit HP 13:35:30 Transponder 296
Date	09.01.2014		
Station no.	44-1 /HF3		
Position	43°57,048N	30°46,912 E	
Water depth	752 m		
Gear on bottom	13:28:00		
Gear out of bottom	13:43:00		
Gear on deck			

Expedition	MSM 34/2		remarks
Date	09.01.2014		Transponder 296
Station no.	45-1 /HF3		
Position	43°57,186N	30°46,771 E	
Water depth	726m		
Gear on bottom	14:04:10		
Gear out of bottom	14:11:30		
Gear on deck			

Expedition	MSM 34/2		remarks Transponder 296
Date	09.01.2014		
Station no.	46-1 /HF3		
Position	43°57,308N	30°46,643 E	
Water depth	700m		
Gear on bottom	14:28:45		
Gear out of bottom	14:36:30		
Gear on deck			

Expedition	MSM 34/2		remarks Transponder 296
Date	09.01.2014		
Station no.	47-1 /HF3		
Position	43°57,440N	30°46,512 E	
Water depth	670m		
Gear on bottom	14:56:40		
Gear out of bottom	15:03:45		
Gear on deck			

Expedition	MSM 34/2		remarks Transponder 296
Date	09.01.2014		
Station no.	48-1 /HF3		
Position	43°57,560N	30°46,377 E	
Water depth	670m		
Gear on bottom	15:20:30		
Gear out of bottom	15:27:00		
Gear on deck			

Expedition	MSM 34/2		remarks Transponder 296
Date	09.01.2014		
Station no.	49-1 /HF3		
Position	43°57,685N	30°46,243 E	
Water depth	650m		
Gear on bottom	15:45:25		
Gear out of bottom	15:53:00		
Gear on deck			

Expedition	MSM 34/2		remarks Transponder 296
Date	09.01.2014		
Station no.	50-1 /HF3		
Position	43°57,811N	30°46,115 E	
Water depth	636m		
Gear on bottom	16:11:20		
Gear out of bottom	16:18:20		
Gear on deck			

Expedition	MSM 34/2		remarks
Date	13.01.2014		Mit HP Transponder 132
Station no.	67-1 /HF4		
Position	43°57,231N	30°46,727 E	
Water depth	713m		
Gear on bottom	15:55:25		
Gear out of bottom	16:10:20		
Gear on deck			

Expedition	MSM 34/2		remarks
Date	13.01.2014		Mit HP Transponder 132
Station no.	68-1 /HF4		
Position	43°57,273N	30°46,679 E	
Water depth	703m		
Gear on bottom	16:24:20		
Gear out of bottom	16:38:20		
Gear on deck			

Expedition	MSM 34/2		remarks HP 17:06:00 Transponder 132
Date	13.01.2014		
Station no.	69-1 /HF4		
Position	43°57,313N	30°46,498 E	
Water depth	696m		
Gear on bottom	16:53:50		
Gear out of bottom	17:14:12		
Gear on deck			

Expedition	MSM 34/2		remarks Mit HP 17:37:55 Transponder 132
Date	13.01.2014		
Station no.	70-1 /HF4		
Position	43°57,363N	30°46,587 E	
Water depth	703m		
Gear on bottom	17:28:50		
Gear out of bottom	17:45:10		
Gear on deck			

Expedition	MSM 34/2		remarks Mit HP 18:06:50 Transponder 132
Date	13.01.2014		
Station no.	71-1 /HF4		
Position	43°57,411N	30°46,680 E	
Water depth	696m		
Gear on bottom	18:00:00		
Gear out of bottom	18:14:00		
Gear on deck			

Expedition	MSM 34/2		remarks Mit HP 18:41:54 Transponder 132 Noise on temperature sensor
Date	13.01.2014		
Station no.	72-1 /HF4		
Position	43°57,405N	30°46,541 E	
Water depth	689m		
Gear on bottom	18:30:40		
Gear out of bottom	18:48:00		
Gear on deck			

Expedition	MSM 34/2		remarks
Date	13.01.2014		Transponder 132 Probe does not stuck in ground, moves with cable and vessel, station stopped
Station no.	73-1 /HF4		
Position	43°57,488N	30°46,454 E	
Water depth	670m		
Gear on bottom	19:04:30		
Gear out of bottom	19:08		
Gear on deck			

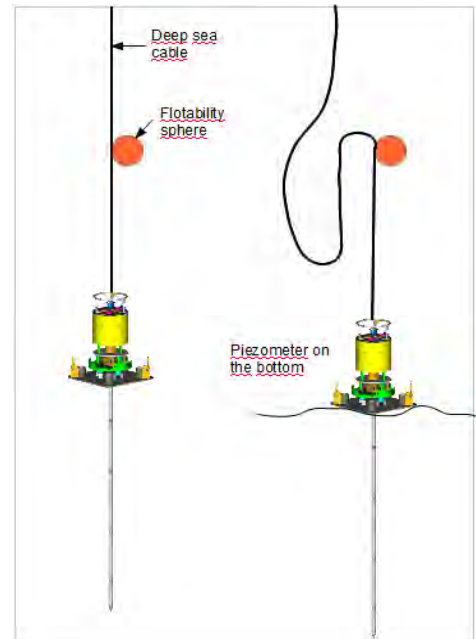
Expedition	MSM 34/2		remarks Second trial 5 m moved Transponder 132 Mit HP 19:19:11
Date	13.01.2014		
Station no.	73-1 /HF4		
Position	43°57,485N	30°46,457 E	
Water depth	674m		
Gear on bottom	19:12:00		
Gear out of bottom	19:26:00		
Gear on deck			

11.7 Piezometer

Mickael Roudaut, Anthony Ferrant

The objectives consisted of the deployment of 2 piezometers during for a period of 2 to 3 years. The IFREMER piezometer consists of two parts of which only one will be recovered at the end of the deployment period. The piezometer is deployed with the help of a deployment frame that was installed in the middle of the after-deck, just under the A-frame. Before the actual deployment of the piezometer, we realised a penetration test using a lance without sensors. This test is important to know the nature of the bottom, whether it is hard or soft sediment. The length of the lance is 10.5 m. If the lance is bent after the test, we shorten the lance until full penetration of the test lance is achieved. When the penetration is correct, the piezometer deployment with a fully equipped lance can be realised. During the cruise, only one test for each piezometer station had to

be realised.



The elements composing the IFREMER piezometer:

A recovering part with :

Acoustic release

Light, VHF

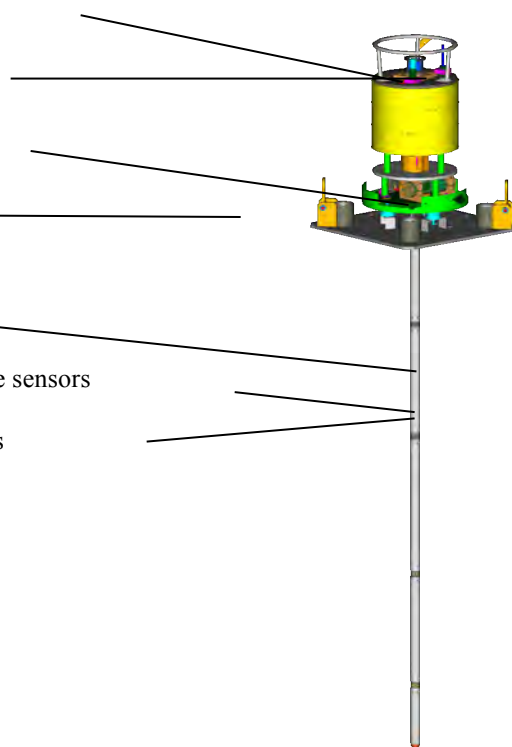
Data logger

A loosing part with :

pipes

differential pressure sensors

temperature sensors



11.7.1 Specifications of the piezometer:

Additional equipment needed for the deployment:

Weight	in the air	in wather
piezo (pipe, sensors, flotability)	350 kg	
ballast	1300 kg	
Piezo + ballast	1650 kg	1000 kg
Dimensions		
recovering part	H = 1,07 m Ø = 0,54 m	
losing part	steel plate : 1 m x 1 m. pipe lenght : 15 m maximum pipe Ø = 63 cm. 3 possibilites lenght : 3m / 1,5 m / 0,75 m	
Sensors	Differential pressure	Temperature
Type	Keller PD-10 LH	thermistance CTN
Precision	+/- 0,5 kPa	+/- 0,05°C
Mesurement	+/- 0,5 kPa	0°C to + 50°C
Maximum pressure	+ 400 kPa / - 300 kPa	
Power		
Type	Lithium 10,8 V / 53,9 Ah	
Autonomy with 5 sensors	200 days (1 mes/1s) or 800 days (1 mes/60s)	
Memory		
Type	SD card 4 Go	
Localisation on surface	Light	Gonio
	Xenon (7300 m max depVHF (chanel 72-156,625 Mhz)	

Maximum depth : 6000 m

- 1 swivel hook between the piezometer ballast and the deep sea cable
- 1 Senthos floatation sphere (-30kg)

11.7.2 Deployment procedure for bridge and deck

1 Lance without pressure sensor

When the weight of the piezometer is in the sea :

- _ go down 20 meters and stop to put floatation sphere on the deep sea cable
- _ go down at 1m/s and when the cable tension decrease, continue to go down 10 meters more
- _ go up to recover floatation sphere and the weight

2 Lance with pressure sensors

- _ when the piezometer is completely in the sea, stop 10 min
- _ go down 20 meters and stop to put floatation sphere on the deep sea cable
- _ go down at 1m/s and stop when piezometer is at about 50 meters from the bottom
- _ after 10 min, go down and when the cable tension decrease, continue to go down 10 meters more
- _ when the weight is released, go up to recover floatation sphere and the weight (speed is not important)



Figure 11.7.1: Deployment of the piezometer